Global Changes in Secondary Atmospheric Pollutants during the 2020 COVID-19 Pandemic

Benjamin Gaubert[1], Idir Bouarar[2], Thierno Doumbia[3], Yiming Liu[4], Trissevgeni Stavrakou[5], Adrien Michel Deroubaix[2], Sabine Darras[6], Nellie Elguindi[7], Claire Granier[8], Forrest Gerhart Lacey[9], Jean-François Müller[10], Xiaoqin Shi[2], Simone Tilmes[1], Tao Wang[11], and Guy P. Brasseur[2]

[1]National Center for Atmospheric Research (UCAR)
[2]Max Planck Institute for Meteorology
[3]Laboratoire d'Aerologie, University de Toulouse, CNRS, UPS
[4]Hong Kong Polytechnic University
[5]Royal Belgian Institute for Space Aeronomy
[6]Observatoire Midi-Pyrenees
[7]Centre national de la recherche scientifique
[8]University of Toulouse
[9]National Center for Atmospheric Research
[10]Royal Belgian Institute for Space Aeronomy (BIRA-IASB)
[11]The Hong Kong Polytechnic University

November 23, 2022

Abstract

We use the global Community Earth System Model to investigate the response of secondary pollutants (ozone O_3, secondary organic aerosols SOA) in different parts of the world in response to modified emissions of primary pollutants during the COVID-19 pandemic. We quantify the respective effects of the reductions in NOx and in VOC emissions, which, in most cases, affect oxidants in opposite ways. Using model simulations, we show that the level of NOx has been reduced by typically 40 % in China during February 2020 and by similar amounts in many areas of Europe and North America in mid-March to mid-April 2020, in good agreement with space and surface observations. We show that, relative to a situation in which the emission reductions are ignored and despite the calculated increase in hydroxyl and peroxy radicals, the ozone concentration increased only in a few NOx-saturated regions (northern China, northern Europe and the US) during the winter months of the pandemic when the titration of this molecule by NO_x was reduced. In other regions, where ozone is NOx-controlled, the concentration of ozone decreased. SOA concentrations decrease in response to the concurrent reduction in the NO_x and VOC emissions. The model also shows that atmospheric meteorological anomalies produced substantial variations in the concentrations of chemical species during the pandemic. In Europe, for example, a large fraction of the ozone increase in February 2020 was associated with meteorological anomalies, while in the North China Plain, enhanced ozone concentrations resulted primarily from reduced emissions of primary pollutants.

Global Changes in Secondary Atmospheric Pollutants during the 2020 COVID-19 Pandemic

Benjamin Gaubert[1], Idir Bouarar[2], Thierno Doumbia[3], Yiming Liu[5], Trissevgeni Stavrakou[6], Adrien Deroubaix[2], Sabine Darras[4], Nellie Elguindi[3], Claire Granier[3,7], Forrest Lacey[1], Jean-François Müller[6], Xiaoqin Shi[2], Simone Tilmes[1], Tao Wang[5], and Guy P. Brasseur[1,2,5]

[1]Atmospheric Chemistry Observations and Modeling Laboratory, National Center for Atmospheric Research, Boulder, CO, [2]Environmental Modeling Group, Max Planck Institute for Meteorology, Hamburg, Germany, [3]Laboratoire d'Aérologie, Université de Toulouse, CNRS, UPS, France, [4]Observatoire Midi-Pyrénées, Toulouse, France, [5]Department of Civil and Environmental Engineering, The Hong Kong Polytechnic University, Hong Kong China, [6]Royal Belgian Institute for Space Aeronomy, Brussels, Belgium, [7]NOAA Chemical Sciences Laboratory/CIRES, University of Colorado, Boulder, CO.

Corresponding author: Guy P. Brasseur (guy.brasseur@mpimet.mpg.de)

Key Points:

- During the Covid-19 lockdown, the atmospheric concentration of primary pollutants (NOx, VOCs, CO, SO_2) was considerably reduced.
- The concentration of secondary pollutants increased in NOx-saturated areas and decreased in NOx-limited areas.
- The response of the chemical system depends strongly on weather variability and on the relative changes in NOx and VOCs emissions.

Abstract

We use the global Community Earth System Model to investigate the response of secondary pollutants (ozone O_3, secondary organic aerosols SOA) in different parts of the world in response to modified emissions of primary pollutants during the COVID-19 pandemic. We quantify the respective effects of the reductions in NOx and in VOC emissions, which, in most cases, affect oxidants in opposite ways. Using model simulations, we show that the level of NOx has been reduced by typically 40 % in China during February 2020 and by similar amounts in many areas of Europe and North America in mid-March to mid-April 2020, in good agreement with space and surface observations. We show that, relative to a situation in which the emission reductions are ignored and despite the calculated increase in hydroxyl and peroxy radicals, the ozone concentration increased only in a few NOx-saturated regions (northern China, northern Europe and the US) during the winter months of the pandemic when the titration of this molecule by NO_x was reduced. In other regions, where ozone is NOx-controlled, the concentration of ozone decreased. SOA concentrations decrease in response to the concurrent reduction in the NO_x and VOC emissions. The model also shows that atmospheric meteorological anomalies produced substantial variations in the concentrations of chemical species during the pandemic. In Europe, for example, a large fraction of the ozone increase in February 2020 was associated with meteorological anomalies, while in the North China Plain, enhanced ozone concentrations resulted primarily from reduced emissions of primary pollutants.

Plain Language Summary

With the reduction in economic activities following the COVID-19 pandemic outbreak in early 2020, most emissions of air pollutants (i.e., nitrogen oxides (NOx), carbon monoxide (CO), sulfur dioxide (SO_2), volatile organic carbon (VOC), black carbon (BC), organic carbon(OC)) have decreased substantially during several months in different regions of the world. This unintended global experiment has given insight on some of the processes that control air quality and offered a glimpse into a potential future in which air quality would be improved. Here, a global atmospheric model is used to assess the changes in the chemical composition of the atmosphere during the pandemic period and in the related chemical processes that lead to the formation of ozone (O_3) and secondary organic aerosols (SOA). The study illustrates the nonlinearity of the air quality response to reduced NOx and VOC emissions, which depends on the chemical environment including the background level of nitrogen oxides. Meteorological variability can lead to anomalies in the

concentration of chemical species with magnitudes that are as large or even larger than the perturbations due to COVID-induced changes in the emissions.

1. Introduction

With the development of the COVID-19 pandemic and the resulting slowdown in economic activity, first in China and then in the rest of the world, anthropogenic emissions of primary pollutants were significantly altered for several months. This unanticipated planet-wide experiment allows us to examine the response of the atmosphere's chemical system and in particular, the formation of secondary compounds such as ozone (O_3) and the fraction of the airborne particles including $PM_{2.5}$ (particles with a diameter smaller than 2.5 micrometers) that is produced in situ. It offers a glimpse into a potential future in which air quality would be improved following structural regulations in the emissions of nitrogen oxides (NOx), carbon monoxide (CO), and volatile organic compounds (VOCs). A reduction in the emissions of the pollutants is expected to modify the level of photo-oxidants present in the atmosphere and the formation of secondary species including ozone (O_3) or secondary organic aerosols (SOA) (Miyazaki et al., 2020; Kroll et al., 2020; Huang et al., 2020). In some polluted geographical areas, the large decrease observed in NOx concentrations might have shifted the chemical regimes from NOx-saturated towards NOx-sensitive conditions. A better understanding of the chemical processes that determine the oxidative potential of the atmosphere and their disruption during the pandemic is therefore useful in developing adequate measures to improve air quality.

The pandemic manifested itself first in China where the first lockdown measures were adopted from the end of January to the month of March. In Europe, North and South America as well as India and the Middle East, lockdowns were imposed with varying degrees of stringency from March onwards and lasted at least until June.

Observations by spaceborne and ground-based instruments during the first months of 2020 highlighted a substantial decrease in the atmospheric concentrations of NO_2 relative to measurements performed during the same period in 2019 (e.g., Bauwens et al., 2020; Le et al., 2020; Liu et al., 2020; Shi and Brasseur, 2020), relative to longer-term averaged data (e.g., Deroubaix et al., 2020) or relative to model-based weather benchmarks (Venter et al. 2020; Keller et al., 2020). Numerous specific studies analyzing on air quality anomalies have focused on

specific regions or urban areas (e.g., Baldasano, 2020; Bedi et al., 2020; Chauhan and Singh, 2020; Fu et al., 2020a; He et al., 2020; Krecl et al., 2020; Menut et al., 2020; Otmani et al., 2020; Rodriguez-Urrego and Rodriguez-Urrego, 2020; Sicard et al., 2020; Siciliano et al., 2020; Zangari et al., 2020 among many others). A large fraction of the observed reductions in air pollutant emissions has been attributed to a drastic disruption in road traffic and in manufacturing operations. In the city of Wuhan, where the pandemic started and very strict lockdown measures were imposed to the entire population, NO_2 and $PM_{2.5}$ concentrations were reduced by approximately 50-60% and 30-40%, respectively, while a large positive anomaly was reported in the concentration of surface ozone (Shi and Brasseur, 2020; Lian et al., 2020; Fu et al., 2020b). For the North China Plain (NCP), the ozone increase was estimated to be larger than 40% (Huang et al., 2020; Shi and Brasseur, 2020; Zhu et al., 2020). Compared to the first months of 2019, measurements made by the spaceborne TROPOMI instrument onboard the Sentinel-5 Precursor satellite in early 2020 showed a decrease in the NO_2 column of typically 40-50% during the lockdown in northern China (Bauwens et al., 2020). Using TROPOMI data, Miyazaki et al. (2020) estimated a reduction of Chinese NOx emissions reaching 36% from early January to mid-February 2020. Several studies assessing the impact of the COVID-19 pandemic on the emissions of greenhouse gases showed for example that the emission of CO_2 decreased by about 11 to 25 % in April 2020 relative to the mean 2019 levels (Le Quéré et al., 2020; Forster et al., 2020). To analyze observational data during the pandemic, all the reported numbers must be disentangled from the long-term changes in pollutant emissions associated, for example, with air quality and climate policies, multi-scale meteorological variability and the occurrence of occasional societal events such as the New Year festivals in China. The need to consider the influence of weather variability (i.e., anomalies in temperature, humidity, circulation, cloudiness, boundary layer stability) during the pandemic has been highlighted by Diamond and Wood (2020), Barré et al. (2020), Deroubaix et al. (2020), Liu and Wang (2020), Ordóñez et al. (2020), Wang and Zhang (2020) and several other authors. Models have the advantage that they can isolate these different effects and derive the response of the atmosphere to the specific forcing mechanisms.

In this study, we use a global earth system model with a comprehensive representation of atmospheric gas phase and aerosol chemistry to analyze the importance of the chemical and meteorological processes that have led to a change in the surface concentrations of primary pollutants (e.g., NOx, CO, VOCs, SO_2, organic and black carbon), secondary photo-oxidants (e.g.,

ozone and radicals such OH, HO_2, RO_2, where R is an organic chain such as CH_3 or C_2H_5) and aerosol particles in several regions of the world in response to the reduced emissions of volatile organic compounds, carbon monoxide and nitrogen oxides during the period January to May 2020. The subsequent situation, linked to the onset of a second wave of the pandemic in late 2020, is not considered in this work.

To quantify the role of different processes that affected the level of pollutants during the COVID-19 pandemic period, different components of the atmospheric system must be carefully examined (Kroll et al., 2020):

(1) the changes in the emissions of primary pollutants resulting from the reduction in economic activities; these include primarily an abrupt disruption in road, air and maritime traffic as well as in industrial activities, but a possible increase in domestic activities;
(2) the changes in chemical regimes and specifically in the formation rate of secondary pollutants associated, for example with a shift from VOC to NOx controlled conditions, and in the formation of ozone and secondary organic aerosols under lower NOx levels;
(3) the changes in the concentration and chemical composition of particulate matter;
(4) the changes in meteorological factors including temperature, humidity, dynamical variability, boundary layer physics, cloudiness, precipitation and the related multi-scale transport processes.

The purpose of the paper is to assess the nonlinear relationship between the synergistic emission reduction of atmospheric primary pollutants during the COVID-19 pandemic and the level of atmospheric photo-oxidants and secondary species (e.g., ozone and secondary organic aerosols) produced in different regions of the world during the early months of 2020.

Ozone is formed during daytime by nonlinear processes at a rate that is determined by the atmospheric concentrations of VOCs and NOx. Under low NOx levels in remote or weakly polluted areas, the ozone production is controlled (or limited) by the concentration of NOx because high NOx concentrations enhance the production of peroxy radicals and subsequently ozone. Ozone is primarily destroyed by reactions involving hydrogenated species leading eventually to the formation of hydrogen peroxide ($HO_2 + HO_2 \rightarrow H_2O_2$), which is scavenged by wet and dry deposition. In very high NOx environments, i.e., in heavily polluted areas including industrial and

urban complexes, nitrogen oxides act as a sink for the OH radical, which slows down the oxidation of VOCs and hence the formation of peroxy radicals. As a result, the ozone production is considerably reduced. Rather, ozone is sequestered by NO to form NO_2 and is further titrated by NO_2 and eventually converted to nitric acid ($NO_2 + OH \rightarrow HNO_3$), which is removed from the atmosphere by wet and dry scavenging. This situation is referred to as NOx-saturated or VOC-controlled conditions. The reduction in VOCs and NOx during the pandemic is therefore expected to have led to a reduction of ozone in NOx-limited regions, but to have caused an increase in the ozone concentration in the most polluted areas, especially during winter when the levels of NOx are the highest. An increased oxidation capacity in the eastern part of China has been reported in Huang et al. (2020), whereas enhanced concentrations of ozone in the North China Plain were reported by Liu and Wang (2020), Shi and Brasseur (2020) and Miyazaki et al. (2020). This question will be further examined in subsequent sections.

The dominant source of secondary organic aerosols is provided by biogenic hydrocarbons including isoprene and terpenes, and by anthropogenic VOCs (linear and aromatic hydrocarbons) resulting from fossil fuel consumption, the industrial and domestic use of solvents and of other products, and from biomass burning. The rate at which the degradation of primary hydrocarbons proceeds, depends on the concentration of oxidants and on the level of nitrogen oxides (NOx) present in the atmosphere (Hallquist et al., 2009). SOA concentrations are expected to be reduced as a result of the reduction in VOC emissions. However, the reduction in NOx tends to increase the SOA production (Ng et al., 2007) under high NOx conditions by increasing the concentration of the OH radical, and therefore to partially offset the SOA decrease caused by the reduced VOC emissions.

The paper is organized as follows. Section 2 provides a short description of the emission reductions that are considered here as a forcing factor to the anomalies in the concentrations of chemical species during the pandemic period. Section 3.1 presents a description of the global earth system model that is adopted to analyze the atmospheric response to this forcing during the pandemic. Section 3.2 focuses on the evaluation of the atmospheric fields derived by the model and compares selected results with surface measurements of key species at different locations in the world. Section 4 provides a global view of the changes that have occurred in the chemical composition of the atmosphere in response to the reduced emissions of primary pollutants and to meteorological

anomalies occurring during the pandemic. Section 5 assesses the calculated changes in the concentration of chemical species in selected regions (China, Europe, North and South America) where lockdowns were imposed during the first months of 2020. This section discusses in particular the respective impact of the reduction in NOx versus VOC emissions as well as the role of meteorological variability on the calculated chemical fields. A summary of the findings and key conclusions are provided in Section 6.

2. Adjustments in Emissions during the Pandemic

The change in the emissions of primary pollutants associated with the COVID-19 pandemic has considerably varied among different economic sectors and geographic areas. The time at which the lockdowns were enforced and the severity of the measures taken to protect the population was different from country to country and even from region to region. Several studies (Guevara et al., 2020; Doumbia et al., 2020) have attempted to estimate these changes in emissions on the basis of available economic information regarding different sectors: transportation (road, air and sea traffic), industrial production, energy consumption and residential activity. Here we adopt the global estimates provided by Doumbia et al. (2020) gridded at a spatial resolution of 0.1 x 0.1 degree (about 10 x 10 km). In this study, adjustment factors were derived for each economic sector and geographic region based on activity data, and the resulting changes in the emissions of a given primary chemical species were calculated at each grid point of the model based on the relative contribution of each sector to the total emission. In some cases, the input data used to derive the adjustment factors was available at the country level, but in some cases, more resolved sub-regional-scale and even local-scale information was used. Some input data, for example the reduction of road traffic intensity, was accessible on a day-to-day basis for major cities in many (but not all) countries, and allowed Doumbia et al. (2020) to provide 10 km resolution emission estimates on a daily basis from January to August 2020. The reduction in the emissions for the shipping and aviation sectors adopted in the present study is also obtained from Doumbia et al. (2020). Figure 1 shows the geographically averaged percentage surface emission adjustment applied during the pandemic in different regions of the world and for different chemical species. In the Northern China Plain, the change in the emissions attributed to the COVID-19 pandemic occurred as early as 23 January 2020 and, as the lockdown was immediately implemented, happened abruptly. The largest reduction in emissions occurred in mid-February 2020. At that

time, the reduction in NOx reached 50% and is explained in large part by the nearly complete shutdown of road traffic. The second largest reduction factor, as estimated by Doumbia et al. (2020), is the decrease of 30% for the emissions of non-methane volatile organic compounds (NMVOC). For carbon monoxide (CO), black carbon (BC) and sulfur dioxide (SO_2), the maximum adjustment factor is close to 0.9 (10% reduction). In the case of organic carbon (OC), an increase of a few percent results from the enhanced domestic activity (stay-at-home policy), particularly related to more extensive cooking and heating during the pandemic period. In the other regions of the world, the COVID-related perturbations in the emissions are most pronounced in mid-March to mid-April at a time where China's emissions were already in a recovery phase. In the European Union and North America, the estimated change in the emissions was largest in April. In South America and India, a sharp decrease appeared in the second half of March followed by a slow recovery from April to June. In Africa, only a small reduction occurred for NOx and VOCs with a maximum reduction in mid-April and a slow recovery afterwards. In all countries, except the Americas, a slight increase in organic carbon is derived during the pandemic.

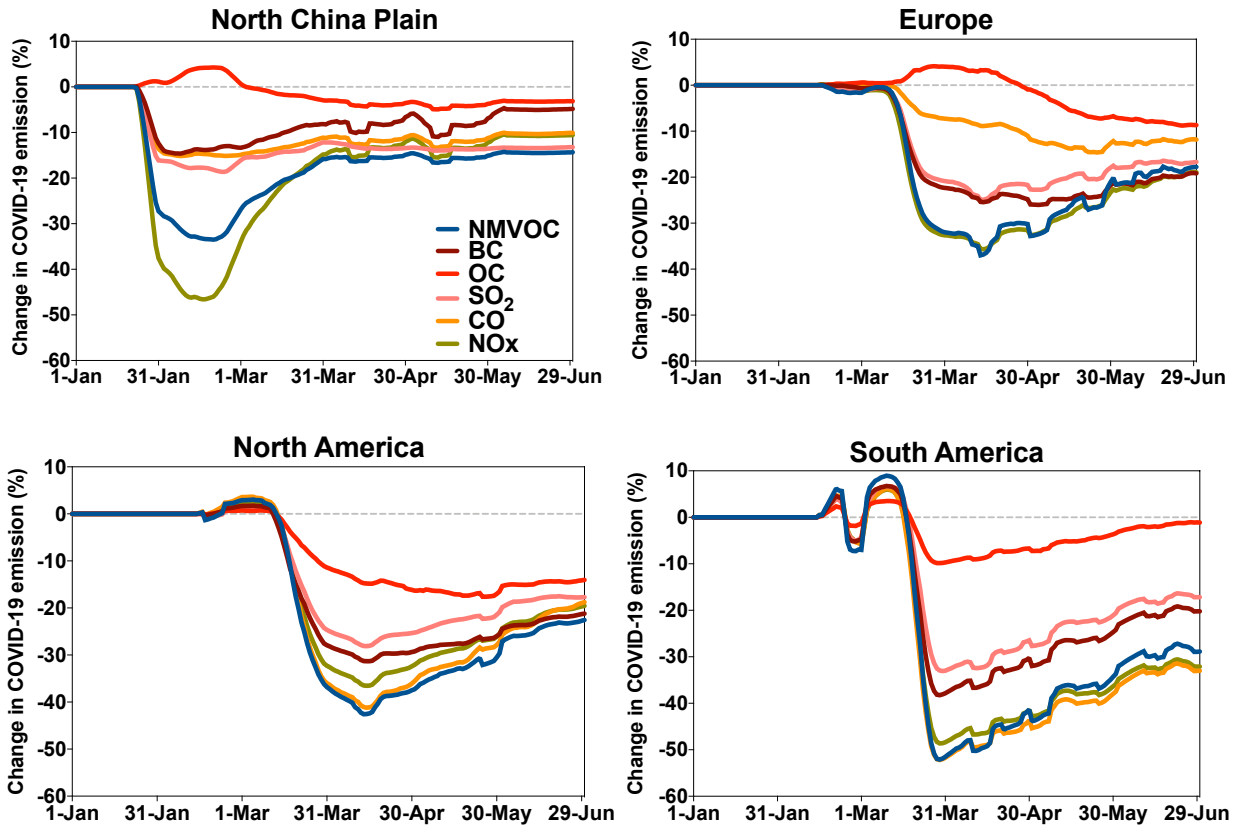

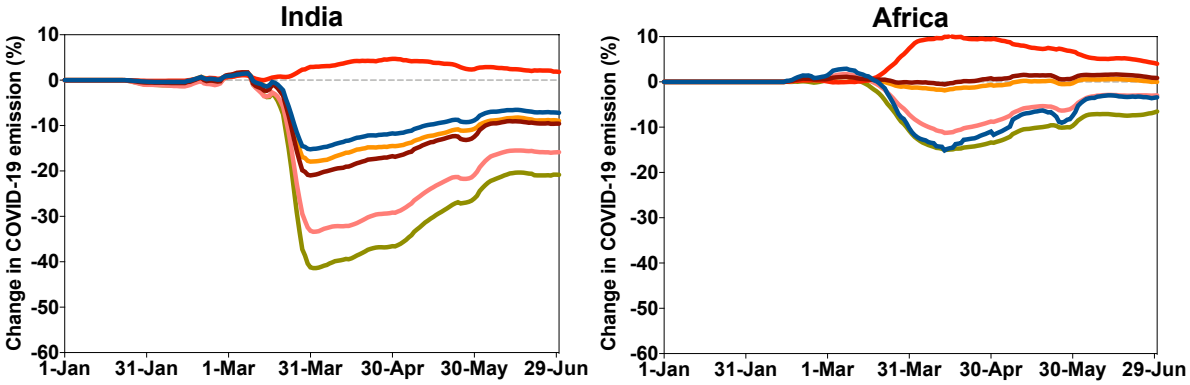

Figure 1. Evolution from 1 January to 30 June 2020 of the daily geographically averaged adjustment factors (percent) for the emissions for nitrogen oxides (NOx), carbon monoxide (CO), sulfur dioxide (SO_2), organic carbon (OC), black carbon (BC) and non-methane volatile organic carbon (NMVOC) in the North China Plain, Europe, North America, South America, India and Africa. A weak filter has been applied to smooth out he high frequency variability in the curves. Based on Doumbia et al. (2020).

Figure 2 shows a global view of the monthly mean percentage reduction in the emissions of NOx CO and SO_2 for January to May 2020. In February, the reduction in the emissions is contained in China. In March and April with lockdown measures imposed in other parts of the world, substantial reductions are seen in the NOx and VOC emissions of Europe, the Middle East, India and North America. In the southern hemisphere, emissions are substantially reduced on both coasts of South America and South Africa. The decrease over the global ocean accounts for the reduced shipping activity in response to the slowdown of the economy.

We should acknowledge here that large uncertainties might reside the aforementioned adjustment factors as discussed in Doumbia et al. (2020). As an example, Guevara et al. (2020) estimated for the period 23 March to 26 April 2020 in Europe an average emission reduction of 33% for NOx, 8% for VOCs and 15% for CO. The average reductions by Doumbia et al. (2020) for the similar period are 33 %, for NOx, 30% for VOCs and 15% for CO. The difference in the VOC emission adjustment factors might be due to a different treatment of the reduction in solvent emissions during the pandemic, as solvents contribute a large share of the anthropogenic VOC emissions in Europe. In the model simulations presented in the following sections, we address this particular uncertainty by considering a case in which the high VOC emission reduction of Doumbia et al. (2020) is adopted (upper limit) and a case in which no reduction in VOC and CO emissions is applied (lower limit).

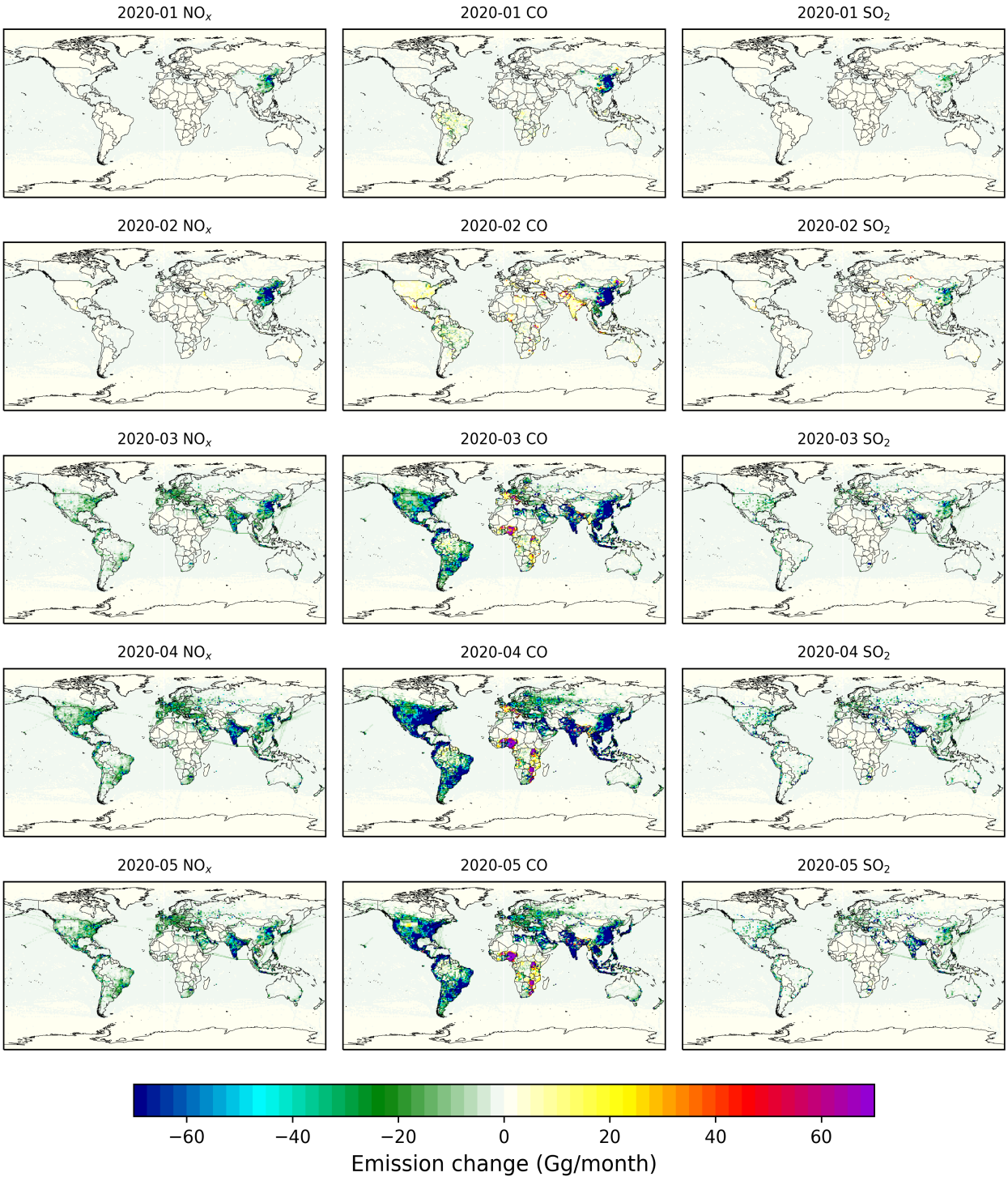

255

256

257 **Figure 2**. Change in the monthly mean emissions of NOx (left) CO (middle) and SO_2 (right) from January
258 2020 (upper panels) to May 2020 (lower panels).

259

260 **3. Global model simulations**

261 **3.1 Community Earth System Model version 2.2 (CESM2.2)**

262 The chemical fields presented in our study are provided by the Community Earth System Model
263 (CESM) version 2.2 that accounts for interactive physical, chemical and dynamical processes
264 (Danabasoglu et al., 2020). The atmospheric component of CESM, the Community Atmosphere
265 Model (CAM-Chem), provides a comprehensive description of atmospheric chemistry and aerosol
266 processes (Gettelman et al., 2019; Tilmes et al., 2019; Emmons et al., 2020; Gaubert et al., 2020)
267 with a spatial resolution of 1.25° in longitude by 0.95° in latitude (about 100 x 100 km^2 at mid-
268 latitude) and with 32 vertical layers from the surface to the pressure height of 3.6 hPa (about 40
269 km altitude). The MOZART Troposphere Stratosphere (TS1) chemistry mechanism includes 221
270 gas phase and aerosol species and 528 chemical and photochemical reactions, and provides
271 therefore a rather comprehensive explicit and interactive representation of tropospheric and
272 stratospheric chemical processes (Emmons et al., 2020). Aerosols are represented by the four-
273 mode Modal Aerosol Model (MAM4, Liu et al., 2016; Mills et al., 2016). The updated Secondary
274 Organic Aerosol parameterization includes the Volatility Basis Set (VBS) approach discussed by
275 Tilmes et al. (2019).

276 In order to accurately represent the meteorological conditions, the wind velocity components and
277 the temperature are nudged towards the Global Modeling and Assimilation Office (GMAO) GEOS
278 Forward Processing (GEOS-FP) meteorological analysis. The GEOS-FP assimilation is performed
279 on the cubed-sphere grid at C720 resolution or 12 km. The data from the three-hourly
280 meteorological horizontal wind and temperature analysis are regridded to the CAM-chem
281 horizontal and vertical resolution. They are nudged with weight calculated at every CAM-Chem
282 physical step (30 min) and with a Newtonian relaxation of about 5 hours. The ocean and sea-ice
283 interfaces are prescribed from a daily analysis of sea surface temperatures (SST, Reynolds et al.,
284 2007).
285
286 The model includes an active coupling between the atmosphere and the Community Land Model
287 version 5 (CLM5; Lawrence et al., 2019), where the deposition of gases and aerosols is calculated.
288 Biogenic emissions are calculated online in CLM5 with the Model of Emissions of Gases and
289 Aerosols from Nature (MEGAN v2.1; Guenther et al., 2012). Daily biomass burning emissions
290 are based on the biomass burning CO_2 emission inventory available from the Quick-Fire Emissions

Dataset (QFED; Darmenov and Da Silva, 2014). The chemical speciation is derived using the Fire INventory from NCAR (FINN) emissions ratios.

The anthropogenic emissions are specified according to the CAMS-GLOB-ANT_v4.2-R1.1 global inventory described by Granier et al. (2019) and Elguindi et al. (2020). This inventory provides monthly-averaged emissions of the main chemical compounds and 25 speciated volatile organic compounds for the 2000-2020 period at a spatial resolution of 0.1x0.1 degree. It is based on the EDGARv4.3.2 inventory developed by the European Joint Research Center (Crippa et al., 2018) and the CEDS emissions (Hoesly et al., 2018), which provide historical emissions for the 6th IPCC Assessment Report (AR6). EDGARv4.3.2 emissions are available until 2012: the emissions are linearly extrapolated to 2020 according to the trends derived from the CEDS emissions for the years 2011-2014. For China, the emissions from MEIC1.3 (Zheng et al. 2018) are used to account for the recent decrease in the emissions of most pollutants in this region. Daily averaged emissions obtained from an interpolation of the monthly averaged emissions are used for the baseline simulations and are adjusted for COVID-related runs by applying the daily adjustment factors discussed in Section 2 (Doumbia et al., 2020).

To evaluate the relative influence of different forcing processes responsible for the variations in the surface concentrations of reactive species, we perform different model simulations that are summarized in Table 1. In cases 1 and 2, referred to as "control" and "climato" cases respectively, the COVID-related reductions are ignored, but, in cases 3 to 5, the long-term trend in surface emissions associated with the evolving economy and air pollution mitigation measures are taken into account. The meteorology varies from year to year with the model being nudged to assimilated observations for the period 2016-2020. In case 2, the same 2020 emissions are used for each year, with, however, the meteorology evolving as in case 1. Case 3 is a repeat of case 1 for the year 2020, but with an adjustment in the emissions for the COVID-19 pandemic period. Cases 4 and 5 are similar, but with adjustments for only NOx and for only VOCs and CO, respectively. Global distributions of simulated chemical species obtained with the controlled case are displayed in Figure S1 of the Supplementary Information.

Table 1. Description of the different model simulations used in the present study

Case	Name	Reduction in	Meteorology	Notes

Emissions				
1	Control (2016 to 2020)	None	GEOS-FP evolving from 2016 to 2020	Long-term emission trends taken into account
2	Climato (2016-2020)	None	GEOS-FP evolving from 2016 to 2020	Simulation from 2016 to 2020 with annually repeated 2020 emissions
3	COVID-All (2020)	All emitted species	GEOS-FP for 2020	Combined emission reduction
4	COVID-NOx (2020)	NOx only	GEOS-FP for 2020	Impact of NOx reduction
5	COVID-VOC (2020)	VOCs and CO only	GEOS-FP for 2020	Impact of VOC and CO reduction

3.2 Model evaluation

We first provide some insight about the performance of the CESM model regarding its ability to reproduce the observed concentration of reactive species at the surface. Since a detailed evaluation of the model is beyond the scope of this paper and has been performed in earlier studies (Emmons et al., 2020), we only compare the calculated time series of ozone and other key atmospheric species (NO_2, CO, SO_2, $PM_{2.5}$) with measurements made at selected locations in different parts of the world. We first show in Figure 3 the global distribution of the monthly mean difference between 2019 and 2020 in the monthly mean NO_2 column derived from TROPOMI measurements in February and compare it with the change in the column as calculated by the model. The comparison between the two figures should be viewed as qualitative since the TROPOMI data are representative of early afternoon measurements while the model results refer to 24-hour average values. Further, both 2019 and 2020 simulations with the meteorology specific for each year have been performed with the same background emissions. In the 2020 case, however, the COVID-adjusted emissions are accounted for. What needs to be stressed here is that, in addition to the NO_2 decrease seen in China during the month of February in response to the economic slowdown, a significant reduction in the NO_2 column is found in northern Europe, in the North Atlantic and in the northern part of the US. Since no lockdown was imposed at that time in Europe and in North America, these changes should be viewed as a fingerprint of meteorological variability. Barré et al. (2020) and Goldberg et al. (2020) stress that meteorological variability complicates the analysis of observed data, and that such natural variations have a large effect when comparing, for example, observations between two consecutive years. The reduction observed in NOx observed in northern Europe during February has generated an increase in ozone (see Figure 8). Interestingly, both the

model and the space observations also show a small NO_2 increase in the southern and eastern part of the US and in the western part of Russia.

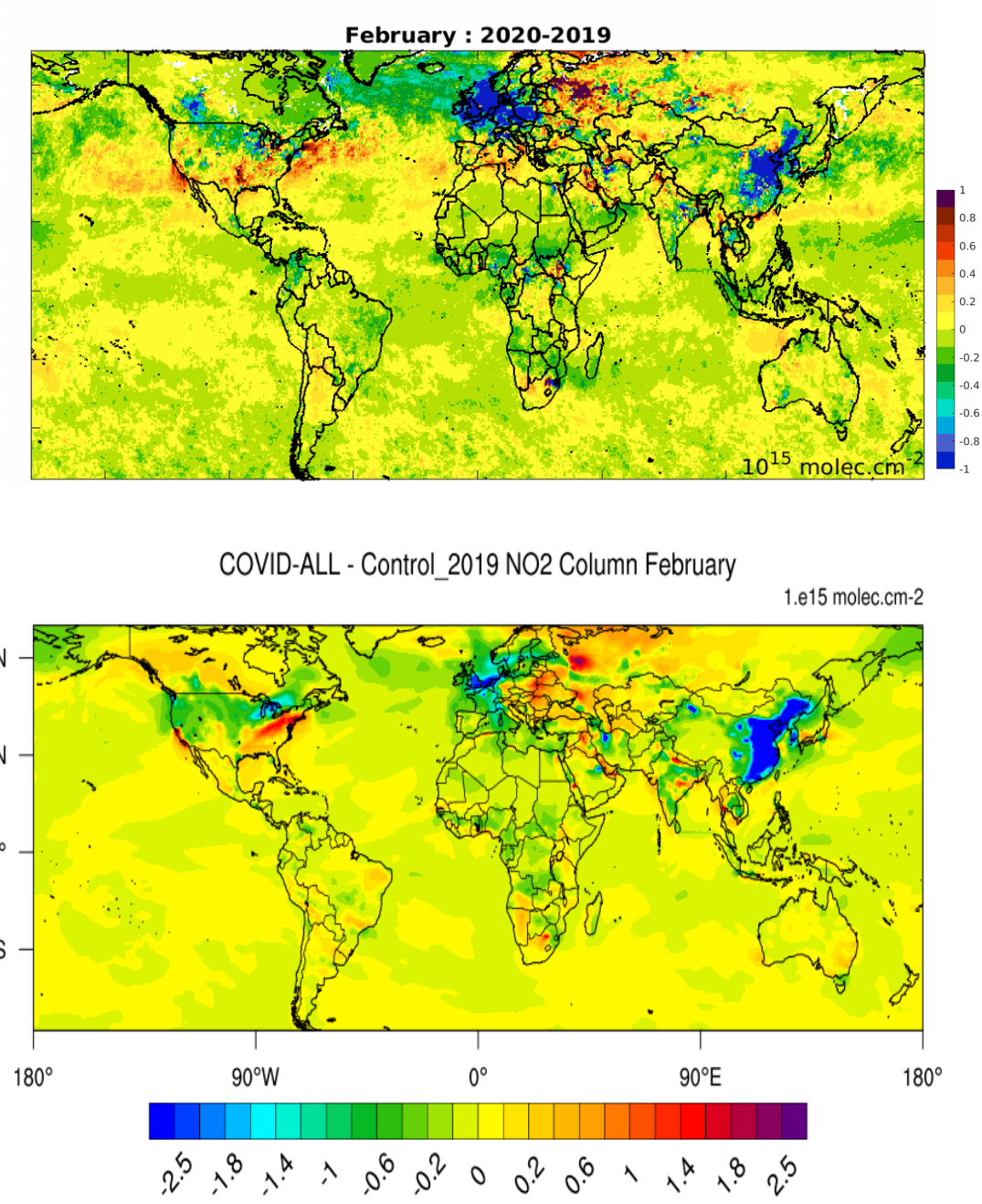

Figure 3. Difference between February 2020 and February 2019 in the global distribution of the monthly mean NO_2 column abundance (10^{15} cm^{-2}) Upper Panel: Observed values derived from TROPOMI satellite instrument. Lower Panel: Model values based on 2019 and 2020 simulations accounting for the reduction in surface emission and meteorological variability.

We now provide comparisons of calculated and observed time series for surface concentrations of

different chemical species in selected regions where measurements are available. We show in Figure 4a-g the evolution of the species concentration between 1 January and 31 May 2020 for two model cases: (1) a baseline case with no correction for COVID-19 effects (case 1 or control case; green curves in the figures) and (2) a perturbed case with emissions adjusted as described above to account for the COVID-19 effect (case 2 or COVID-All case; red curves in the figures). The differences between these two cases are further addressed in Section 3.3. We also show as supplemental information (Figure S2) the evolution of the ozone mixing ratio averaged over areas of about 100 x 100 km^2 around 6 European cities. The observations represent an average of the measurements made at monitoring stations in these areas. The outputs of the simulations are first interpolated to the location of these stations and, as for the observational data, are averaged over the chosen area.

In most regions, the model reproduces relatively well the chemical composition of the lower layers of the atmosphere. The long-term average evolution of the concentrations calculated by the model are influenced mainly by emissions from primary species and by chemical processes that occur in the atmosphere, while day-to-day variability is directly dependent on atmospheric dynamics and other meteorological processes. Data from monitoring stations are influenced by local emissions and by small-scale dynamic processes that cannot be captured by a model with a relatively coarse spatial resolution. Further, monitoring stations are often located in areas prone to high air pollution. Polluted areas may therefore be oversampled relative to the spatial averages provided by the model. In Europe and in the Sao Paulo region, we address this issue by removing from our analysis the data from stations located in areas with a population density larger than 1500 inhabitants per km^2, which is the threshold adopted by the European Union to define "high-density areas".

We evaluate the model results by comparing the surface concentrations averaged over relatively large areas with the average of measurements made in these areas (Table 1). Model outputs are bi-linearly interpolated to each selected station. We then calculate the mean concentration and the standard-deviation of all selected stations to construct the daily time series. In Europe, we use four criteria to calculate the daily averages and select the stations of the European network (AQ e-Reporting database) according to the following criteria: (i) 70% of hourly data must be available to calculate the daily average, (ii) a maximum of 10% of missing values on daily averages, (iv) the urban stations are not taken into account (threshold of 1500 inhabitants per km^2), (iv) the altitude

of the station is lower than 300 m. These selection criteria are especially important over Southwestern Europe because of the large variability in the environment (urban, rural, mountain) compared to Northern Europe. For the São Paulo region (CETESB network), we use the three criteria (i, ii and iii). For the three domains of North America (Air Quality System Data Mart database of US Environmental Protection Agency), we use two criteria (i and ii). For the North China Plain (China Environmental Observation Network), only one criterion (i) is used because this area is a continuously urbanized and represents a flat area.

Table 2. Domain names, acronyms, coordinates of the south-western and north-eastern corners of the domain's frames, and the number of stations per species retained in the present study.

Domain Name	Domain Acronym	Coordinates	Species (Number of Stations)
North China Plain	NCP	(112°E; 34°N) to (119°E; 42°N)	NO_2 (220), CO (220), O_3 (220), SO_2 (220), $PM_{2.5}$ (220)
Northern Europe	N-Eu	(1°W; 47°N) to (11°E; 54°N)	NO_2 (151), CO (16), O_3 (156), SO_2 (35), Ox (115), $PM_{2.5}$ (53)
Southwestern Europe	SW-Eu	(9°W; 39°N) to (3°E; 45°N)	NO_2 (32), CO (9), O_3 (42), SO_2 (19), Ox (29), $PM_{2.5}$ (10)
Northeastern USA and Southern Canada	NE-US	(126°W; 36.5°N) to (94°W; 52°N)	NO_2 (122), CO (81), O_3 (233), $PM_{2.5}$ (257)
Southern USA	S-US	(94°W; 24°N) to (66°W; 36.5°N)	NO_2 (43), CO (27), O_3 (113), $PM_{2.5}$ (86)
Western USA	W-US	(94°W; 24°N) to (66°W; 52°N)	NO_2 (243), CO (120), O_3 (417), $PM_{2.5}$ (291)
Sao-Paulo	Sao-P	(47.5°W;24°S) to (45.5°W;22°S)	NO_2 (6), CO (1), O_3 (47), SO_2 (3), Ox (4), $PM_{2.5}$ (3)

The model results obtained for the North China Plain (32^0 – 40^0 N, 112.5^0 – 120^0 E) show that the model satisfactorily reproduces the concentrations of NO_2, ozone and Ox (= O_3 + NO_2) as well as their temporal variability (Figure 4a). The model also underestimates the CO concentration by a factor of 1.5-2 during and after April 2020. In the case of SO_2, the agreement of the model with the observation is satisfactory, except during the months of January and February when the modeled concentrations and their temporal variability are considerably higher than in the observations. During this period, the model also underestimates the concentrations and temporal variability of atmospheric particles ($PM_{2.5}$) and CO. The repeated high peaks in $PM_{2.5}$, which are observed, but whose amplitude is underestimated by the model, show acute haze episodes as those reported for example in Beijing (Li et al., 2020). The high correlation of the model overestimation for SO_2 with the observed $PM_{2.5}$ concentration suggests that the aerosols might be a significant

414 SO_2 sink in winter in this region, as recently proposed by Cheng et al. (2016) to explain the inability
415 of the models to reproduce the observed sulfate production during haze events.
416
417 In northern Europe (Figure 4b), the calculated concentrations of NO_2, ozone and Ox are generally
418 in good agreement with observations. However, the calculated concentrations of CO are about
419 40% lower than the observations. This discrepancy, also noted in Northern China in April and
420 May, repeats itself in most regions of the northern hemisphere and remains an open scientific
421 question since it appears in most models unless their emissions have been artificially increased
422 (Stein et al., 2014) or observationally constrained using data assimilation (Gaubert et al., 2016,
423 2020). The calculated SO_2 variability is larger than observed and the concentration values
424 generally higher than observed.
425
426 In southwestern Europe (Figure 4c), the concentrations of CO, NO_2, SO_2 and $PM_{2.5}$ are
427 underestimated by the model, while the concentrations of ozone and Ox are overestimated. The
428 concentration ratio O_3/NO_2 is too high, perhaps due to an overestimation of the NO_2 photolysis
429 rate during this period that was unusually cloudy.
430
431 In the USA (Figures 4d-f), the concentrations of NO_2 are in fair agreement with measurements in
432 the northeastern (NE) US and southern Canada; there are, however, lower than observations in the
433 southern and western regions of the US. Ozone is in fair agreement with measurements in the NE
434 US, but overestimated in the southern and western parts of the country. CO is underestimated in
435 all regions. $PM_{2.5}$ are underestimated in the NE and western US and in good agreement in the
436 southern region.
437
438 In Sao Paulo, Brazil (Figure 4g), the temporal evolutions of ozone, Ox and $PM_{2.5}$ are correctly
439 simulated despite a large underestimation of NO_2 (factor 3-4). SO_2 is underestimated by a similar
440 factor. It should be noted, however, that, in this very heterogeneous megapolis, the NO_2 and SO_2
441 measurements vary greatly from one location to another and that these differences cannot be taken
442 into account by a model whose mesh size is of the same order of dimension of the city. CO
443 concentrations are in fair agreement with observed values.

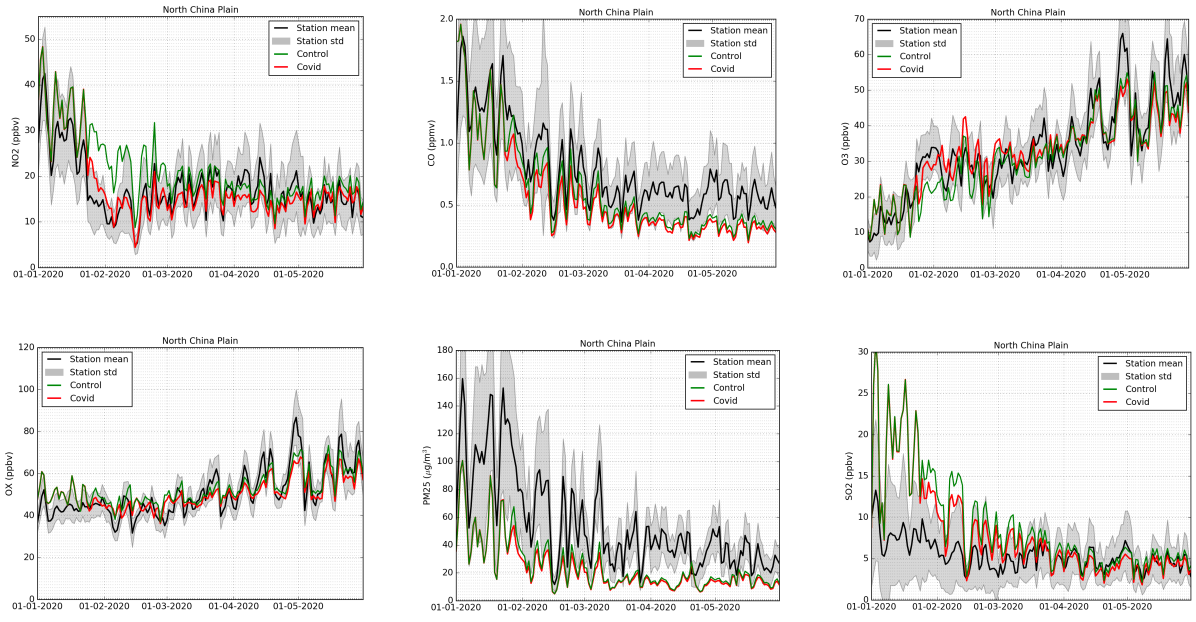

Figure 4a. Evolution for the period 1 January – 31 May 2020 of the surface concentration of NO_2, CO, O_3, Ox, SO_2 and $PM_{2.5}$ in the North China Plain. Black curve: measurements from monitoring stations. Green curve: model control case. Red curve: model case with emissions modified to account for the effect of the COVID-19 pandemic.

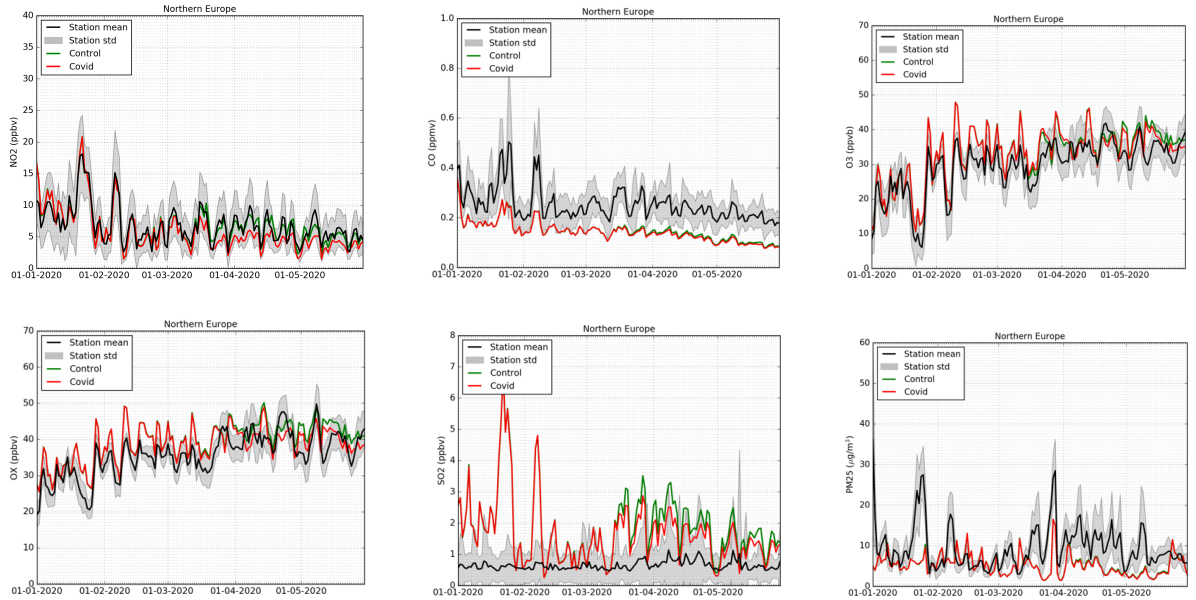

Figure 4b. Evolution for the period 1 January – 31 May 2020 of the surface concentration of NO_2, CO, O_3, Ox, SO_2 and $PM_{2.5}$ in northern Europe. Black curve: measurements from monitoring stations. Green curve: model control case. Red curve: model case with emissions modified to account for the effect of the COVID-19 pandemic.

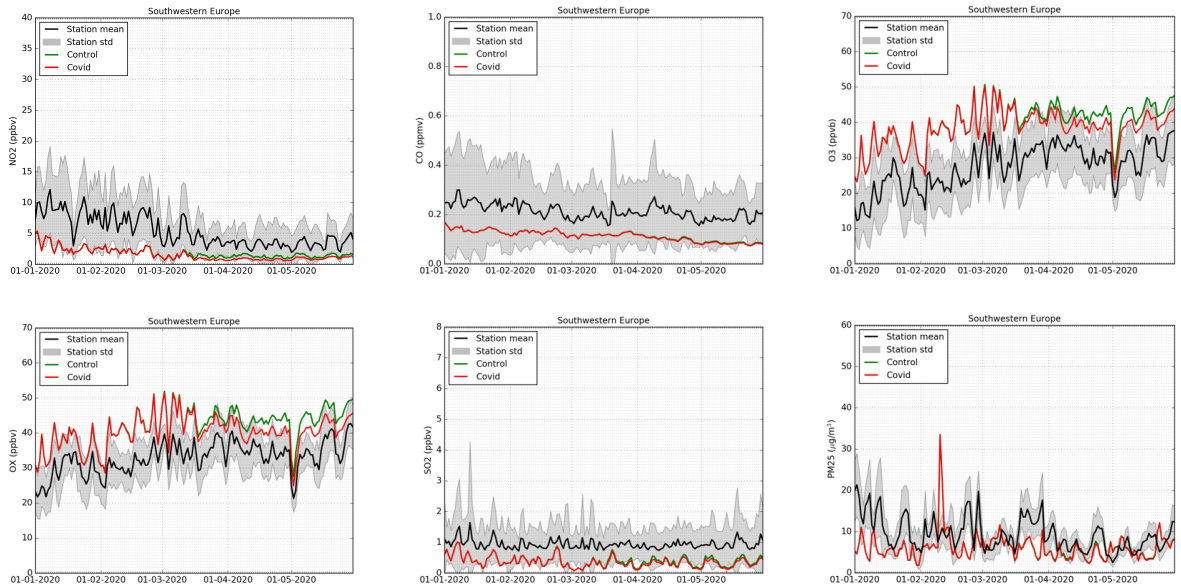

Figure 4c. Evolution for the period 1 January – 31 May 2020 of the surface concentration of NO_2, CO, O_3, Ox, SO_2 and $PM_{2.5}$ in southwestern Europe. Black curve: measurements from monitoring stations. Green curve: model control case. Red curve: model case with emissions modified to account for the effect of the COVID-19 pandemic.

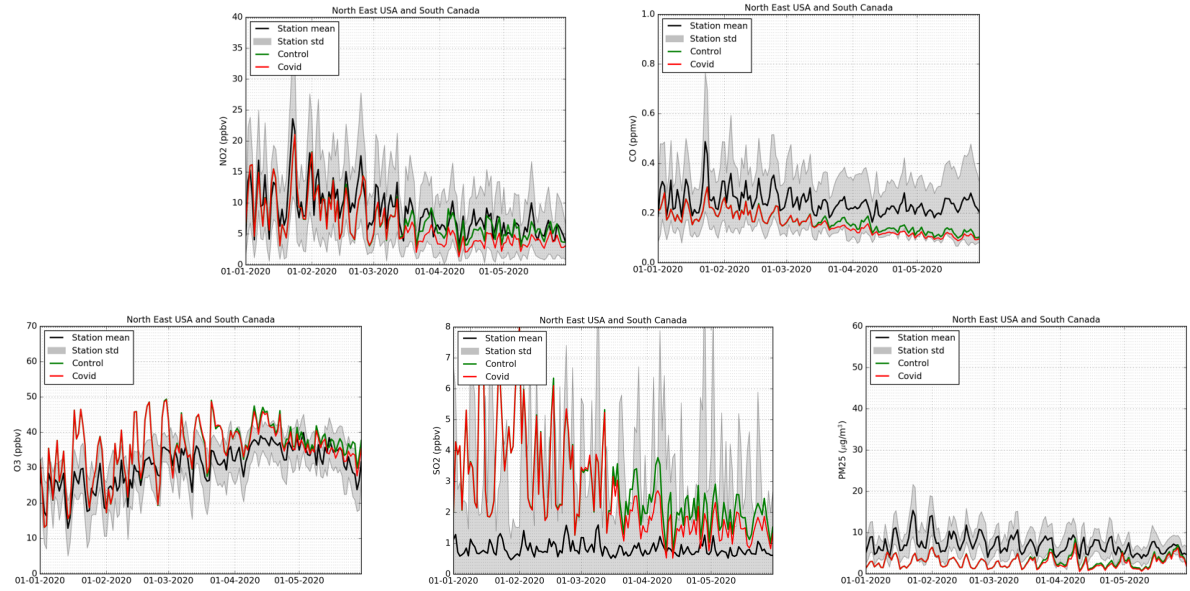

Figure 4d. Evolution for the period 1 January – 31 May 2020 of the surface concentration of NO_2, CO, O_3, SO_2 and $PM_{2.5}$ in Northeastern USA and South Canada. Black curve: measurements from monitoring stations. Green curve: model control case. Red curve: model case with emissions modified to account for the effect of the COVID-19 pandemic.

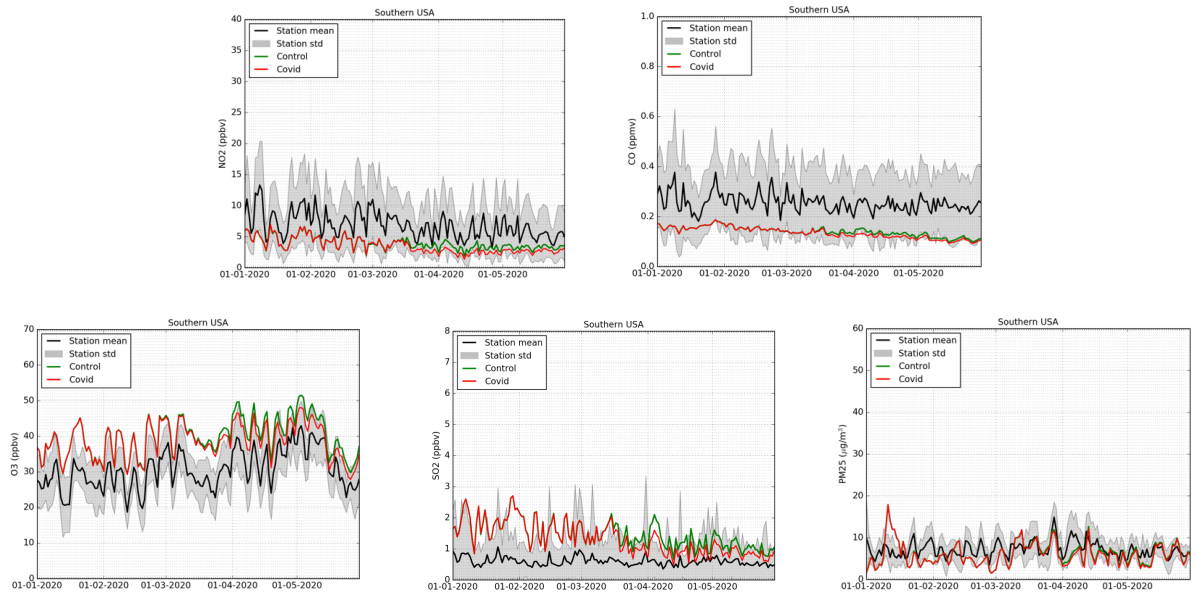

Figure 4e. Evolution for the period 1 January – 31 May 2020 of the surface concentration of NO_2, CO, O_3, SO_2 and $PM_{2.5}$ in Southern USA. Black curve: measurements from monitoring stations. Green curve: model control case. Red curve: model case with emissions modified to account for the effect of the COVID-19 pandemic.

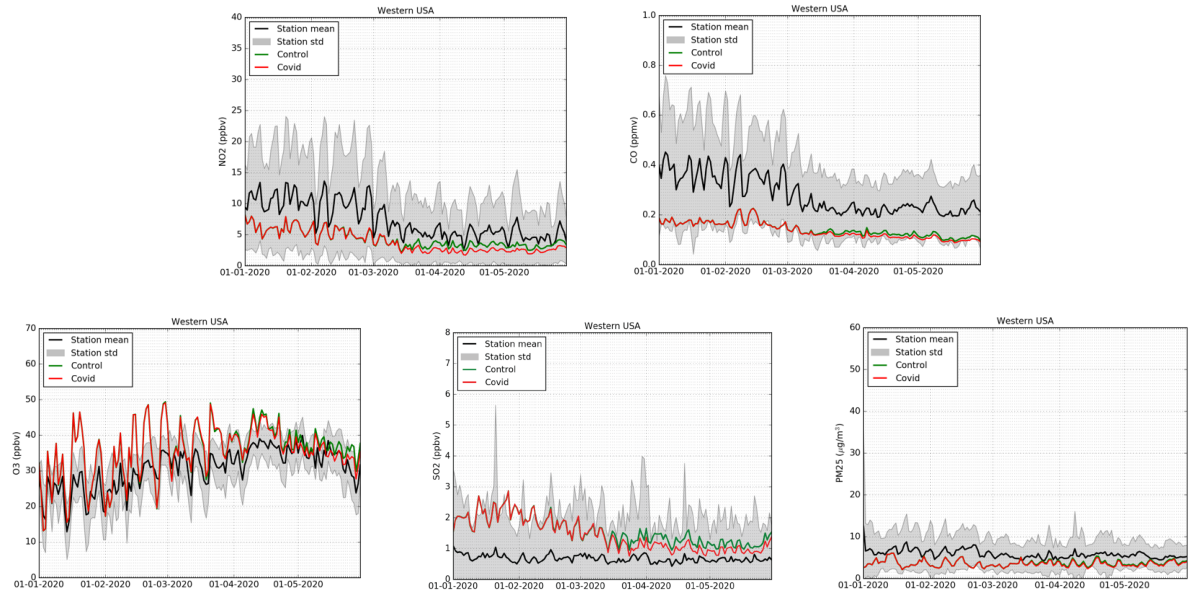

Figure 4f. Evolution for the period 1 January – 31 May 2020 of the surface concentration of NO_2, CO, O_3, SO_2 and $PM_{2.5}$ in Western USA. Black curve: measurements from monitoring stations. Green curve: model control case. Red curve: model case with emissions modified to account for the effect of the COVID-19 pandemic.

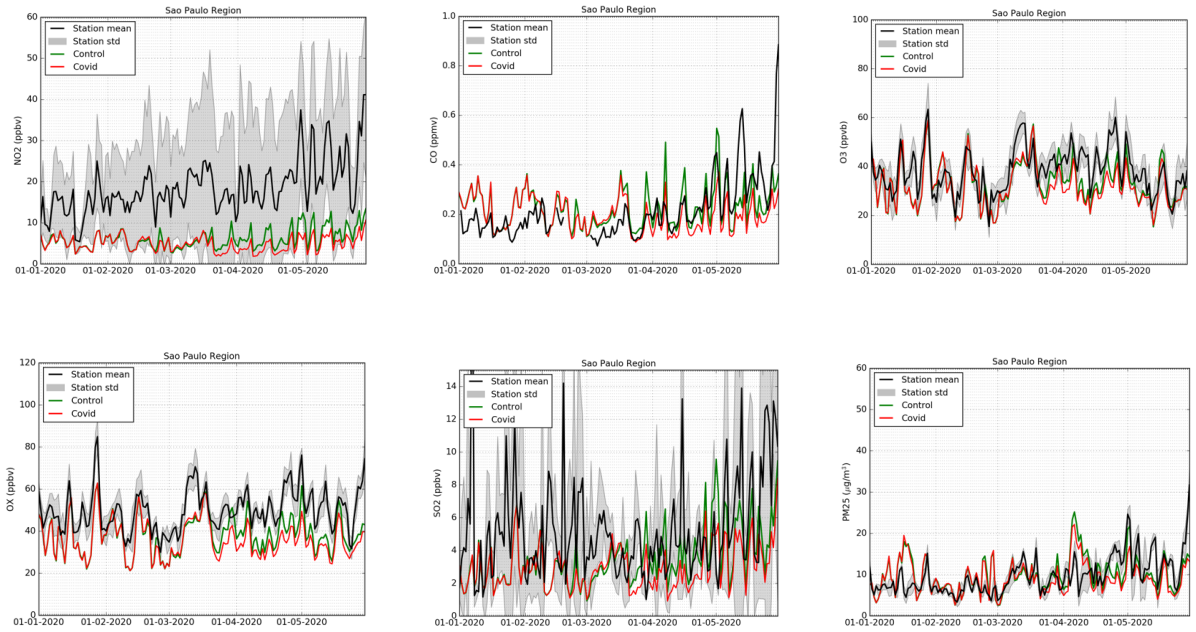

Figure 4g. Evolution for the period 1 January – 31 May 2020 of the surface concentration of NO_2, CO, O_3, Ox, SO_2, and $PM_{2.5}$ in the region of Sao Paulo. Black curve: measurements from monitoring stations. Green curve: model control case. Red curve: model case with emissions modified to account for the effect of the COVID-19 pandemic.

Finally, an examination of the ozone concentration in several densely populated areas of Europe (Figure S2), shows a good agreement between the model and the ground measurements, particularly near Berlin, Hamburg and Paris. In the area around London, Milan and Madrid, however, the model slightly overestimates the concentration of this gas in January, but the difference is reduced in the following months.

4. Changes in surface air quality during the COVID-19 pandemic

We now examine the global response of the chemical composition to the changes in the surface emissions during the pandemic. For this purpose, we compare the model results obtained with and without the modified emissions (COVID-all minus Baseline) as described above. In order to isolate the impact of the changes in emissions, we constrain the model in both cases by the same meteorological input corresponding to the year 2020. We also show how the particular dynamical situation in 2020 has produced anomalies relative to a multi-year averaged meteorology. We present panels that provide the percentage change in the monthly mean surface concentration of key chemical species for two different months: February and April, which correspond to the peak

time of the lockdown episode in China and in the rest of the world, respectively. Model results for other months are provided as Supplementary Information (Figure S3). Note that the patterns presenting relative changes may be very different from patterns of absolute changes. In this section, we focus on global aspects. A more detailed analysis of the chemical processes that are responsible for the calculated changes in selected regions of the world is provided in Section 4.

4.1 Response to changes in surface emissions of primary pollutants

When examining the changes in the surface abundance of nitrogen oxides resulting from the synergic emissions of NOx and VOCs (Figure 5), we note a reduction in the concentration during February that amounts to 30-50% in China, particularly in the Northern China Plain (i.e., north of the Yangtze River) and in the western province of Xinjiang. No significant reduction is yet detected in other parts of the world. Only a small decrease of a few percent is found over the oceans, particularly along the ship tracks and accounts for the assumed slowdown in international shipping activities. In April, the calculated NOx reduction in China is a factor of two smaller than two months earlier, but the impact of the pandemic has now reached most regions of the world. Reductions of typically 40% are derived by the model in India, Western Europe, Saudi Arabia, Canada, South Africa and in the southern hemisphere, Bolivia, Peru and Ecuador. In Eastern Europe, New Zealand, the east coast of Australia and most regions of the United States and Brazil, the surface concentration of NOx is reduced by 20-30%. Very small changes are calculated for Central Africa, the center and western coast of Australia, the Asian regions of Russia and Iran. The absence of reduction calculated for Iran is consistent with the observations derived by the TROPOMI instrument (Bauwens et al., 2020).

The response of ozone during the lockdown of February is characterized by a concentration increase of typically 20-40% in the northeastern part of China. A small spot with a similar increase is found in the province of Xinjiang. In April, the ozone increase in China is vanishing, but changes in the concentration of this gas have now spread in other regions of the world. The largest relative surface ozone reductions are found in the tropics (5 – 20%), specifically in northern Peru and Ecuador as well as along the Indian coasts, in Indonesia and in Malaysia. Some increases are noted in a few regions including northern Europe, eastern Canada (Québec) and northeastern United States (East Coast, Chicago). Such specific situations will be further discussed in Section 4.

The changes in the monthly mean surface concentration of the hydroxyl radical (OH), which

provides indications about the change in the oxidation potential of the atmosphere, is characterized during the month of February by an increase to typically 30-40% in northeastern and northwestern China. At the same time, the model highlights a decrease in the southern and southwestern regions of the country. During the month of March and April, an increase of OH concentration has become apparent in Northern Europe. The level of OH, however, decreases in the southern part of Europe. In the populated regions of Canada and the northeastern United States, OH concentration anomalies are positive. In the southern hemisphere, the OH concentration usually decreases, except in urban areas such as Santiago, Buenos Aires, Sydney and Melbourne, where positive anomalies are derived. The level of OH is also reduced during the pandemic, along the ship tracks.

Formaldehyde, which is directly emitted from combustion and industry, is also produced as an intermediate species in the photooxidation of primary hydrocarbons, a process that is influenced by the presence of nitrogen oxides. For this oxygenated VOC, we note a reduction in the surface concentration of 10-30% in China during February 2020. In April, reductions of the same order of magnitude are found in Canada, southern Europe, South Africa as well as along the Pacific and Atlantic coasts of South America.

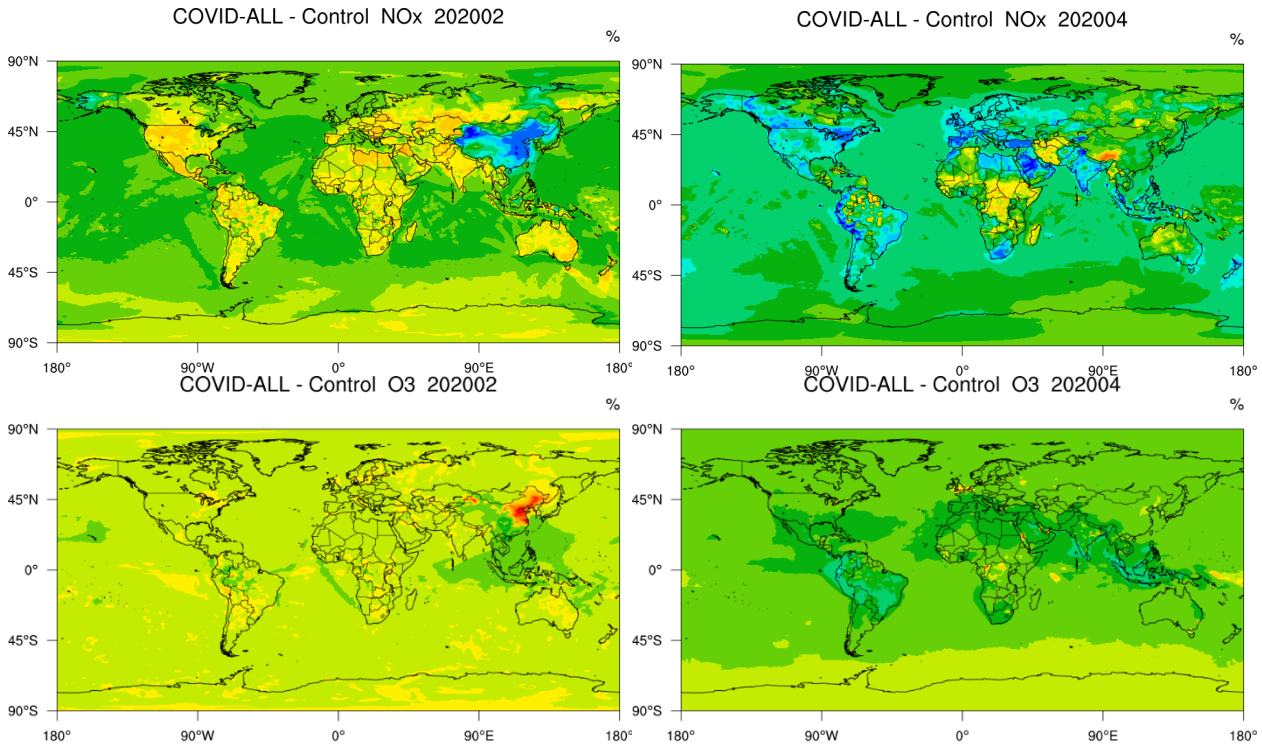

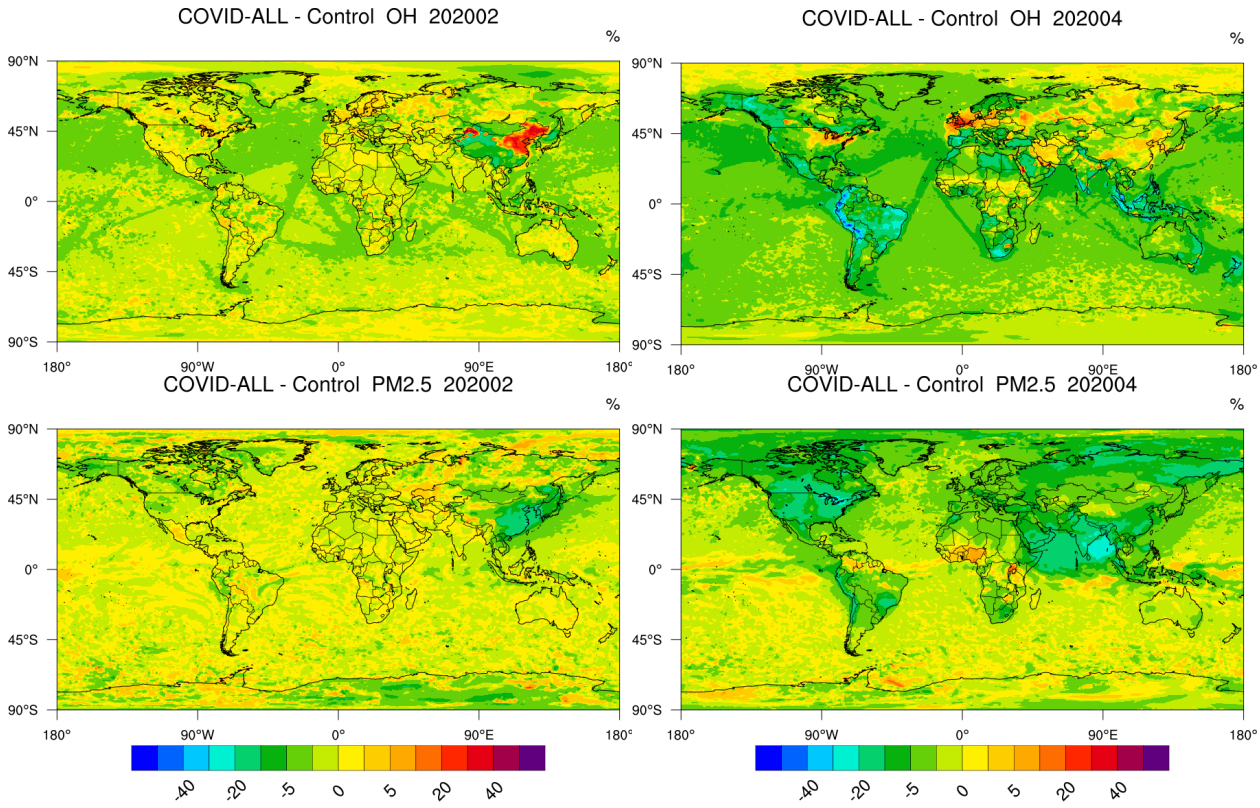

Figure 5. Relative change (percent) in February and April 2020 in the global monthly mean concentration of (from top to bottom) of NOx, ozone, OH and $PM_{2.5}$ resulting from the change to the adopted surface emissions of primary pollutants during the COVID-19 pandemic period.

When considering the changes in particulate matter as calculated by the model, we note (Figure 5) that the concentration of $PM_{2.5}$ first decreased by nearly 20% in China during the month of February. Later in April, it was reduced by 10 – 20% in India, the US and Canada and by about 10% in Europe. A fraction of this reduction is attributed to the decrease of the direct emission of particulate matter during the pandemic. However, the change in the emission of gas-phase precursors and in their photo-oxidation processes under reduced NOx concentrations must also be considered. We address this issue by examining the changes affecting the quantity of SOA as derived by the model, based on the oxidation scheme described by Tilmes et al. (2020). Figure 6 shows that, according to the model (COVID-All case), the SOA concentration was substantially reduced, during February 2020 in China (up to 40 %) and later during April in other parts of the world including the eastern US and a large area of South America. A fingerprint of the reduced SOA concentration extends in a plume over the northern Pacific Ocean. Interestingly, if only the NOx emissions had been reduced (case 4 or COVID-NOx), the concentration of SOA would have increased in northern part of China (February and April) as well as in the region surrounding the

English Channel (April) where the oxidation capacity increased after the pandemic outbreak. A smaller increase in SOA is seen in India, eastern Brazil and the eastern US. If only the VOC and CO emissions had been reduced (case 5 or COVID-VOC), the SOA concentration would have decreased everywhere. The patterns of the SOA in response to the combined decrease in NOx and VOCs/CO emissions is similar to the patterns derived for the COVID-VOC case, but with smaller concentration reductions in high NOx regions such as northern China during wintertime.

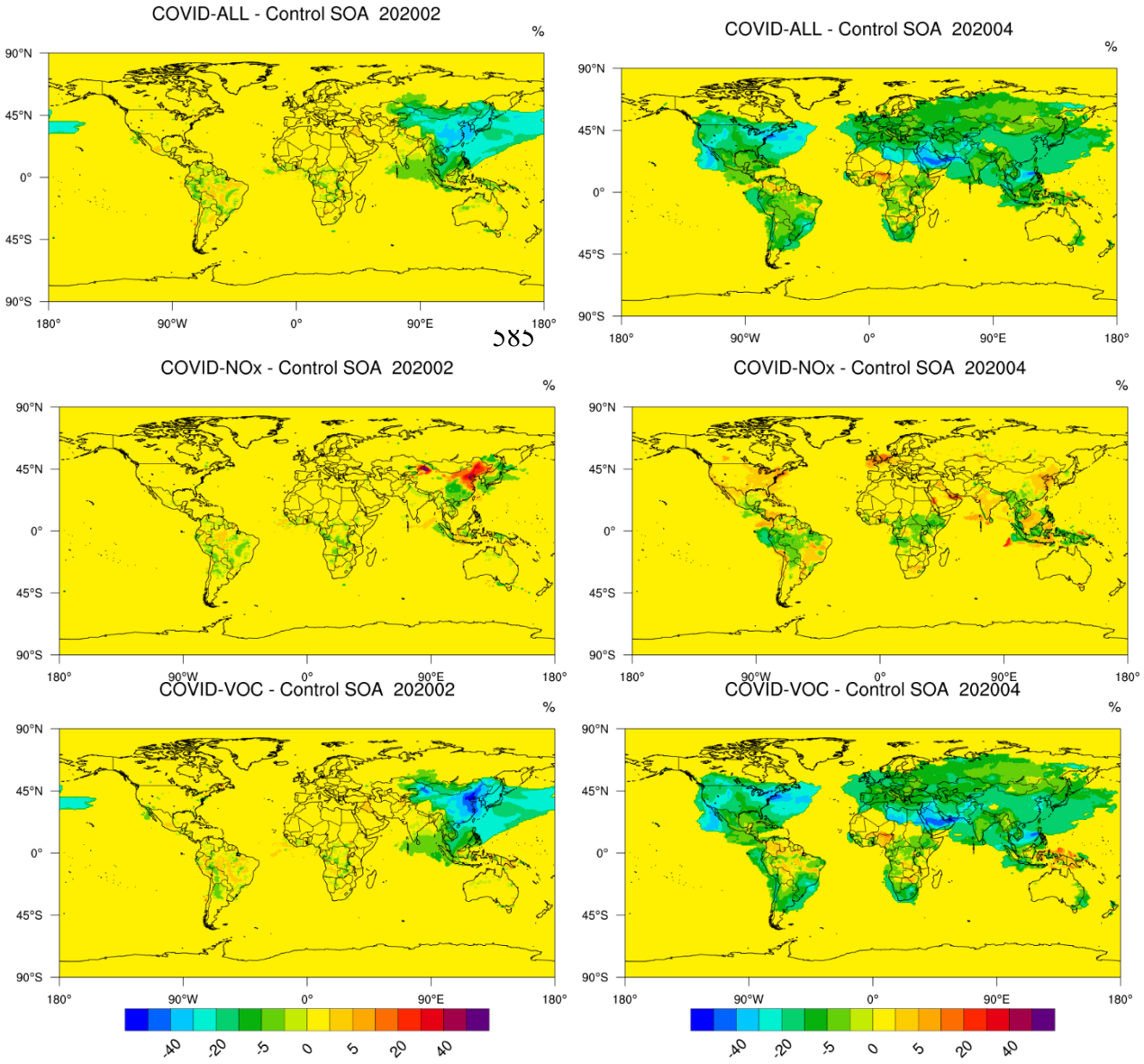

Figure 6. Relative change in the concentration of secondary organic aerosols (SOA) resulting from reduced emissions of primary pollutants during the COVID-19 pandemic for February (left panels) and April 2020 (right panels). Upper panels: all emissions reduced; middle panels: reduction of NOx emissions only; lower panels: reduction in VOC and CO emissions only.

592

593 **4.2 Effect of meteorological anomalies**

594 The analysis of observed changes in the chemical composition during the pandemic must carefully
595 assess the influence of meteorological variability and, when examining monthly mean values, of
596 weather anomalies for the month under consideration. The early months of 2020 were strongly
597 affected by weather events, for example by the passage of two storms (Ciara and Dennis) in
598 northern Europe during the month of February and the influence of two other storms (Karine and
599 Myriam) in southern Europe (Petetin et al., 2020; Barré et al., 2020). We assess to what extent
600 meteorological variability during the pandemic has generated variations in the calculated chemical
601 fields. This information should help in the analysis of observations that are affected by both the
602 COVID-related changes in the emissions and by weather anomalies (combined atmospheric
603 dynamics, temperature, cloudiness, precipitation, atmospheric stability, etc.). For this purpose, we
604 derive the difference in the surface temperature and monthly mean ozone concentrations in 2020
605 (COVID-All case) relative to the average concentrations derived from a model simulation
606 conducted for five consecutive years (called here "pseudo-climatology" for the period 2016 to
607 2020). In this last case (referred to as the Climato-case or Case 2), the surface emissions are subject
608 to their usual seasonal variations, but their values are repeated from one year to the other. The
609 corresponding global fields of surface temperature and percentage ozone anomaly, calculated for
610 February and April 2020, are shown in Figure 7.

611 In February, besides variations occurring over the oceans, we note a small impact of the mesoscale
612 weather situation on the monthly mean ozone fields in China during the COVID pandemic
613 (February 2020). A positive ozone anomaly of 5 – 10%, however, is seen along a line that stretches
614 from northern India to Europe. This anomaly reaches about 10% in northern Europe including the
615 north of France, the Benelux countries, the UK and Germany. In Spain, the ozone anomaly is
616 negative. A negative anomaly of up to 20% is derived in northern China, Mongolia and Russia. In
617 the US, a positive anomaly of a few percent is seen in the vicinity of Chicago and along the Rocky
618 Mountains, while there is a small negative anomaly elsewhere. In South America, the largest ozone
619 anomaly is found along the Andes in Peru and Ecuador.

620 In April, the patterns of variations relative to our 5-year pseudo climatology are characterized as
621 follows: positive anomalies in southern China (5 – 10%) and in South Asia (20 – 30%), in northern

and eastern Europe (5 – 10%) as well along the Rockies in the US and Canada (10 – 20%) and along the Andes in Argentina, Bolivia, Peru, Ecuador and Colombia (20 – 30%); negative anomaly in Russia (10 – 20%), in Spain and the southwest of France (5 – 15%).

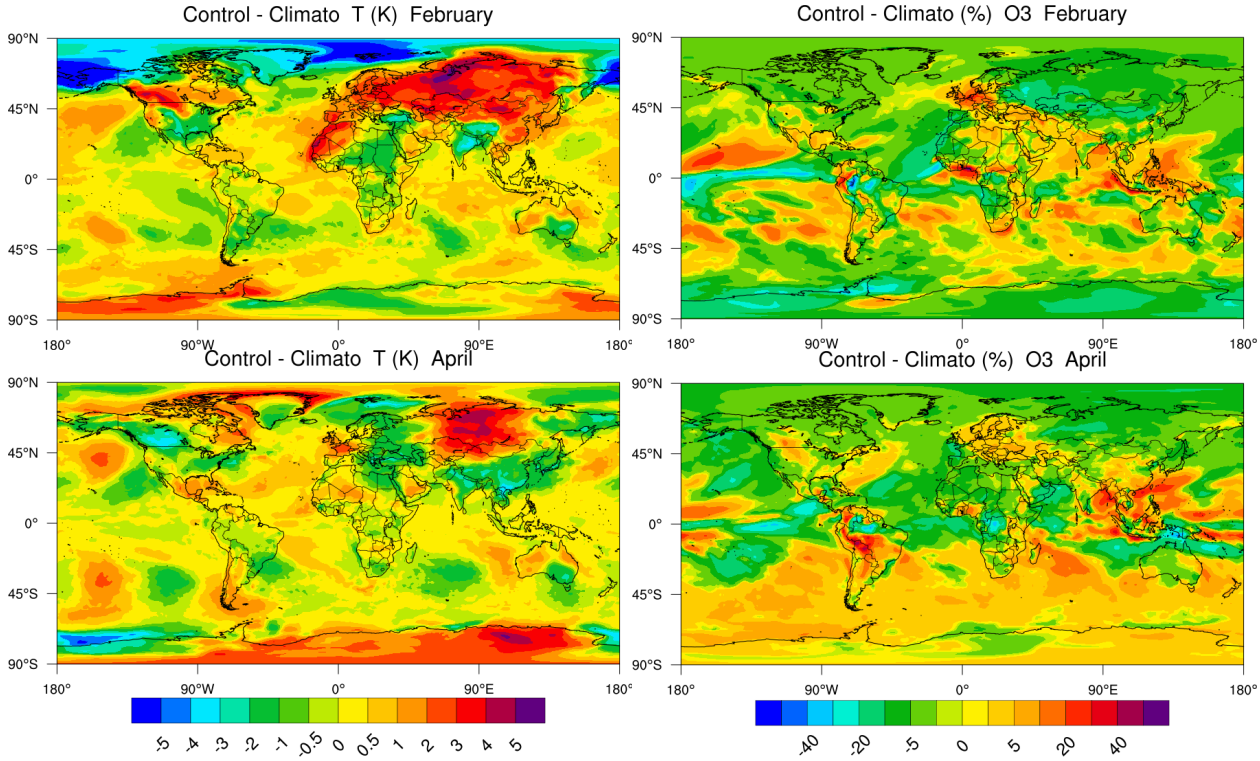

Figure 7. Anomalies in monthly mean surface temperature (K) and ozone concentration (percent) in 2020 relative to a 5-year monthly mean ("pseudo-climatology" for 2016 -2020) highlighting the perturbation effects of the meteorological situation during the year of the pandemic (2020).

4.3 Combined effects

Finally, we show in Figure 8 the response in February and April 2020 of the surface ozone concentration to the *combined* effects of the entire COVID-related emission adjustments and of the meteorological anomalies. This purpose is to reproduce as closely as possible the real changes in ozone relative to the monthly mean values averaged over 5 years (2016-2020) without accounting for long-term trends in emissions (COVID-All minus Climato cases). In February, the model produces positive anomalies for ozone in northern China, northwestern Europe, in the center of the US, in the region of the Great Lakes and in the Middle-East. In April, ozone is higher than the pseudo-climatological values in northern Europe, in southern China, along the Rockies near the US-Canadian border, along the Andes in South America and in the eastern Pacific.

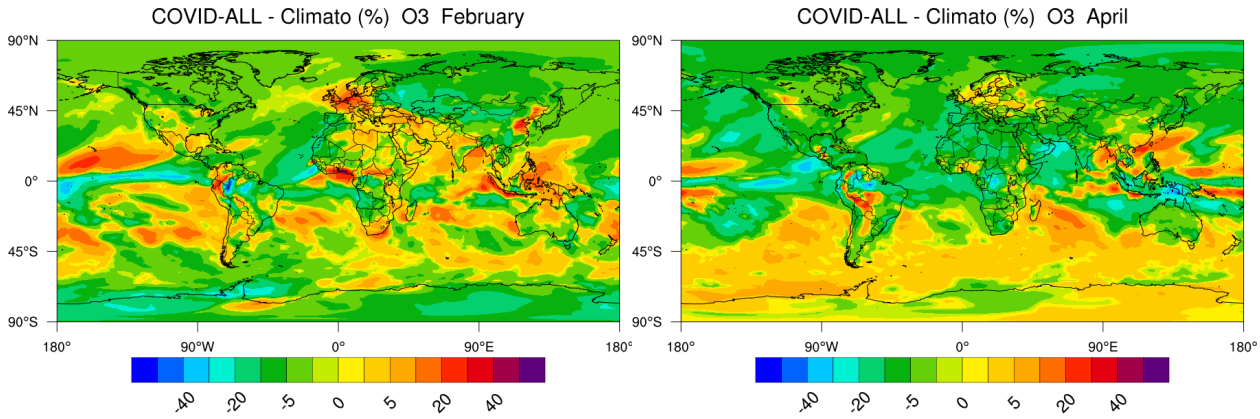

641

642 **Figure 8.** Relative change (percent) in February and April 2020 in the global monthly mean concentration
643 of ozone resulting from the combined changes in surface emissions of primary pollutants during the
644 COVID-19 pandemic period and the meteorological anomalies during the same period.

645 We summarize the results of our model simulations (Table 3) by providing values (orders of
646 magnitude) that characterize the ozone changes in different populated regions of the world during
647 the middle of the pandemic (monthly mean values for February in China and for April in the rest
648 of the world). We compare the relative importance of the contributions of chemistry (reduced
649 emissions) and meteorological anomalies in 2020; we also show the response to the two combined
650 forcing processes.

651 **Table 3**. Relative changes (orders of magnitude in percent) in the monthly mean values of the
652 surface concentrations of ozone as calculated for different regions (non-urban conditions).
653 Changes due to modified emissions during the pandemic, to specific meteorological anomalies of
654 2020 (relative to the average from a "pseudo-climatology of years 2016-2020) and to the combined
655 effects.

Region	Emission Adaptation	Meteorological Anomaly	Combined Effects
February 2020			
North China Plain	0 to +30	0 to +5	+20 to +30
Southern China	-10 to -5	-5 to +5	-20 to -5
April 2020			
India	-15 to -5	-5 to +5	-20 to -10
Northern Europe (UK, Benelux,	+2 to + 5	+2 to +5	0 to +5

Germany, northern France)			
Southwestern Europe (south of France, Spain)	-10 to -5	-20 to -5	-20 to -10
Northeastern US and southern Canada	+2 to +5	-5 to + 2	-2 to +20
Eastern Brazil	-25 to -10	-5 to +15	-20 to -10
Peru Ecuador	-35 to -25	+5 to +25	-20 to -10
South Africa	-10 to -5	-5 to +2	-15 to -5

5. Process analysis and discussion

To identify the chemical processes that explain the changes in the concentrations of secondary pollutants (e.g., ozone, SOA), we now examine, in more detail than in Section 3, the response of a set of chemical species, which contribute to the formation and destruction of these secondary pollutants. We focus on several regions of the world, which are differentiated by the intensity of incident solar radiation and by environmental conditions such as, for example, the level of nitrogen oxides in the boundary layer. We take advantage of the fact that the season that corresponds to the lockdowns was different in different regions of the world. To quantify the respective role of nitrogen oxides and carbon compounds, we consider in addition to the simulations (COVID-All) considered in Section 3 two additional cases: in one of them (COVID-NOx), only the reduction of nitrogen oxide emissions are taken into account, while in the second case (COVID-VOC), only VOC and CO emissions are reduced.

5.1. Air quality in China during the pandemic

Our first case focuses on the significant changes that took place in China during the 2020 lockdown (Zhang et al., 2020). To analyze the response of secondary species, it is first useful to determine the distribution of chemical regimes (VOC/NOx control of ozone) during the winter period (February). To estimate if a region is NOx-limited or NOx-saturated (VOC-limited), we represent in Figure 9 the ratio R of the production of H_2O_2 relative to the production of HNO_3. When R is

greater than 0.2 (red zone), the ozone production is controlled by the level of nitrogen oxides, while if it is less than 0.06 (blue zone), the region is NOx-saturated and the ozone formation is controlled by the atmospheric level of VOCs (Tonnesen et al., 2000; Zhang et al., 2009; Fu et al., 2020b). The white zone shown in the figure corresponds to an intermediate situation. We note that, in continental areas where population density and the economic activity are low or moderate and over the oceans, ozone is, as expected, NOx-limited. In the north of China, in India, Korea, Japan, Kyrgyzstan, Kazakhstan and certain highly urbanized zones (e. g., Hong Kong and Guangzhou, Taipei), ozone is NOx-saturated and therefore VOC-limited. This condition corresponds to a winter and early spring situation. In summer, however, when the concentration of NOx is lower, the area with VOC-limited conditions is reduced. In China during the lockdown period, the limit between the VOC and NOx controlled regions is located along a line extending from approximately Lanzhou in the center of China to Xiamen along the ocean in the vicinity or Taiwan. Inside the NOx-limited regions, urban centers are often VOC-limited areas.

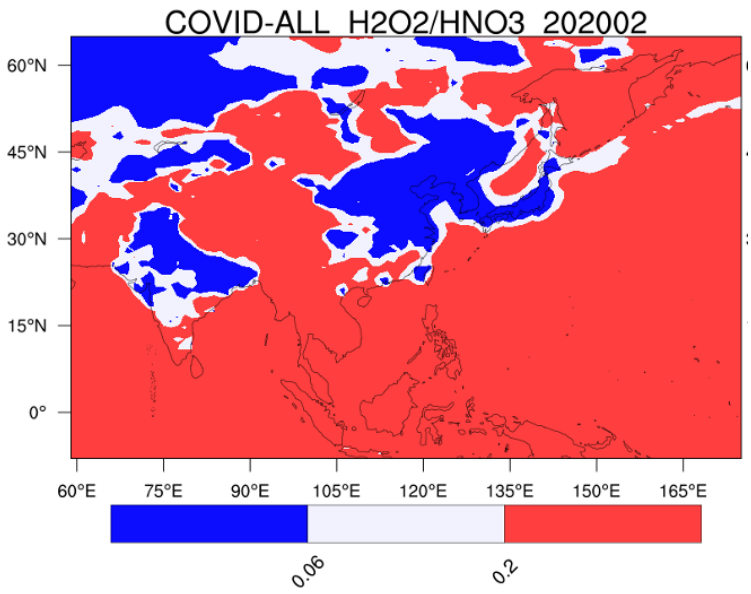

Figure 9. Ratio between the production rate of hydrogen peroxide and nitric acid, a measure of the chemical conditions governing the formation of ozone. Geographical areas in which ozone is NOx controlled (red) and NOx-saturated or VOC controlled (blue). The white area represents an intermediate situation.

Figure 10 shows that, during the lockdown of February, the surface concentration of NOx was severely reduced (40-50%) in most areas of eastern China and in the northwest of the country. At the same time, the concentration of ozone increased in the northeastern part of China and locally in several large urban areas of other regions as evidenced by surface observations (e.g., Shi and Brasseur, 2020; Huang et al., 2020; Liu and Wang, 2020). Further, a reduction in ozone occurred

699 in the southern part of the country. This result is consistent with the results of the regional modeling
700 study of Liu and Wang (2020) and with surface observations (e.g., Lian et al., 2020; Fu et al.,
701 2020b). To further address this question, we show how surface NOx and ozone would have
702 responded according to the model if only the emissions of VOC or of NOx had been reduced.

703 **5.1.1 COVID-VOC case: Reduction only in the VOC and CO emissions**

704 If *only* VOC and CO emissions are reduced, while the emissions of other species including NOx
705 remain unchanged in China during February 2020, the ozone and peroxyacetyl nitrate (PAN)
706 concentrations as calculated by the model decrease in the North China Plain by 20-30% and 30-
707 50%, respectively. A substantial reduction in the concentration levels of hydrogen radicals (HOx
708 = OH + HO_2) also occurrs, but the concentration of NOx slightly increases due to the reduced loss
709 rate via HNO_3 formation, the reduced formation of organic nitrates and peroxynitrates and the
710 reduced uptake of NOx by SOA. With the adjustment factors adopted for VOCs, the model derives
711 a reduction of around 30% for OH, 50% or higher for HO_2, 50% for CH_3O_2, 20-30%, for
712 formaldehyde, 20% for hydrogen peroxide and 20% for nitric acid in the North China Plain (see
713 also Figure S4). The concentration of OH, however, is slightly enhanced (5 to 10%) outside this
714 particular region. The concentration of the NO_3 radical, which is a major oxidant during nighttime,
715 slightly increases (typically 2-5 %) in most regions of China except in the North China plain, where
716 it decreases by as much as 30 %. The decrease in the level of HOx directly results from the
717 reduction in the sources of these radicals, including the reactions of alkenes with ozone, the
718 photolysis of formaldehyde and of other carbonyls and the photolysis of nitrous acid (HONO)
719 since the heterogeneous formation of this last compound on the surface of aerosol particles is
720 reduced as the aerosol concentration (including the concentration of SOA and sulfates) has
721 decreased. Under the assumptions adopted here, the HO_2 to OH ratio declines since the conversion
722 of OH to HO_2 by CO and VOCs is slowed down, while the conversion of HO_2 back to OH slightly
723 accelerates due to slightly enhanced NOx concentrations. We note that the relatively large
724 reduction in HO_2 and CH_3O_2 (more than 50%) together with a smaller increase in NOx (10-30%)
725 leads to a decrease in the photochemical production of ozone.

726 **5.1.2 COVID-NOx case: Reduction only in the NOx emissions**

727 If we make a simulation in which *only* the NOx emissions are reduced during the pandemic, the
728 response to the chemical system is very different (opposite sign) than in the previous case. Under

729 our assumption, the concentrations of OH and HO_2 increase by 50% or more, mostly in the
730 northeastern part of China. The concentrations of methyl peroxy (CH_3O_2) and formaldehyde
731 (HCHO) increase by 10-20%. The increase in HOx is attributed primarily to a reduced
732 recombination of OH with NO_2, which leads to the reduction in the HNO_3 concentration derived
733 by the model. Since the photolysis of HCHO is a significant source of HOx radicals, the increase
734 in the concentrations of OH and HO_2 radicals also results from the enhanced concentration of
735 formaldehyde (Li et al., 2020). The reduction in the NO concentration tends to shift the balance
736 between HO_2 to OH towards HO_2. The concentration levels of the NO_3 radical and of PAN are
737 enhanced in northern China and particularly in the region of Beijing (up to 50% for both species),
738 but are reduced in southern China. The response of ozone (increase in northern China and decrease
739 in southern China) results from synergetic changes in both the production and destruction rates of
740 the molecule. First, the simultaneous reduction in NOx, and enhancement in HO_2 and CH_3O_2
741 concentrations result, according to the model, in a *reduced* photochemical ozone production rate
742 of 20-30%. Second, the titration of ozone by NO_2, a major loss for ozone in the highly polluted
743 areas of northern China, is reduced, while the direct ozone loss due to the enhanced levels of OH
744 and HO_2 increased. Taking into consideration these two processes acting in different directions,
745 we find a resulting ozone loss that is *reduced*. This suggests that the most important factor
746 explaining the ozone increase in northern China is the reduction of the ozone titration by NO_2. In
747 southern China, where the background levels of nitrogen oxides are lower and solar radiation
748 intensity is higher, the reduction in NOx has led to an *enhanced* net ozone destruction and hence
749 a reduction in the surface concentration of this molecule except in cities where the ozone
750 concentration increases. As expected, the net ozone production rate calculated for February 2020
751 (Figure 8) is positive in northeastern China and negative in other regions.

752 **5.1.3 COVID-All case: Reduction in the NOx, VOC, CO and aerosol emissions**

753 The response of the surface composition, when all emission adjustments for the emissions are
754 taken into consideration, leads to an intermediate situation between the two cases described above.
755 In fact, the response of most chemical species to the NOx and VOC emission reduction generally
756 happens in opposite directions. When the two effects are combined, the reduction in NOx is of the
757 order of 40% in the North China Plain and in the northwest of the country. The increase in HO_2
758 and CH_3O_2 is of the order of 50% and that of OH around 30%. The mean concentration of the NO_3
759 radical increases by up to 50% in the urbanized regions of Beijing and Shanghai. The decrease in

HCHO concentration is limited to 10-20% (Figure S4). PAN and SOA concentrations decrease only by a few percent in the northern China, but decrease more substantially (20-30%) in the central and southern parts of the country. The exact quantitative response of PAN and SOA depends critically on the relative amplitude of the VOC and NOx emission reduction. It would have been positive in the North China Plain during February if the adopted VOC emission reduction had been somewhat smaller. In the case of SOA, a plume with decreased concentration values in noticeable over Korea, Japan and the Western Pacific Ocean. The change in ozone is positive in the northeastern part of China (about 30%) and negative in the southern part of the country (about 10%). As seen in the figures, the most pronounced changes in the concentration level of most chemical species are located in the North China Plain and further north. Additional model results are provided in Figure S4 of the Supplementary Information.

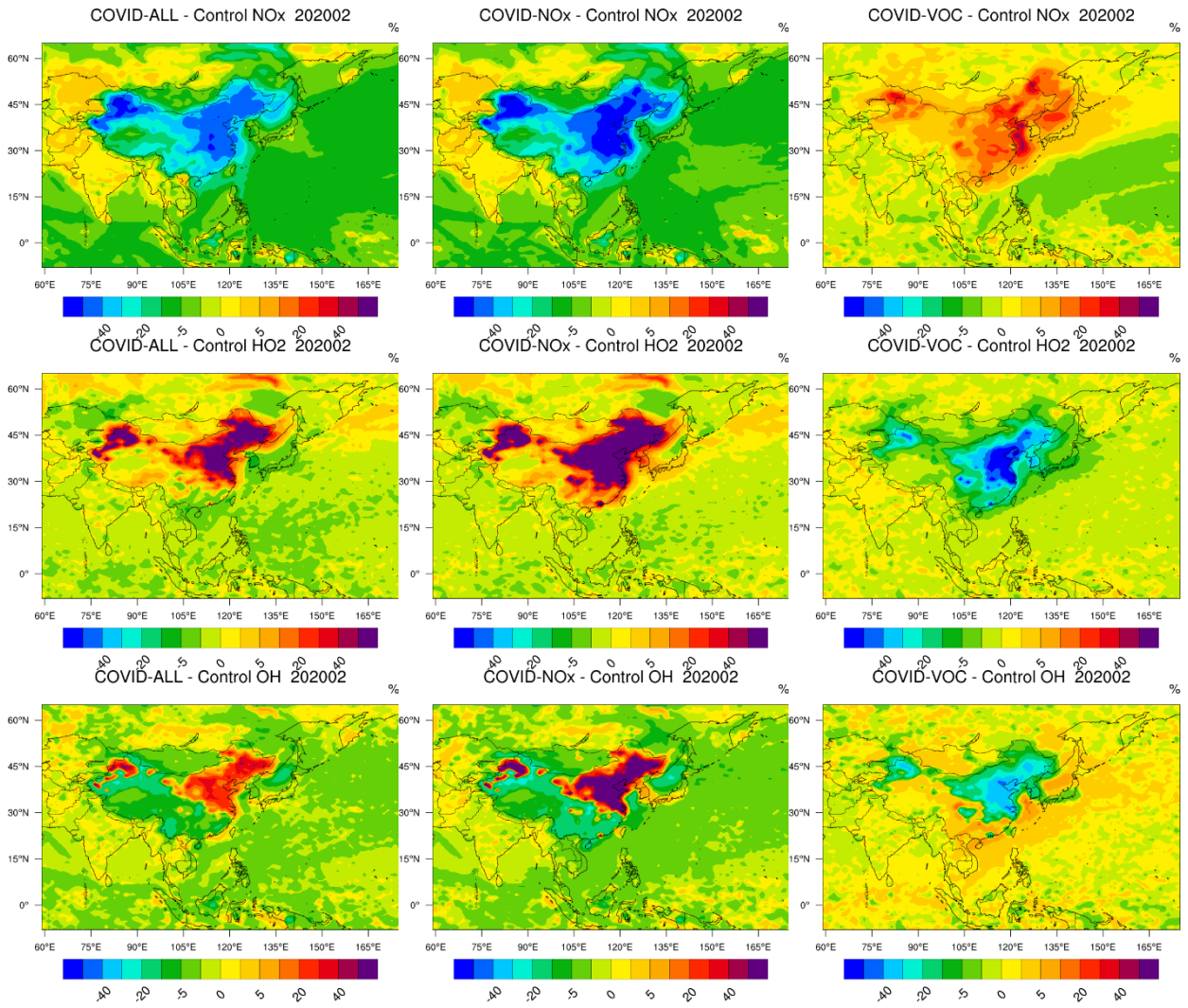

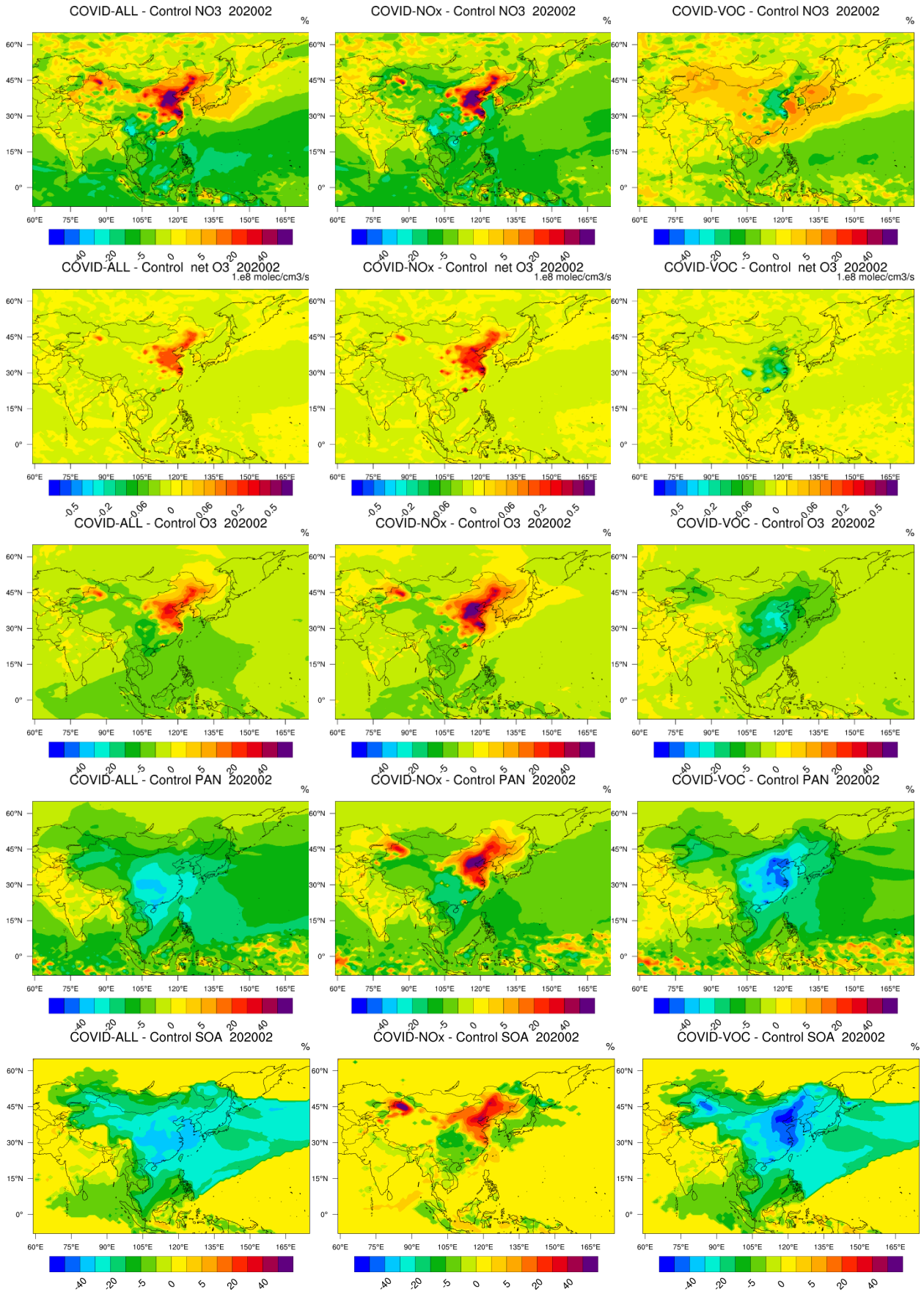
COVID-ALL - Control NO3 202002
COVID-NOx - Control NO3 202002
COVID-VOC - Control NO3 202002
%
COVID-ALL - Control net O3 202002
COVID-NOx - Control net O3 202002
COVID-VOC - Control net O3 202002
1.e8 molec/cm3/s
COVID-ALL - Control O3 202002
COVID-NOx - Control O3 202002
COVID-VOC - Control O3 202002
COVID-ALL - Control PAN 202002
COVID-NOx - Control PAN 202002
COVID-VOC - Control PAN 202002
COVID-ALL - Control SOA 202002
COVID-NOx - Control SOA 202002
COVID-VOC - Control SOA 202002
60°N
45°N
30°N
15°N
0°
60°E
75°E
90°E
105°E
120°E
135°E
150°E
165°E
-40
-20
-5
0
5
20
40
-0.5
-0.2
-0.06
0
0.06
0.2
0.5

780 **Figure 10.** Percentage change in several chemical variables in China in response to reduced emissions of
781 primary pollutants in February 2020 during the COVID-19 pandemic. Panels from the top to the bottom:
782 NOx, HO_2, OH and NO_3; net ozone production (cm^{-3} s^{-1}), ozone. PAN and SOA. Left column: reduction in
783 all emission; center panel: reduction in NOx emissions only; right panel: reduction in VOC and CO
784 emissions only.

785

786 In order to provide some insight on the relative forcing effects of the emission reduction during
787 the pandemic and of the meteorological variability, we provide in Figure 11 an estimate of the
788 ozone anomaly generated by weather dynamics and by the combined effects of the two forcing
789 factors. Wang and Zhang (2020) provide a detailed assessment of the effects of meteorological
790 elements during the pandemic period. Our model simulations as nudged towards the GEOS-FP
791 meteorology show that during February 2020 and relative to our 5-year "pseudo-climatology",
792 Eastern China was abnormally warm by 1.5 to 2.5 K and subject to high cloud fraction; northern
793 China was 2-4 K warmer with cloud fraction lower relative to the previous 5 year average. During
794 this month, ozone anomalies associated with meteorological variability were dominant in the
795 tropical regions south of China, but were relatively weak on the Chinese mainland. Abnormally
796 low ozone was found along the border between China and Mongolia related to the abnormally high
797 NO_2 concentration calculated during February 2020. The increase in the monthly mean ozone
798 concentration in the North China Plain (up to 5%) predicted by the model in response to
799 meteorological anomalies adds to the ozone perturbation caused by the reduction in emissions.
800 Our simulations suggest that chemical disturbances rather than meteorological anomalies explain
801 the ozone concentration increase in the North China Plain during February 2020. Shorter time
802 fluctuations linked to specific weather conditions should be considered in a finer analysis to
803 explain, for example, the acute air pollution episodes reported in several urban areas during
804 January and February 2020 (Wang et al., 2020). In southern China, where the perturbed chemistry
805 tended to reduce ozone, a small positive anomaly is visible along the South China Sea. The change
806 resulting from the two simultaneous effects is however negative except in the urban zone of
807 Guangzhou/Hong Kong/Macao. In short, the enhancement in the level of oxidants in the North
808 China Plain appears to be primarily a direct consequence of the reduction on chemical emissions
809 triggered by the pandemic, but could have been facilitated by unfavorable weather conditions.

810

811

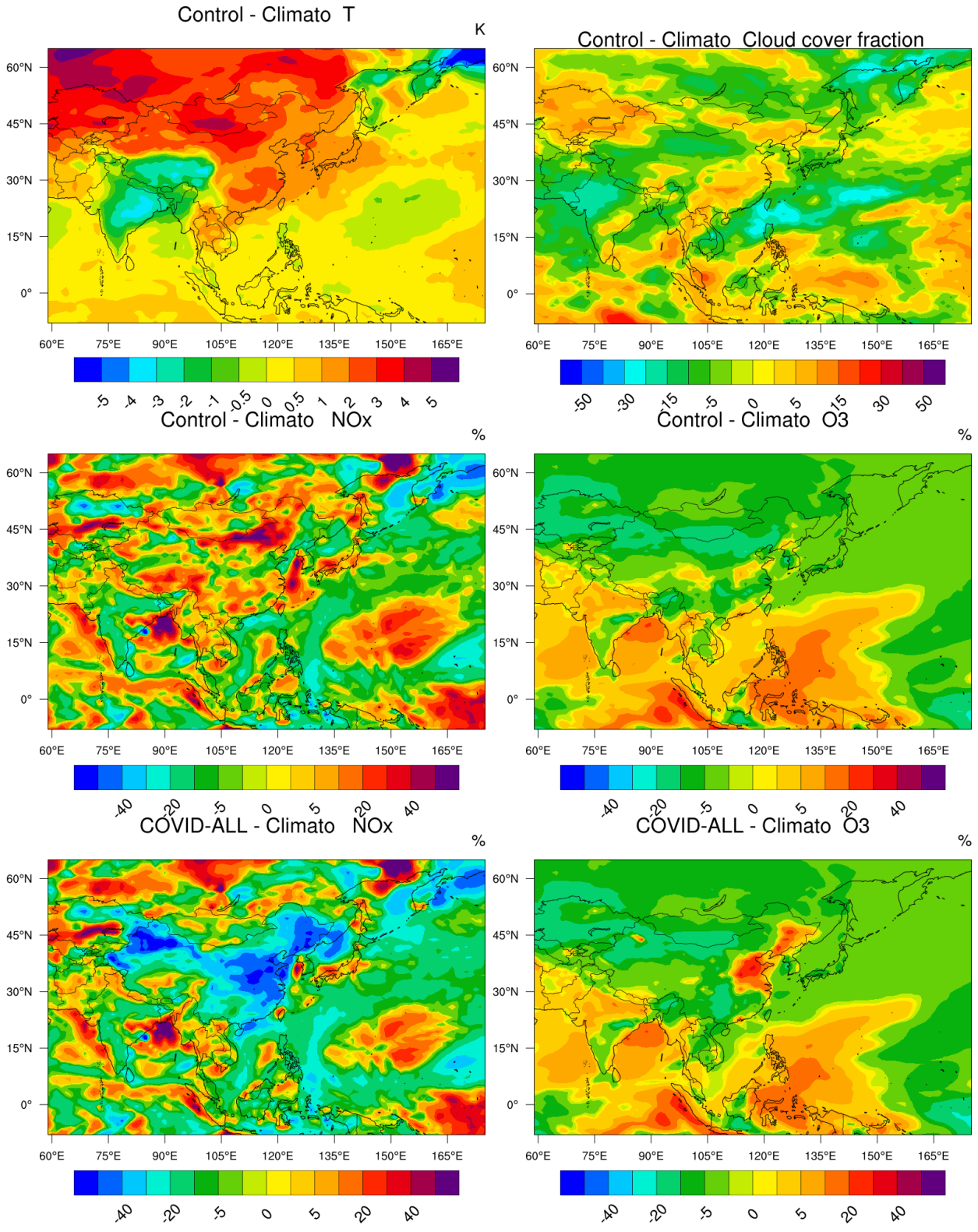

812

813

814

815 **Figure 11.** Percentage change in the monthly mean ozone surface concentration in Asia for February 2020
816 relative to the value averaged over 5 years (2016 to 2020) for the same period of the year. Left Panel:
817 Response taking into account the adjustment of the emissions associated with the pandemic and the
818 meteorological anomaly. Right panel: ozone response only to the meteorological anomaly.

5.2. Air quality in Europe during the pandemic

The situation in Europe during the pandemic is somewhat similar to what was derived in China including a small increase of the ozone concentration in highly polluted areas. We first show in Figure 12 that, during the period of the lockdowns (15 March to 15 April), the ozone production in most regions of Europe was controlled by NOx except in the most densely populated areas where the influence of VOC was significant.

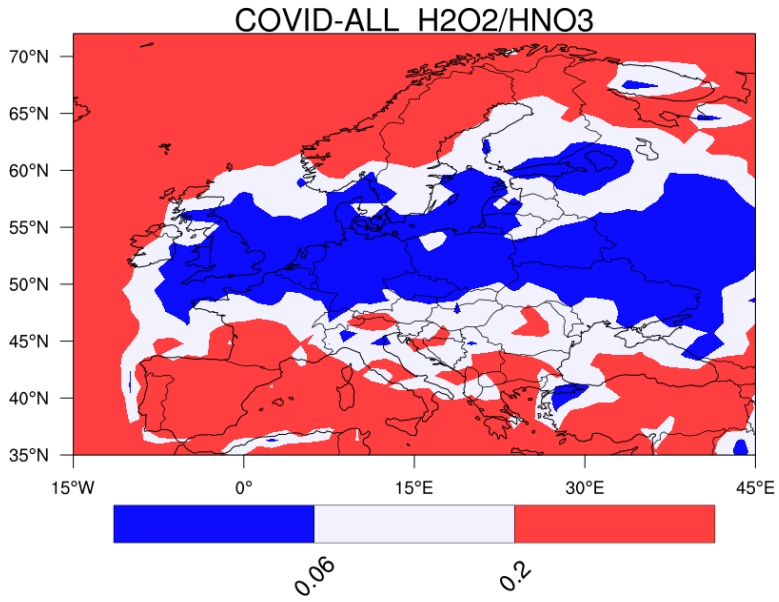

Figure 12. Ratio between the production rate of hydrogen peroxide and nitric acid, a measure of the chemical conditions governing the formation of ozone. The geographical area in which ozone is NOx controlled is shaded in red and VOC controlled in shaded in blue. The white area represents an intermediate situation between fully NOx and VOC controlled situations.

In Figure 13, we show that, in March-April 2020, the relative reduction in NOx concentrations associated with the reduced emissions covers the entire European continent, but with the most pronounced effects occurring in the western and southern part of the continent (30-50% in areas of Spain, France and Switzerland; 20-30% in Germany Eastern Europe and Scandinavia). This reduction is accompanied by an increase in the level of photo-oxidants (OH, ozone) that is most pronounced in the UK, Belgium, the Netherlands, northern France and in the western part of Germany. The ozone increase in this area is typically 5 to 10%, while the OH increase reaches 30%. In southern Europe, ozone concentrations are reduced by 5 to 10%. The net ozone production

slightly increases over most of the continent with a notable exception in Spain. The largest values are found again in the region extending from the UK to western Germany with hot spots in several urban or industrial areas. These patterns of ozone change are consistent with the regional model simulations performed by Menut et al. (2020) for western Europe. They derive on 28 March 2020 ozone anomalies (relative to a "business as usual" reference case) that are positive in the geographical area extending from in northern France and the UK to Germany and Poland. Negative anomalies are found in southern France and Spain. Ozone concentrations are also abnormally high in the Po valley (northern Italy) and in several large European cities, including in southern Europe (Madrid, Barcelona, Rome, Naples Marseille, Toulouse).

The same type of behavior is found in our global model when only NOx emissions are reduced, but with reinforced changes in secondary products. When only VOC emissions are reduced, ozone decreases by 2 to 5 percent with the largest response located in an area extending from the Atlantic to Germany in the vicinity of the English Channel. In this area, OH concentrations are 5 to 10% lower than in the baseline case. Finally, we note again, in this particular case, a slight increase in the concentration of NOx (2 percent with higher values of 5 percent over the sea east and west of the UK) resulting from a reduced conversion of nitrogen species to nitro-organic compounds.

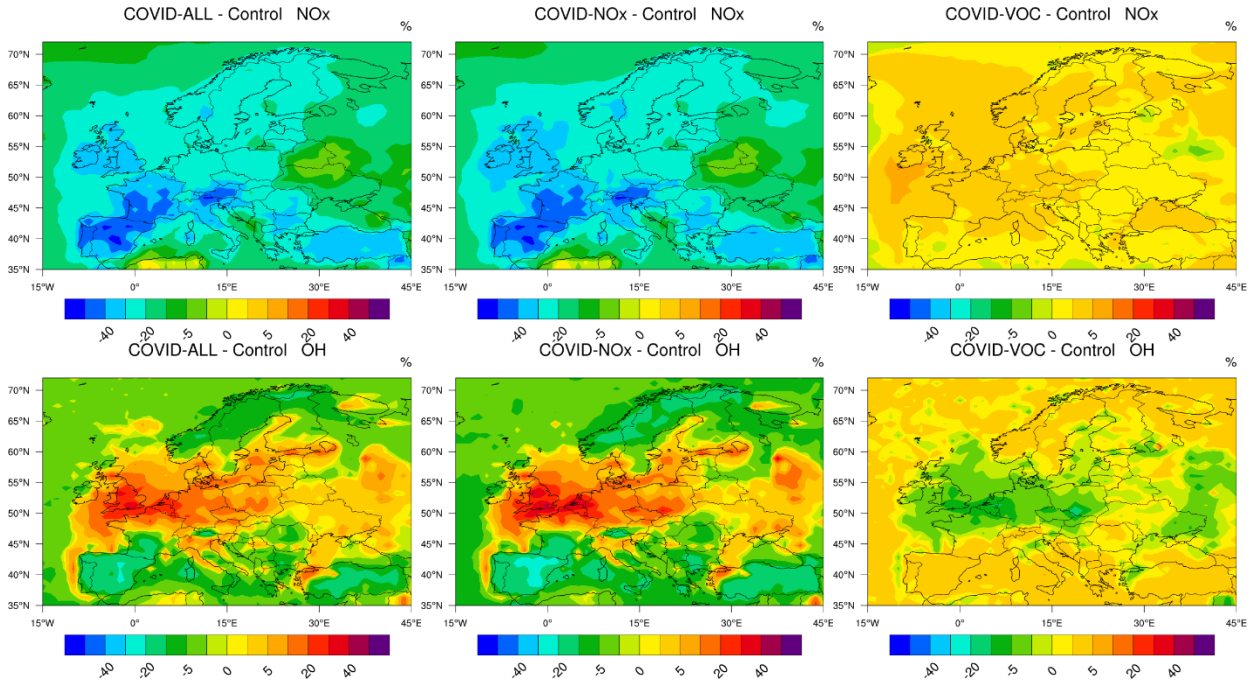

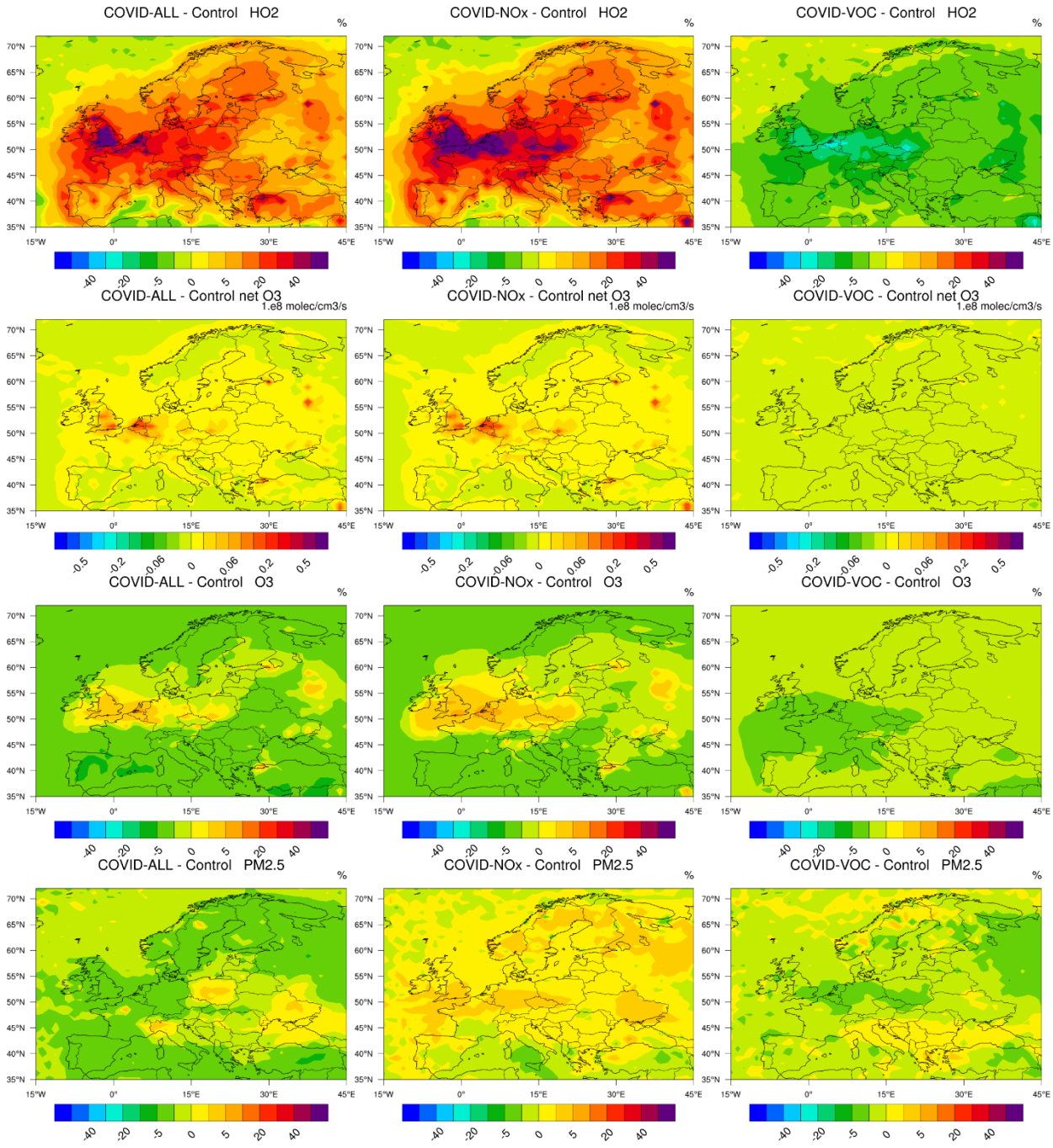

Figure 13. Percentage change in the surface concentration and in the net ozone production across Europe in response to the emissions of primary pollutants adjusted for the COVID-19 pandemic period of 15 March-14 April 2020. From top to bottom: NOx, OH, HO_2, net ozone production (cm^{-3} s^{-1}), ozone concentrations. Left column: reduction in all emissions; center panel: reduction in NOx emissions only; right panel: reduction in VOC and CO emissions only.

We now examine the effects of meteorological anomalies on the calculated changes in the surface concentrations of NOx, HO_2 and ozone. Figure 14 shows the changes in the concentration of several chemical species in response to the anomalies in the meteorology in March-April 2020.

Meteorological analyses (Deroubaix et al., 2020; Ordóñez et al., 2020) show that this period was characterized by unusual clear sky periods in central and northern Europe and cloudy skies in southwestern Europe. Figure 14 also shows the anomaly in temperature and in cloud cover calculated by the model for the month of April 2020 relative to a 5-year "pseudo-climatology". During this particular month, the temperature is higher than the mean value in France, in Spain, near the Baltic Sea and in Eastern Europe. Abnormal low cloudiness is predicted in Central Europe extending from France to the Black Sea and from Italy to Denmark. Cloudiness, however, is higher than normal in Spain, Turkey and part of Norway.

When considering only the effect of meteorological variability and ignoring the adjustments in the emissions, we see that, during the 15 March – 14 April period, the level of nitrogen oxides is abnormally high at the western edge of the European continent, as well as in France and in large parts of Italy and Central Europe. It is low along the eastern coast of Spain and in the southeastern part of Scandinavia. The change in NOx concentrations, when combining the emission reductions and the meteorological effects (COVID-All – Climato) is more pronounced than in the "emission reduction" case (see Figure 13). Meteorological anomalies play therefore a substantial role. In the case of HO_2, meteorological perturbations reinforce the disturbances resulting from the changes adopted for the emissions. The same reinforcement is also found in the case of ozone. In fact, for this particularly species, meteorological anomalies are responsible for most of the changes in the surface concentrations. The ozone increase attributed to the combined reductions in NOx and VOC emissions is visible only in the region that covers the southern UK, the Benelux, and parts of Germany, as well as the eastern coast of Spain and areas in the Mediterranean. In summary, contrary to what has been found for China, a large fraction of the ozone increase noted in Europe during the pandemic must be attributed to meteorological anomalies (Ordóñez et al., 2020); the reduction in pollutant emissions has substantially affected only a few specific regions of the continent.

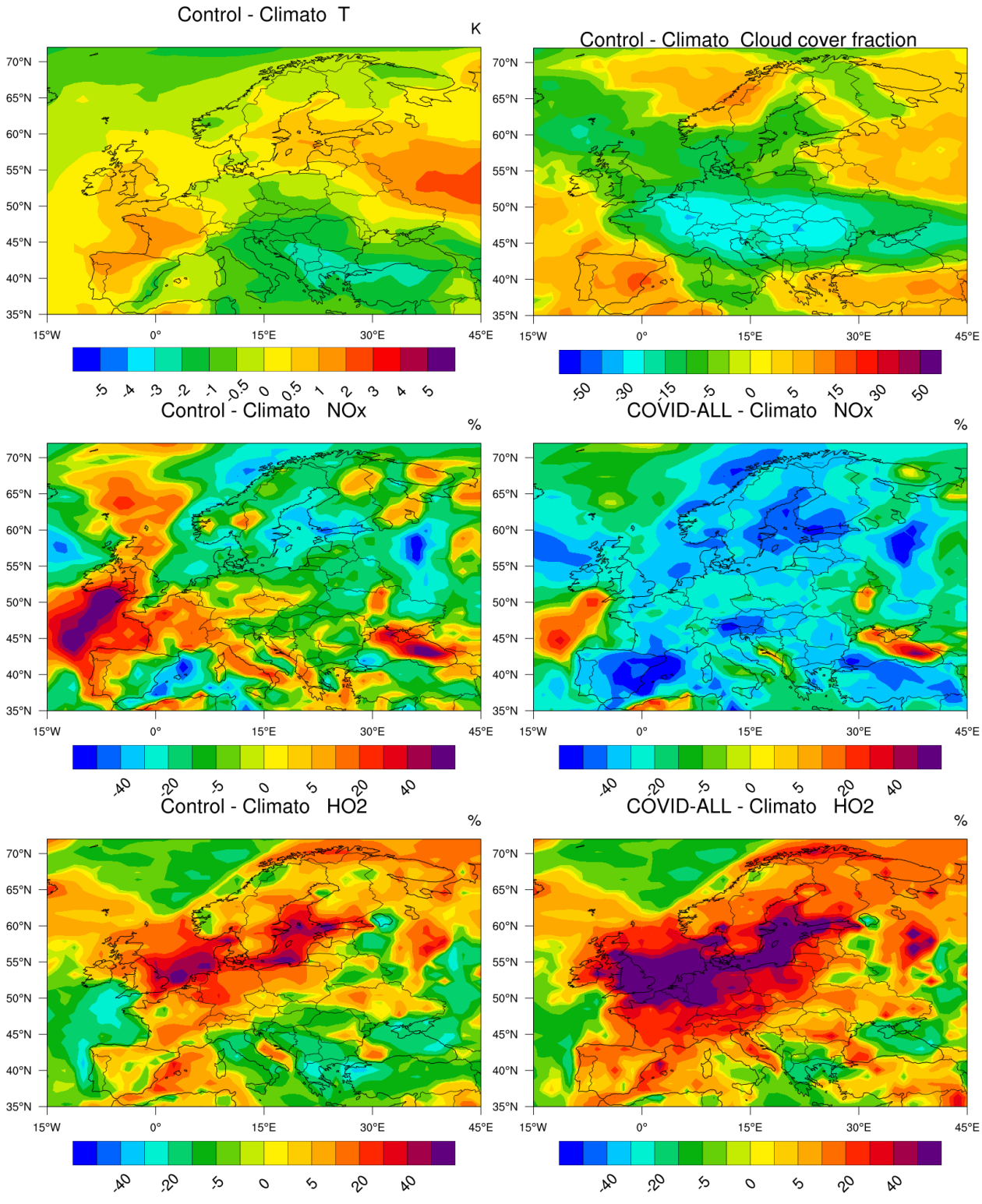
Control - Climato T
K
Control - Climato Cloud cover fraction
Control - Climato NOx
%
COVID-ALL - Climato NOx
%
Control - Climato HO2
%
COVID-ALL - Climato HO2
%
70°N
65°N
60°N
55°N
50°N
45°N
40°N
35°N
15°W
0°
15°E
30°E
45°E

900

901

902

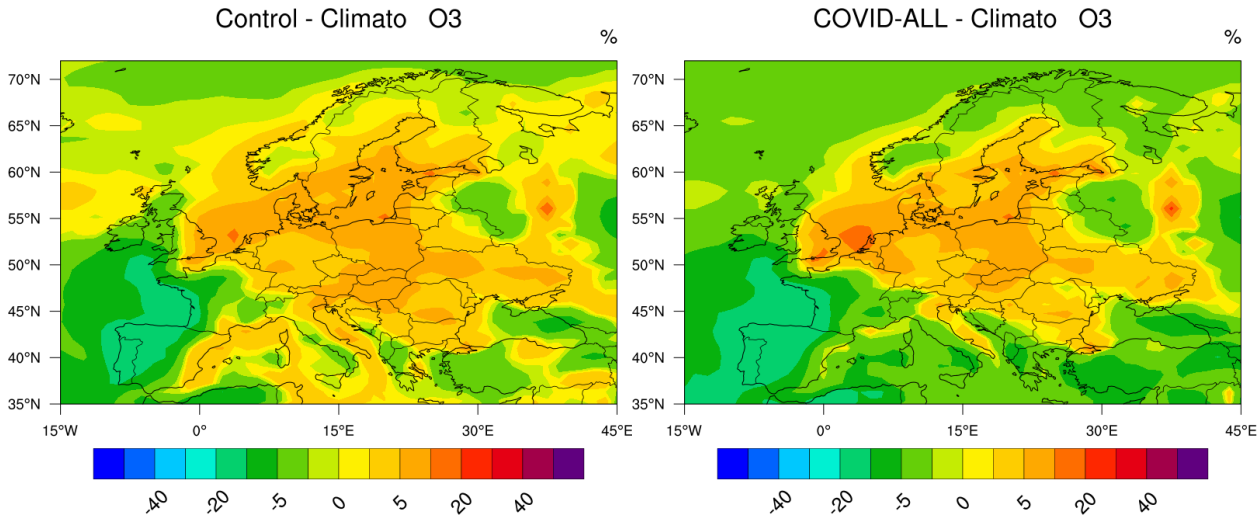

Figure 14. Percentage change in the surface concentration of ozone across Europe during the period 15 March-14 April 2020 relative to the value averaged over 5 years (2016 to 2020) for the same period of the year. Left Panel: Response taking into account the adjustment of the emissions associated with the pandemic and the meteorological anomaly. Right panel: ozone response only to the meteorological anomaly.

5.3. Air quality in North America during the pandemic

We now examine the results provided by the model in North America (COVID-All case) and focus again on the period 15 March to 14 April 2020. In most of the regions, particularly in rural areas, ozone is NOx-limited during the spring conditions (Figure 15). However, in a region extending from the US East Coast to Alberta in Canada including the region of the Great lakes and part of the Middle West, ozone is VOC controlled.

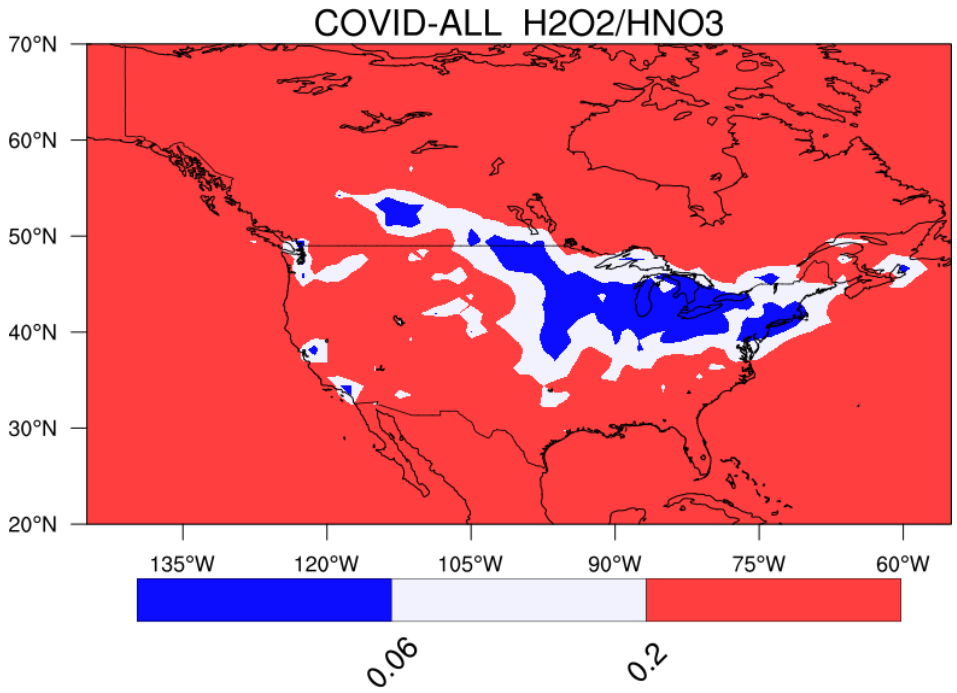

Figure 15. Ratio between the production rate of hydrogen peroxide and nitric acid, a measure of the chemical conditions governing the formation of ozone. The geographical area in which ozone is NOx controlled is shaded in red and VOC controlled in shaded in blue. The white area represents an intermediate situation between fully NOx and VOC controlled situations.

In relative terms, the largest decrease in NOx concentrations is found in southern Canada (30-40%) as well as in the northeastern US (40-50%), notably near the Great Lakes and along the St Lawrence River (Figure 16). Substantial reductions in NOx are also noticeable along the west coast (20-30%) and in the western and southern states of the US and in Mexico (20-30%).

The surface concentration of the hydroxyl and peroxy radicals has increased most in the region of the Great Lakes, along the US-Canadian Border (including the region of Calgary), in the central plain of the US, as well as in urban areas of the west coast including Los Angeles, San Francisco and Seattle (5-15% for OH, 30-50% for HO_2 and CH_3O_2). The reduction in formaldehyde is relatively small (less than 10%) except in southern Canada and the region of the St Lawrence, where it reaches 10 to 20% (Figure S5). The change in the net ozone production rate during March-April (see Figure S5) is limited to a few percent and so is the change in the surface ozone concentration. Since ozone is NOx-controlled in rural areas, the reduction in NOx leads to a small ozone decrease, mostly in the central and southern parts of the US. Only small ozone increases (2-10%) in response to the changes in emissions are noticeable in the model results for the period 15 March – 14 April, and are located around the Great Lakes, particularly near densely populated

940 urban areas like New York, Boston, Toronto, Chicago, Calgary, Los Angeles and San Francisco.
941 The bottom right panel in Figure 15 provides the response of ozone resulting from a reduction in
942 the NOx emissions only (no VOC and CO emission reduction, COVID-NOx case). The patterns
943 are the same as those discussed for the COVID-All simulations with, however, more pronounced
944 ozone increases along the US-Canadian border and in the urban areas of the west coast. Chen et
945 al. (2020) analyzed data acquired from 28 urban and sub-urban air quality stations across the
946 United States that showed widespread nonuniform NOx reductions relative to a pre-lockdown
947 reference as well as mixed and relatively minor changes (less than 20%) in ozone. Additional
948 model results are provided in Figure S5 of the Supplementary Information.
949
950

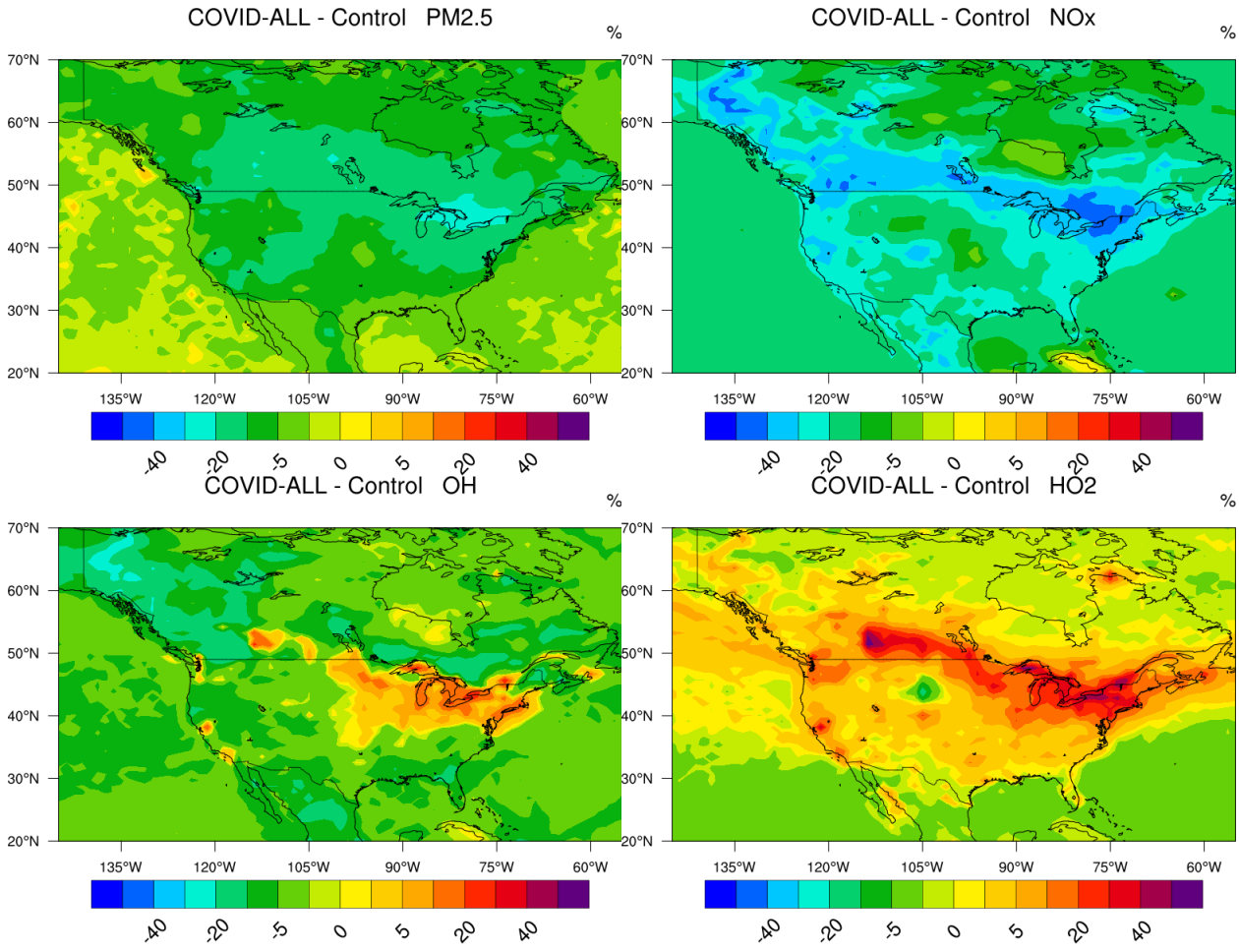

951
952

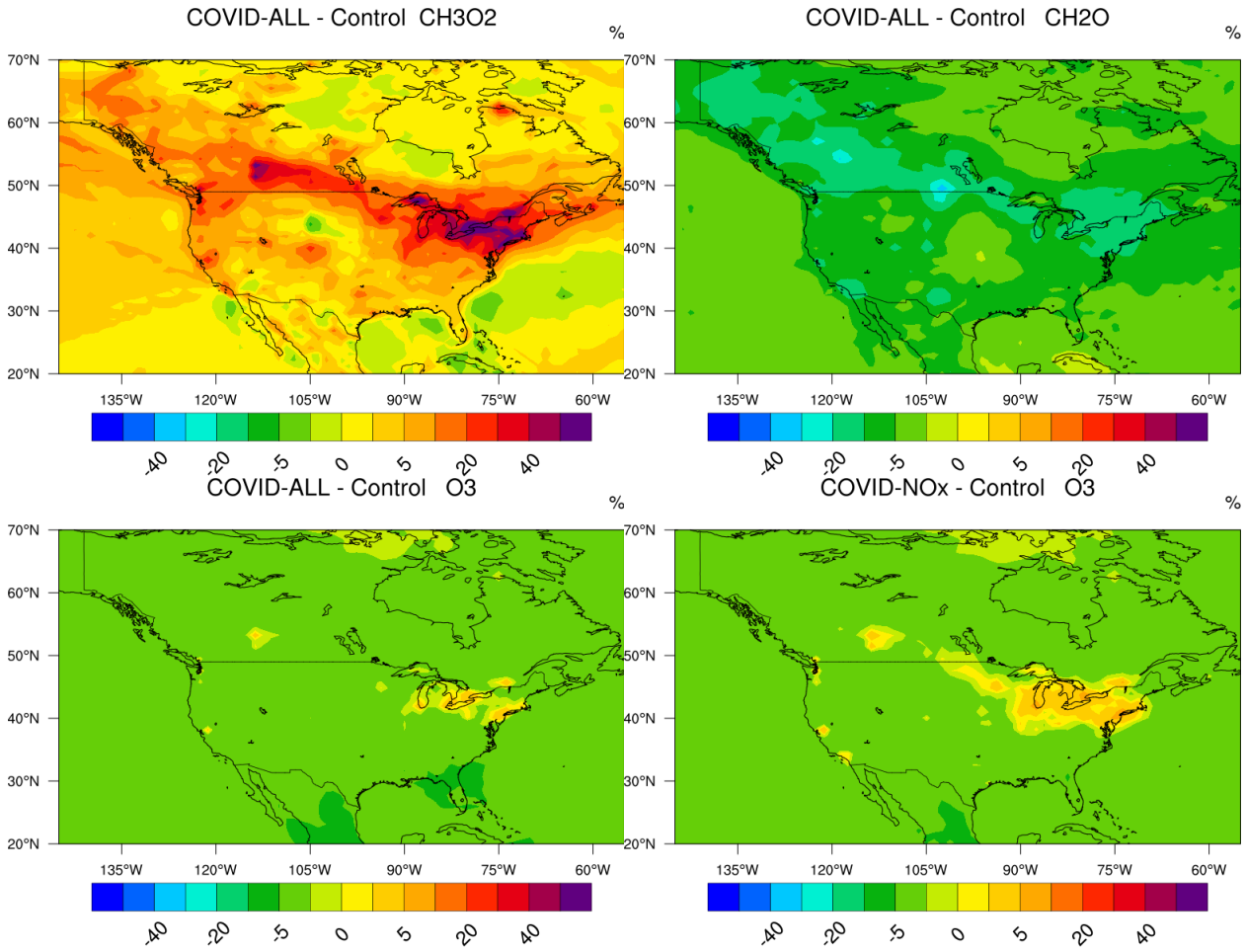

Figure 16. Percentage change in the surface concentration of (from top left to bottom right) $PM_{2.5}$, NOx, OH, HO_2, CH_3O_2, HCHO, and ozone several chemical species across North America in response to adjusted emissions of primary pollutants during the COVID-19 period of 15 March-14 April 2020. All calculated fields result from a COVID-All simulation except the bottom right panel which is obtained from a COVID-NOx simulation (no reduction in VOC and CO emissions).

5.4. Air quality in South America during the pandemic

In South America (Figure 17), a significant reduction in the surface concentration of nitrogen oxides is derived for the period 15 March – 14 April, specifically along the Atlantic coast in Brazil (25 - 35%) and the Pacific coast in Peru and Ecuador (30 – 40%). Reductions of 30 to 40% are also found in the region of Buenos Aires, Argentina and Santiago, Chile. The reduction in formaldehyde is generally limited to a few percent across the continent since a large source of this compound is due to biogenic emissions, which is unchanged in this simulation. Except in urban areas, the level of OH decreases (20 – 25% in eastern Brazil; 30 – 40% in Peru and Ecuador). However, the concentration of HO_2 increases by 5 – 10% in Chile, eastern Brazil and eastern

Argentina, specifically in and near large South American metropolitan areas (Sao Paulo-Rio de Janeiro region, Buenos Aires, Santiago, Lima, Guayaquil). The concentration of nitric acid decreases along both coasts (30% in Brazil; 40 - 50% in Peru and Ecuador) and that of hydrogen peroxide slightly increases (up to 5 %) in Chile, in the region of Sao Paulo and Rio de Janeiro as well as in the northern part of the South American continent. A small reduction in the surface ozone concentration (5 – 10%) is derived in Brazil and a larger decrease (15 – 20%) is calculated in Peru and Ecuador. Cazorla et al. (2020) note that in the city of Quito, Ecuador, the average ozone level during the lockdown in April was not significantly different from the ozone level in January, which they attribute to unusually high cloudiness and to frequent precipitation during the month of April.

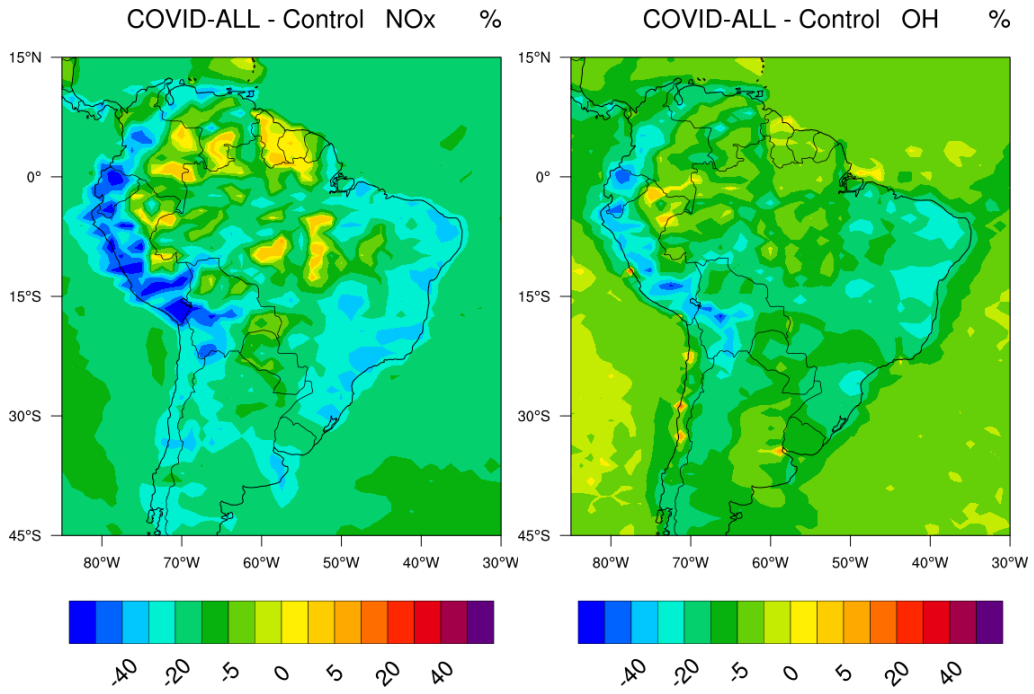

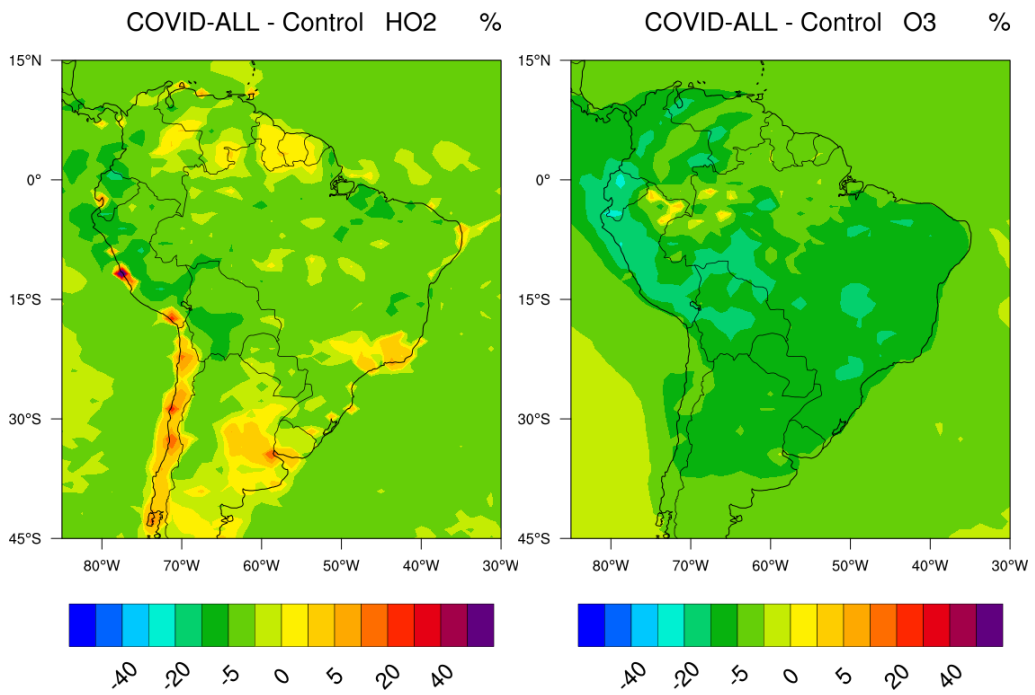

Figure 17. Percentage change in the surface concentration of several chemical species across South America in response to adjusted emissions of primary pollutants during the COVID-19 period of 15 March-14 April 2020.

6. Summary and conclusions

The world-wide disruption in the economic activities during the COVID-19 pandemic in early 2020 has generated large perturbations in the emissions of air pollutants. These perturbations have been prominent first in China where the pandemic outbreak was reported, and later in other countries of both hemispheres. The response of photo-oxidants to the simultaneous reductions in NOx, VOC and CO emission has varied according to the geographic location and the time of the year. In the NOx-saturated region of northeastern China, which was hit by the pandemic under winter conditions, an increase in the concentrations of ozone, OH, HO_2, and RO_2 radicals was derived by the model. The concentration of the NO_3 radical, a powerful nighttime oxidant, and of PAN, a secondary pollutant was also increased in the North China Plain. The reduced NOx emissions also led to less titration of ozone, a reduced conversion of OH by NO_2 and an increased HO_2/OH concentration ratio. Further, even though the intensity of solar radiation is low during February, the photochemical production of ozone and OH was not suppressed. However, the strong decrease in NO resulting from reduced activities during the pandemic was not compensated by a sufficiently large increase in peroxy radicals, so that the overall ozone production by the limiting HO_2 + NO and RO_2 + NO reactions was reduced during the month of February. The ozone

concentration increase was therefore due primarily to a relatively larger reduction in the ozone loss. In the NOx-limited region of southern China, the concentration of ozone and other photooxidants decreased because their formation rate, favored by NOx, was reduced, except in VOC-limited urban areas like Guangzhou or Hong Kong, where the model predicted ozone enhancements.

In the other regions of the world during the peak of the lockdown period (corresponding to Northern Hemisphere spring and Southern Hemisphere fall), the oxidation level was also disturbed by the reduced emissions of ozone precursors. During April 2020, for example, the level of oxidants including ozone was enhanced in the regions of Europe where the background level of NOx is relatively high. In response to the perturbed emissions of pollutants, ozone concentrations increased in a region extending from the UK to Germany, and OH levels increased in most of western Europe except in Spain. In North America, the reduced emissions led to enhanced concentrations of oxidants along the US-Canadian border and ozone concentrations increased slightly in the region of the Great Lakes. In South America, during this period of late summer and early fall, the level of photo-oxidants decreased except in metropolitan areas where elevated concentrations of OH and HO_2 were calculated by the model.

The level at which the oxidizing capacity of the atmosphere changed in Northern China and to a lesser extent in Europe and North America, as well as the related increase in the concentration of secondary products such as ozone, OH, HO_2, NO_3 and PAN depends on the relative amplitude in the change in VOC and in NOx emissions. Both forcing processes act in different directions. Therefore, if the VOC emission reduction adopted here was overestimated, the formation of the secondary species would be somewhat underestimated. In this case, a more likely description of the response of the atmosphere during the pandemic should be intermediate between the fields provided by the COVID-All and COVID-NOx simulations.

These results are obtained by model simulations that isolate the changes in surface emissions and consider them as the only forcing mechanism. However, meteorological variability provides an additional forcing mechanism that produces substantial changes in the monthly mean concentrations of chemical species; these changes can be comparable and, in some cases, larger than the chemical response to emission reductions. In China, although large-scale meteorological anomalies as derived by the model during the month of February may have contributed to the ozone increase in the North China Plain, the largest effect should be attributed to chemical

perturbations related to the reduction in emissions. In most areas of Europe, however, the situation was different: during the acute period of the pandemic between 15 March and 14 April 2020, most of the ozone increase calculated by the model was associated primarily with weather anomalies rather than the emission reduction. Chemical perturbations contributed significantly to the ozone increase, but only in a limited region extending from the UK to Germany and including the Benelux countries.

In summary, the simulations performed by the global atmospheric model (CESM v.2.2) with a detailed chemical scheme (MOZART TS1 mechanism) driven by emission changes of primary pollutants and forced by realistic weather conditions reproduce reasonably well the changes observed in the chemical composition of the atmosphere, and specifically in the perturbations of surface ozone and other oxidants during the COVID-19 pandemic. At least qualitatively, the response of the atmosphere to the gigantic chemical experiment that took place in the atmosphere during the first half of 2020 is found to be explained to a satisfactory degree by our current understanding of the photochemical theory, in particular in what concerns ozone formation. This unexpected global event allows us, however, to address unresolved questions related to the nonlinear atmospheric system with its complex chemical regimes including the mechanisms that control the formation of secondary pollutants under different chemical environments. More detailed and specific studies that investigate regional responses to emission reductions together with mesoscale and local weather variability should be conducted with higher resolution models.

Data availability

CESM2.2.0 is a publicly released version of the Community Earth System Model and freely available online (at www.cesm.ucar.edu, last access: 2 October 2020). Air Quality e-Reporting (AQ e-Reporting) (2020). For Europe, the observational dataset is provided by the Air Quality e-Reporting (AQ e-Reporting), available at https://www.eea.europa.eu/data-and-maps/data/aqereporting-8 (permanent link: b21a537e763e4ad9ac8ccffe987d6f77), last access: November 4, 2020. For São Paulo region, the observational dataset is provided by the CETESB Network of the environmental state agency of São Paulo, available at https://qualar.cetesb.sp.gov.br/qualar/home.do, last access: November 4, 2020. For the North China Plain region, the observational dataset is provided by the China Environmental Observation Network operated by the China National Environmental Monitoring Center, available at http://www.cnemc.cn/en/, last access: November 4, 2020. For the USA, the observational dataset is provided by the US Environmental Protection Agency, Air Quality System Data Mart [internet database], available at http://www.epa.gov/ttn/airs/aqsdatamart, last access: October 26, 2020. This publication contains modified Copernicus Sentinel-5 TROPOMI data for 2019–2020.

TROPOMI data versions 1.2.2 and 1.3.0 used here are available at https://s5phub.copernicus.eu.

Acknowledgments

We would like to acknowledge the high-performance computing support from Cheyenne (doi:10.5065/D6RX99HX) provided by NCAR's Computational and Information Systems Laboratory of the National Center for Atmospheric Research (NCAR), sponsored by the US National Science Foundation (NSF). This material is based upon work supported by the National Center for Atmospheric Research, which is a major facility sponsored by the National Science Foundation under cooperative agreement no. 1852977. We also acknowledge the support of the AQ-WATCH European project, a HORIZON 2020 Research and Innovation Action (GA 870301). The CAMS-GLOB-ANT dataset has been developed with the support of the CAMS (Copernicus Atmosphere Monitoring Service), operated by the European Centre for Medium-Range Weather Forecasts on behalf of the European Commission as part of the Copernicus Programme. T.W. and Y.L. acknowledge support by the Hong Kong Research Grants Council (T24-504/17-N and A-PolyU502/16). This work has also been partly supported by the TROVA and ICOVAC projects of the European Space Agency (ESA).

Author contributions:

Conceptualization: Guy Brasseur, Benjamin Gaubert, Claire Granier, Tao Wang
Production of emissions: Sabine Darras, Thierno Doumbia, Nellie Elguindi, Claire Granier
Analysis of surface observations: Idir Bouarar, Adrien Deroubaix, Forrest Lacey, Yiming Liu, Xiaoqin Shi
Analysis of space observations: Trissevgeni Stavrakou
Model simulations: Benjamin Gaubert, Simone Tilmes
Analysis of the model results: Guy Brasseur, Idir Bouarar, Benjamin Gaubert, Jean-François Müller, Simone Tilmes.
Writing -original draft: Guy Brasseur, Benjamin Gaubert
Writing -review and editing: All authors.

References

Baldasano, J. M. (2020). COVID-19 lockdown effects on air quality by NO_2 in the cities of Barcelona and Madrid (Spain). *Science of the Total Environment*, *741*, 140353, https://doi.org/10.1016/j.scitotenv.2020.140353

Barré, J., Petetin, H., Colette, A., Guevara, M., Peuch, V.-H., … Kouznetsov, V. (2020) Estimated lockdown induced European NO_2 changes, *Atmospheric Chemistry and Physics Discussions*, https://doi.org/10.5194/acp-2020-995

Bauwens, M., Compernolle, S., Stavrakou, T., Müller, J.-F., van Gent, J., Eskes, H., … Zehner, C. (2020). Impact of coronavirus outbreak on NO_2 pollution assessed using TROPOMI

and OMI observations. *Geophysical Research Letters*, *47*, e2020GL087978. https://doi.org/10.1029/2020GL087978

Bedi, J. S., Dhaka, P., Vijay, D., Aulakh R.S., & Gill, J.P.S. (2020). Assessment of Air Quality Changes in the Four Metropolitan Cities of India during COVID-19 Pandemic Lockdown. *Aerosol and Air Quality Research*, *20*, https://doi.org/10.4209/aaqr.2020.05.0209

Cazorla, M., Herrera E., Palomeque, E., & Saud, N. (2020). What the COVID-19 lockdown revealed about photochemistry and ozone production in Quito, Ecuador, *Atmospheric Pollution Research*, https://doi.org/10.1016/j.apr.2020.08.028

Chauhan, A., & Singh R.P. (2020). Decline in PM2.5 concentrations over major cities around the world associated with COVID-19. *Environmental Research*, *187* (109634), https://doi.org/10.1016/j.envres.2020.109634

Chen, L.-W., Chien, L.-C, Li, Y., & Lin, G. (2020) Nonuniform impacts of COVID-19 lockdown on air quality over the United States, Science of the Total Environment, 745, 141105, https://doi.org/10.1016/j.scitotenv.2020.141105

Cheng, Y., Zheng, G., Wei, C., Mu, Q., Zheng, B.,… Su, H. (2016) Reactive nitrogen chemistry in aerosol water as a source of sulfate during haze events in China, *Science. Advances*., *2*, e1601530. doi: 10.1126/sciadv.1601530

Crippa, M., Guizzardi, D., Muntean, M., Schaaf, E., Dentener, F., van Aardenne, … Janssens-Maenhout, G. (2018) Gridded emissions of air pollutants for the period 1970–2012 within EDGAR v4.3.2, *Earth Syst. Sci. Data, 10*, 1987–2013, https://doi.org/10.5194/essd-10-1987-2018

Danabasoglu, G., Lamarque, J.-F., Bacmeister, J., Bailey, D. A., DuVivier, A. K., Edwards, J., et al. (2020). The Community Earth System Model Version 2 (CESM2). *Journal of Advances in Modeling Earth Systems*, 12, e2019MS001916. https://doi.org/10.1029/2019MS001916.

Darmenov, A., & da Silva, A.M. (2014). The QuickFire Emissions Dataset (QFED)—Documentation of versions 2.1, 2.2 and 2.4, NASATM-2013-104606, vol. 35, 183 pp. (data available at: https://portal.nccs.nasa.gov/datashare/iesa/aerosol/emissions/QFED/v2.4r6/, last access: 17 January 2020).

Deroubaix, A., Brasseur, G., Gaubert, B., Labuhn, I., Menut, L., Siour, G., & Tuccella, P. (2020) Response of surface ozone concentration to emission reduction and meteorology during the COVID-19 lockdown in Europe, submitted to *Meteorol. Appl.*

Diamond, M. S. and R. Wood (2020) Limited Regional Aerosol and Cloud Microphysical Changes Despite Unprecedented Decline in Nitrogen Oxide Pollution During the February 2020 COVID-19 Shutdown in China. *Geophysical Research Letters*, 47, https://doi.org/10.1029/2020GL088913,

Doumbia, T., Granier, C., Elguindi, N., Bouarar, I., Darras, S., Brasseur, G., … Wang, T. (2020) Changes in global air pollutant emissions during the COVID-19 pandemic: a dataset for atmospheric chemistry modeling, submitted to *Earth. Sys. Sci. Data*

1152 Elguindi, N., Granier, C., Stavrakou, T., Darras, S., Bauwens, M., Cao, … Zheng, B. (2020)
1153 Intercomparison of Magnitudes and Trends in Anthropogenic Surface Emissions from
1154 Bottom-Up Inventories, Top-Down Estimates, and Emission Scenarios. *Earth's Future*,
1155 8: e2020EF001520. doi:10.1029/2020EF001520

1156 Emmons, L. K., Schwantes, R. H., Orlando, J. J., Tyndall, G., Kinnison, D., Lamarque, J.-F., …
1157 Pétron, G. (2020). The Chemistry Mechanism in the Community Earth System Model
1158 version 2 (CESM2). *Journal of Advances in Modeling Earth Systems*, *12*,
1159 e2019MS001882. https://doi.org/10.1029/2019MS001882

1160 Forster, P. M., Forster, H. I., Evans, M. J., Gidden, M. J., Jones, C. D., Keller, C. A., … Turnock,
1161 S.T. (2020) Current and future global climate impacts resulting from COVID-19. *Nature*
1162 *Climate Change*, https://doi.org/10.1038/s41558-020-0883-0

1163 Fu, F., Purvis-Roberts, L., Williams, B. (2020a), Impact of COVID-19 pandemic lockdown on
1164 air pollution of 20 major cities around the world, submitted to *AGU Advances*

1165 Fu, X., Wang, T., Gao, J., Wang, P., Liu, Y., Wang, S., Zhao, B., Xue, L. (2020b). Persistent
1166 Heavy Winter Nitrate Pollution Driven by Increased Photochemical Oxidants in Northern
1167 China, *Environmental Science & Technology*, *54* (7) 3881-3889

1168 Gaubert, B., et al. (2016), Toward a chemical reanalysis in a coupled chemistry-climate model:
1169 An evaluation of MOPITT CO assimilation and its impact on tropospheric composition,
1170 *J. Geophys. Res. Atmos.*, 121, 7310– 7343, doi:10.1002/2016JD024863.

1171 Gaubert, B., Emmons, L.K., Reader, K., Tilmes, S., Miyazaki, K., … Ren, X. (2020). Correcting
1172 model biases of CO in East Asia: impact on oxidant distributions during KORUS-AQ.
1173 *Atmos. Chem. Phys. Discuss*., https://doi.org/10.5194/acp-2020-599.

1174 Gettelman, A., Mills, M. J., Kinnison, D. E., Garcia, R. R., Smith, A. K., Marsh, D. R., … Randel,
1175 W.J. (2019). The whole atmosphere community climate model version 6 (WACCM6).
1176 *Journal of Geophysical Research: Atmospheres, 124*,
1177 https://doi.org/10.1029/2019JD030943.

1178 Goldberg, D. L., Anenberg, S. C., Griffin, D., McLinden, C. A., Lu, Z. & Streets, D. G. (2020).
1179 Disentangling the Impact of the COVID-19 Lockdowns on Urban NO2 From Natural
1180 Variability. *Geophysical Research Letters, 47*, https://doi.org/10.1029/2020GL089269.

1181 Granier, C., Darras, S., Denier van der Gon, H., Doubalova, J., Elguindi, N., Galle, B., …
1182 Sindelarova, K. (2019). The Copernicus Atmosphere Monitoring Service global and
1183 regional emissions, Copernicus Atmosphere Monitoring Service (CAMS),
1184 doi:10.24380/d0bn-kx16

1185 Guenther, A. B., Jiang, X., Heald, C.L., Sakulyanontvittaya, T., Duhl, T., Emmons, L.K. & Wang
1186 X. (2012). The Model of Emissions of Gases and Aerosols from Nature version 2.1
1187 (MEGAN2.1): An extended and updated framework for modeling biogenic emissions,
1188 *Geosci. Model Dev*., *5*, 1471–1492, doi:10.5194/gmd-5-1471-2012

1189 Guevara, M., Jorba, O., Soret, A., Petetin, H., Bowdalo, D., Serradell, K., … Garcia-Pando, C.P.
1190 (2020). Time-resolved emission reductions for atmospheric chemistry modelling in
1191 Europe during the COVID-19 lockdowns. *Atmospheric Chemistry and Physics,*
1192 https://doi.org/10.5194/acp-2020-686, in review.

Hallquist, M., Wenger, J.C., Baltensperger, U., Rudich, Y., Simposon, D., Claeys, M., … Wildt, J., (2009). The formation properties and impact of secondary: Current and emerging issues, *Atmospheric Chemistry and Physics*, *9*, 5155-5236, https://doi.org/10.5194/acp-9-5155-2009.

He, G., Pan Y. and Tanaka T. (2020). The short-term impacts of COVID-19 lockdown on urban air quality pollution in China. *Nature Sustainability*, https://doi.org/10.1038/s41893-020-0581-y,

Hoesly, R. M., Smith, S. J., Feng, L., Klimont, Z., Janssens-Maenhout, G., Pitkanen, … Zhang, Q. (2018). Historical (1750–2014) anthropogenic emissions of reactive gases and aerosols from the Community Emissions Data System (CEDS), *Geosci. Model Dev*., *11*, 369–408, https://doi.org/10.5194/gmd-11-369-2018

Huang, X., Ding, A., Gao, J., Zheng, B., Zhou, D., Qi, X., … He, K. (2020) Enhanced secondary pollution offset reduction of primary emissions during COVID-19 lockdown in China, *National Science Review*, https://doi.org/10.1093/nsr/nwaa137

Krecl, P., Targino, A. C., Oukawa G. Y. & and Cassino, R. P., (2020). Drop in urban air pollution from COVID-19 pandemic: Policy implications for the megacity of São Paulo. *Environmental Pollution*, *265*, 114883, https://doi.org/10.1016/j.envpol.2020.114883.

Keller, C. A., Evans, M. J., Knowland, K. E., Hasenkopf, C. A., Modekurty, S., Lucchesi, R. A., Oda, T., Franca, B. B., Mandarino, F. C., Díaz Suárez, M. V., Ryan, R. G., Fakes, L. H., and Pawson, S. (2020). Global Impact of COVID-19 Restrictions on the Surface Concentrations of Nitrogen Dioxide and Ozone, Atmos. Chem. Phys. Discuss., https://doi.org/10.5194/acp-2020-685.

Kroll J. H., Heald, C. L., Cappa, C. D., Farmer, D. K., Fry, J. L., Murphy, J. G., & Steiner A. (2020). The complex chemical effects of COVID-19 shutdowns on air quality, *Nature Chemistry,* 12, 777-779

Lawrence, D. M., Fisher, R. A., Koven, C. D., Oleson, K. W., Swenson, S. C., Bonan, G., … Zeng, X. (2019). The Community Land Model version 5: Description of new features, benchmarking, and impact of forcing uncertainty. *Journal of Advances in Modeling Earth Systems, 11*, 4245– 4287. https://doi.org/10.1029/2018MS001583

Le, T., Wang, Y., Liu, L., Yang, J., Yung, Y. L., Li, G., & Seinfeld, J. H. (2020). Unexpected air pollution with marked emissions reductions during the COVID-19 outbreak in China. *Science*, https://doi.org/10.1126/science.abb7431

Le Quéré, C., Jackson, R. B., Jones, M. W., Smith, A. J. P., Abernethy, S., Andrew, R. M. … Peters, G. P. (2020). Temporary reduction in daily global CO_2 emissions during the COVID-19 forced confinement. *Nature Climate Change*, https://doi.org/10.1038/s41558-020-0797-x

Li, K., Jacob, D. J., Liao, H., Qiu, Y., Shen L., Zhai, S., Bates, K. H., Sulprizio, M. P., Song, S., Lu, X., Zhamg, Q., & Zheng, B. (2020) Ozone pollution in the North China Plain spreading into late-winter haze season, *Proceedings of the national Academy of Sciences,* submitted.

Lian, X., Huang, J., Huang, R., Liu, C., Wang, L. & Zhang, T. (2020). Impact of city lockdown on the air quality of COVID-19-hit of Wuhan city. *Science of the Total Environment, 742*, 140556, https://doi.org/10.1016/j.scitotenv.2020.140556.

1236 Liu, F., Page A., Strode S. A., Yoshida Y., Choi S., Zheng B., Lamsal L. N., Li C., Krotkov N.
1237 A., Eskes H., van der A R., Veefkind P., Levelt P. F., Hauser O. P. & Joiner J. (2020).
1238 Abrupt decline in tropospheric nitrogen dioxide over China after the outbreak of COVID-
1239 19. *Science Advances 6*(28), https://doi.org/10.1126/sciadv.abc2992,

1240 Liu, X., Ma, P.-L., Wang, H., Tilmes, S., Singh, B., Easter, R. C., Ghan, S. J., & Rasch P.J.
1241 (2016). Description and evaluation of a new four-mode version of the Modal Aerosol
1242 Module (MAM4) within version 5.3 of the Community Atmosphere Model. *Geoscientific*
1243 *Model Development*, *9* (2), 505–522. https://doi.org/10.5194/gmd-9-505-2016

1244 Liu, Y. & Wang, T. (2020). Diverse response of atmospheric ozone to COVID-19 lockdown in
1245 China, arXiv preprint arXiv:2008:10851, https://arxiv.org/abs/2008.10851.

1246 Menut, L., Bessagnet, B., Siour, G., Mailler, S., Pennel R., & Cholakian A. (2020). Impact of
1247 lockdown measures to combat COVID-19 on air quality over western Europe, *Science of*
1248 *the Total Environment, 741*, 140426, https://doi.org/10.1016/j.scitotenv.2020.140426

1249 Miyazaki, K., Bowman, K., Sekiya, T., Jiang, Z., Chen, X., Eskes, H., et al. (2020). Air quality
1250 response in China linked to the 2019 novel coronavirus (COVID-19) lockdown.
1251 *Geophysical Research Letters*, 47, e2020GL089252.
1252 https://doi.org/10.1029/2020GL089252

1253 Mills, M. J., Schmidt, A., Easter, R., Solomon, S., Kinnison, D. E., Ghan, S. J., … Gettelman, A.
1254 (2016). Global volcanic aerosol properties derived from emissions, 1990–2014, using
1255 CESM1c(WACCM), *Journal of Geophysical Research: Atmospheres*, *121*, 2332–2348.
1256 https://doi.org/10.1002/2015JD024290

1257 Ng, N. L., Chhabra P. S., Chan A. W. H., Surratt J. D., Kroll J. H., Kwan A. J., McCabe, D.C.,
1258 Wennberg P. O., Sorooshian A., Murphy S. M., Dalleska N. F., Flagan R. C. & Seinfeld,
1259 J. H. (2007). Effect of NOx level on secondary organic aerosol (SOA) formation from the
1260 photooxidation of terpenes, *Atmospheric. Chemistry &. Physics, 7*, 5159–5174,
1261 www.atmos-chem-phys.net/7/5159/2007/

1262 Ordóñez, C., Garrido-Perez, J. M., García-Herrera, R. (2020). Early spring near-surface ozone in
1263 Europe during the COVID-19 shutdown: Meteorological effects outweigh emission
1264 changes, *Science of The Total Environment*, *747,* 141322,
1265 https://doi.org/10.1016/j.scitotenv.2020.141173

1266 Otmani, A., Benchrif, A., Tahri, M., Bounakhla, M., Chakir, E. M., El Bouch, M., & Krombi, M.
1267 (2020). Impact of COVID-19 lockdown on PM_{10}, SO_2 and NO_2 concentrations in Salé
1268 City (Morocco). *Science of The Total Environment*, *735* (139541),
1269 https://doi.org/10.1016/j.scitotenv.2020.139541

1270 Petetin, H., Bowdalo, D., Soret, A., Guevara, M., Jorba, O., Serradell, K., and Pérez García-
1271 Pando, C. (2020). Meteorology-normalized impact of the COVID-19 lockdown upon
1272 NO_2 pollution in Spain, *Atmos. Chem. Phys.*, 20, 11119–11141,
1273 https://doi.org/10.5194/acp-20-11119-2020.

1274 Reynolds, R. W., Smith, T. M., Liu, C., Chelton, D. B., Casey, K. S. & Schlax M. G. (2007).
1275 Daily high-resolution blended analyses for sea surface temperature, *Journal of Climate*,
1276 *20,* 5473-5496, https://doi.org/10.1175/2007JCLI1824.1

Rodriguez-Urrego, D. & Rodriguez-Urrego, L. (2020). Air quality during the COVID-19: PM2.5 analysis in the 50 most polluted capital cities in the world. *Environmental Pollution, 266*, 115042, https://doi.org/10.1016/j.envpol.2020.115042

Shi, X., & Brasseur, G. P. (2020). The Response in Air Quality to the Reduction of Chinese Economic Activities during the COVID-19 Outbreak. *Geophysical Research Letters*, *47*, e2020GL088070. https://doi.org/10.1029/2020GL088070.

Sicard, P., De Marco, A., Agathokleous, E., Feng, Z., Xu, X., Paoletti, E., Rodriguez, J. J. D., & Calatayud V. (2020). Amplified ozone pollution in cities during the COVID-19 lockdown. *Science of the Total Environment*, *735* (139542), https://doi.org/10.1016/j.scitotenv.2020.139542

Siciliano, B., Carvalho, G., da Silva, C. M., Arbilla, G. (2020). The impact of COVID-19 partial lockdown on primary pollutant concentrations in the atmosphere of Rio de Janeiro and Sao Paulo megacities (Brazil). *Bulletin of Environmental Contamination and Toxicology, 105*, 2-8, https://doi.org/10.1007/s00128-020-02907-9

Siciliano, B., Dantas, G., da Silva, C. M., & Arbilla, G. (2020). Increased ozone levels during the COVID-19 lockdown: Analysis for the city of Rio de Janeiro, Brazil. *Science of the Total Environment*, *737*, 139765, https://doi.org/10.1016/j.scitotenv.2020.139765

Stein, O., Schultz, M. G., Bouarar, I., Clark, H., Huijnen, V., Gaudel, A., ... Clerbaux, C. (2014). On the wintertime low bias of Northern Hemisphere carbon monoxide found in global model simulations. Atmospheric Chemistry and Physics, 14, 9295–9316. https://doi.org/ 10.5194/acp-14-9295-2014.

Tilmes, S., Hodzic, A., Emmons, L. K., Mills, M. J., Gettelman, A., Kinnison, D. E., … Liu, X., (2020). Climate forcing and trends of organic aerosols in the Community Earth System Model (CESM2). *Journal of Advances in Modeling Earth Systems, 11*, 4323–4351. https://doi.org/10.1029/2019MS001827.

Tonnesen, G. S. & Dennis, R. L. (2000). Analysis of radical propagation efficiency to assess ozone sensitivity to hydrocarbons and NOx 1. Local indicators of instantaneous odd oxygen production sensitivity. *J. Geophys. Res., 105* (D7), 9213− 9225

Veefkind, J. P., Aben, I., McMullan, K., Föorster, H., de Vries, J., Otter, G., et al. (2012), TROPOMI on the ESA Sentinel-5 Precursor: A GMES mission for global observations of the atmospheric composition for climate, air quality and ozone layer applications. *Remote Sensing of Environment*, 120, 70–83. https://10.1016/j.rse.2011.09.027

Venter, Z.S., Aunan, K., Chowdhury, S. & Lelieveld, J. (2020). COVID-19 lockdowns cause global air pollution declines, *Proc. Nat. Acad. Sci. (PNAS),* https://doi.org/10.1073/pnas.2006853117

Wang, X. & Zhang, R. (2020). How did air pollution change during the COVID-19 outbreak in China, *Bulletin of the American Meteorological Society*, https://doi.org/10.1175/BAMS-D-200102.1

Wang, P., Chen, K., Zhu, S., Wang, P. & Zhang, H. (2020). Severe air pollution events not avoided by reduced anthropogenic activities during COVID-19 outbreak, *Resources, Conservation and recycling, 158*, https://doi.org/10.1016/j.resconrec.2020.104814

Zangari, S., Hill, D. T., Charette, A. T. & Mirowsky, J. E (2020.Air quality changes in New York City during the COVID-19 pandemic. *Science of the Total Environment 742* (140496), https://doi.org/10.1016/j.scitotenv.2020.140496

Zhang, Y., Wen, X. Y., Wang, K., Vijayaraghavan, K., & Jacobson, M. Z. (2009) Probing into regional O_3 and particulate matter pollution in the United States: 2. An examination of formation mechanisms through a process analysis technique and sensitivity study. *J. Geophysical Research*, *114*, https://doi.org/10.1029/2009JD011900

Zhang, R., Zhang, Y., Lin, H, Feng, X., Fu, T-M., & Wang, Y. (2020). NOx emission reduction and recovery during COVID-19 in East China, *Atmosphere, 11*, 433 doi:10.3390/atmos11040433.

Zheng, B., Tong, D., Li, M., Liu, F., Hong, C., Geng, G., Li, H., Li, X., Peng, L., Qi, J., Yan, L., Zhang, Y., Zhao, H., Zheng, Y., He, K., and Zhang, Q. (2018) Trends in China's anthropogenic emissions since 2010 as the consequence of clean air actions, Atmos. Chem. Phys., 18, 14095–14111, https://doi.org/10.5194/acp-18-14095-2018,.

Zhu, S., Poetscher, J., Shen, J., Wang, S., Wang, P. & Zhang H. (2020) The “seasaw” impacts between reduced emissions and enhanced AOC on O3 during COVID-19, arXiv:2009.11714 [physics.ao-ph]

Supplementary Information

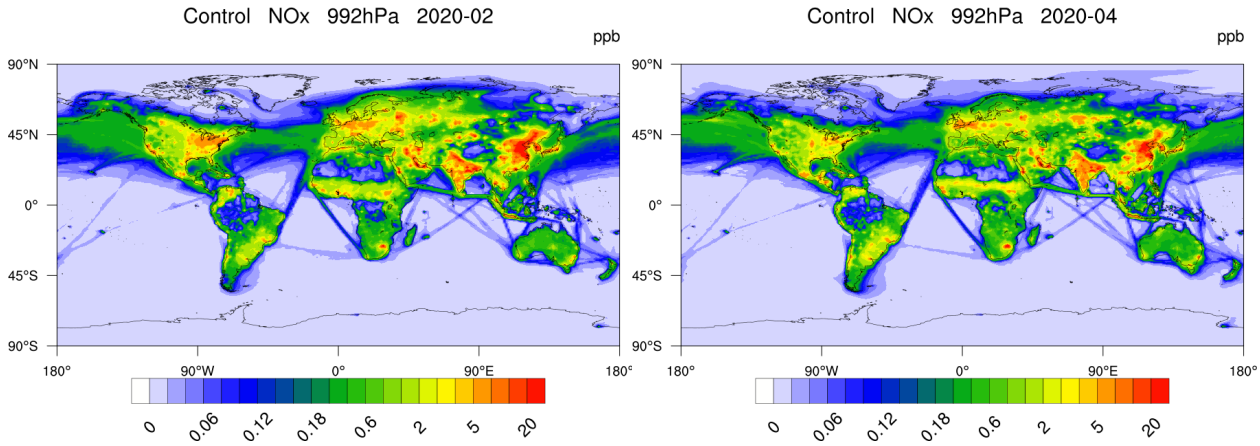

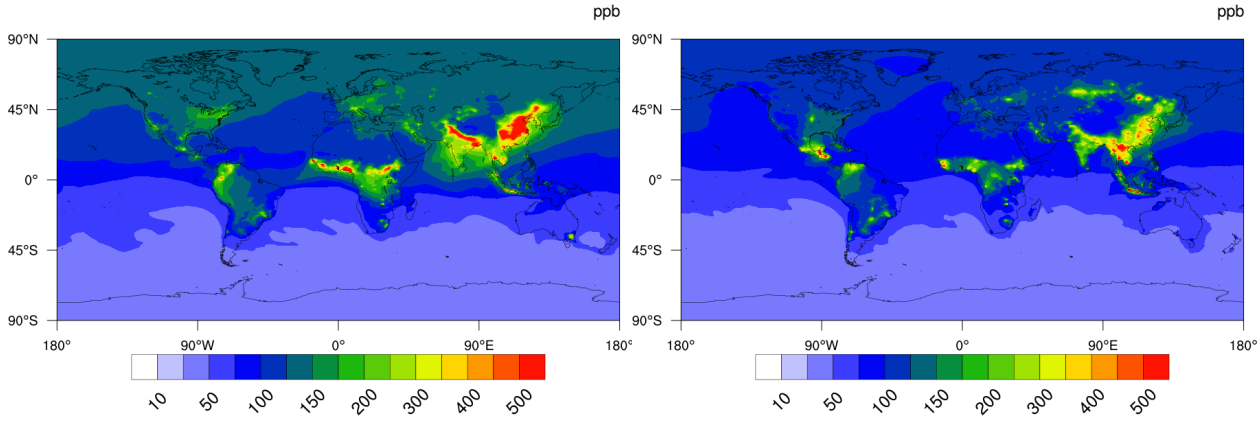

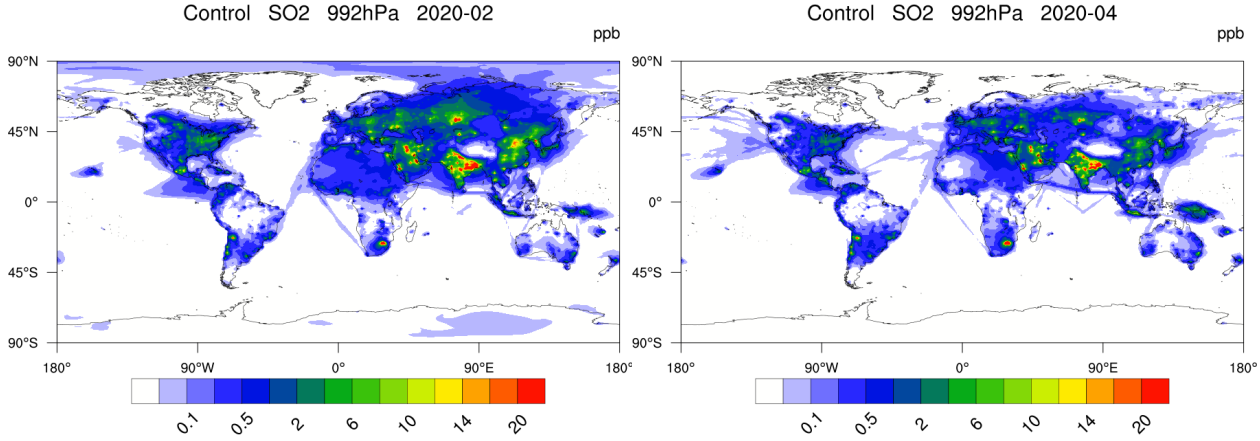

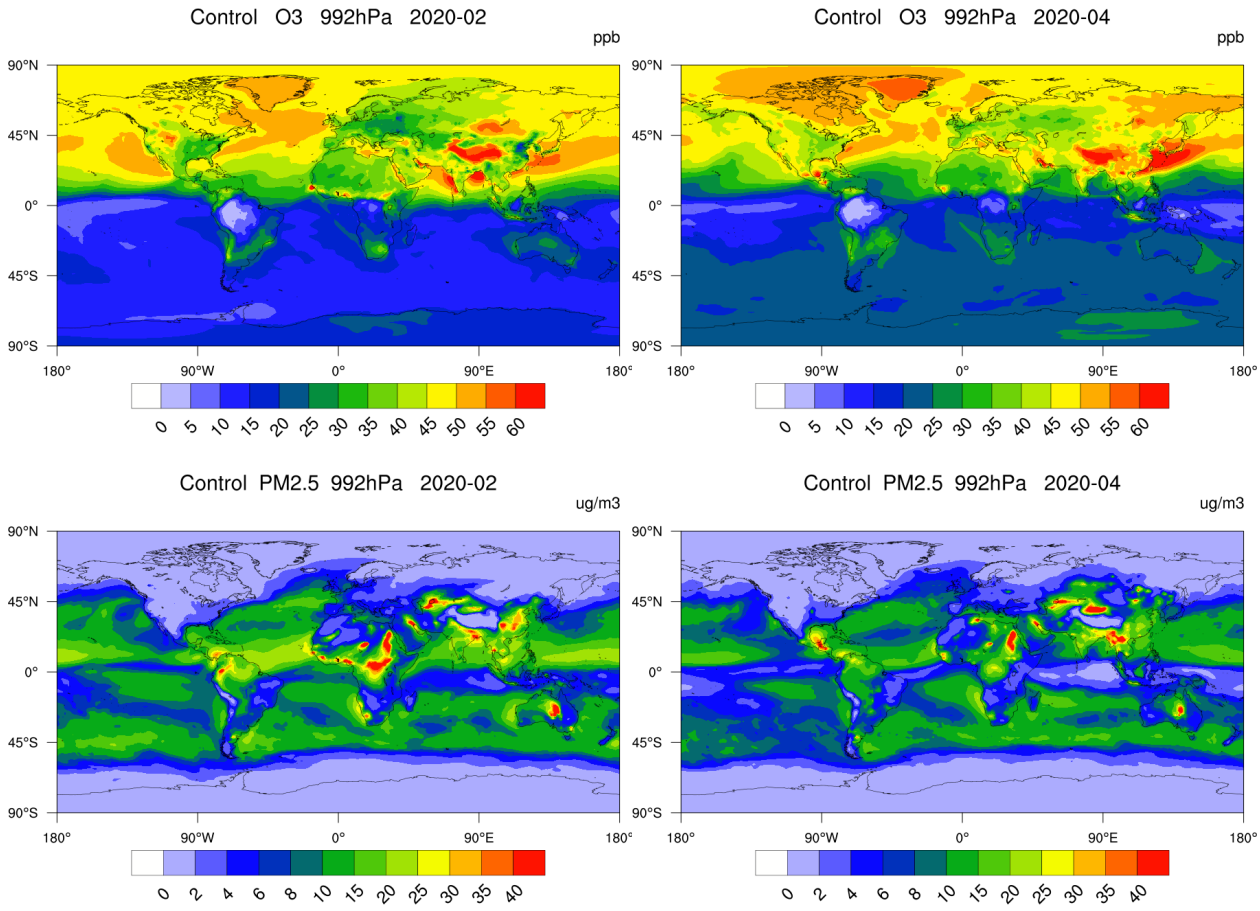

Figure S1. Global distribution of the surface mixing ratio of (from top to bottom) NO_2, CO, SO_2, O_3 and $PM_{2.5}$ (ppbv) for the month of February (left column) and April (right column) resulting from the control simulation of the CESM model.

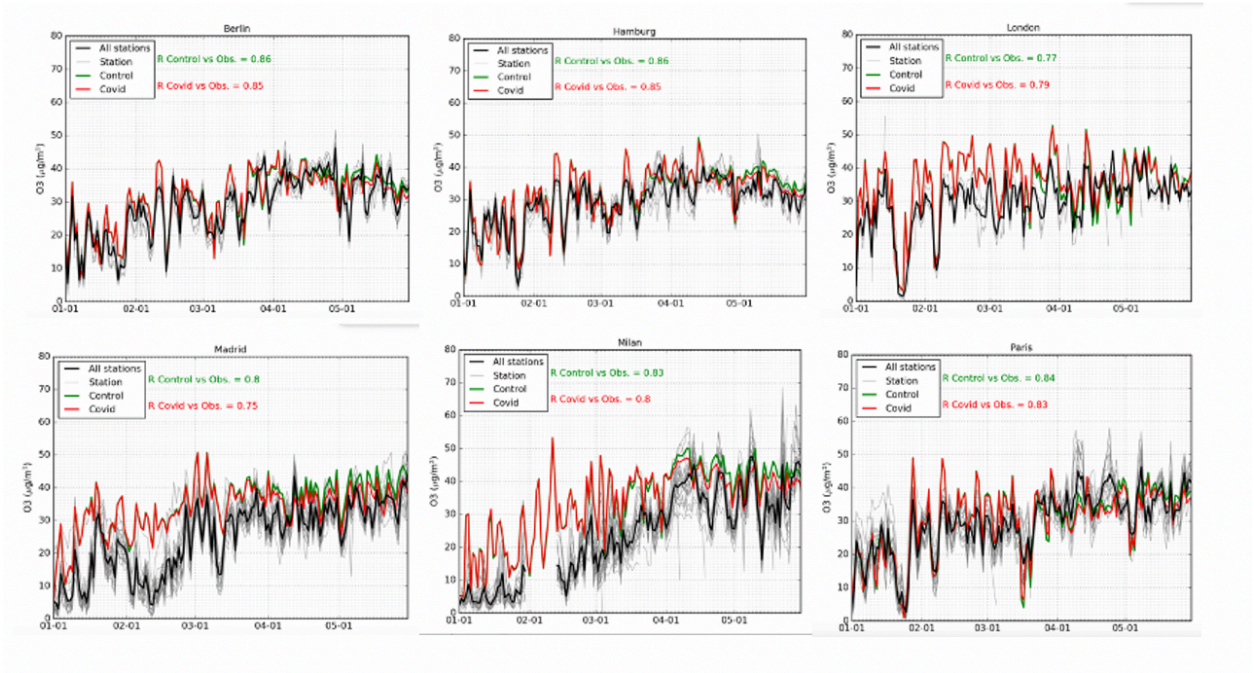

Figure S2. Evolution for the period 1 January – 31May 2020 of the surface concentration of ozone in the urban areas of Berlin, Hamburg, London, Madrid, Milan and Paris. Black curve: measurements from monitoring stations. Green curve: model baseline case. Red curve: model case with emissions modified to account for the effect of the COVID-19 pandemic.

Reduction in all anthropogenic emissions (COVID-ALL)
NOx

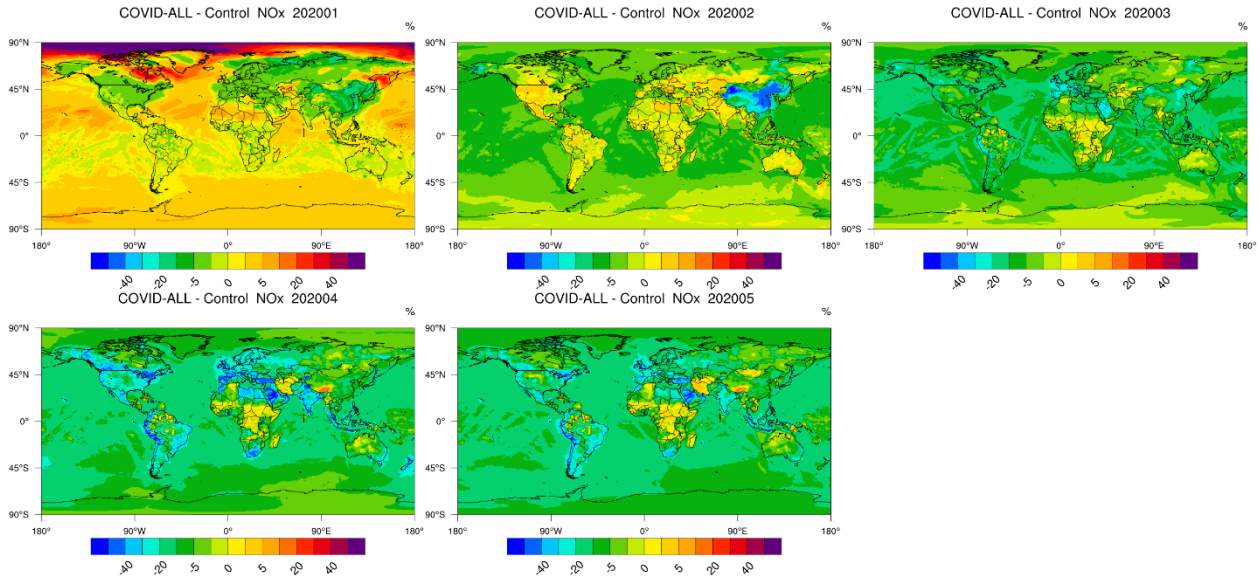

Reduction in all anthropogenic emissions (COVID-ALL)
O3

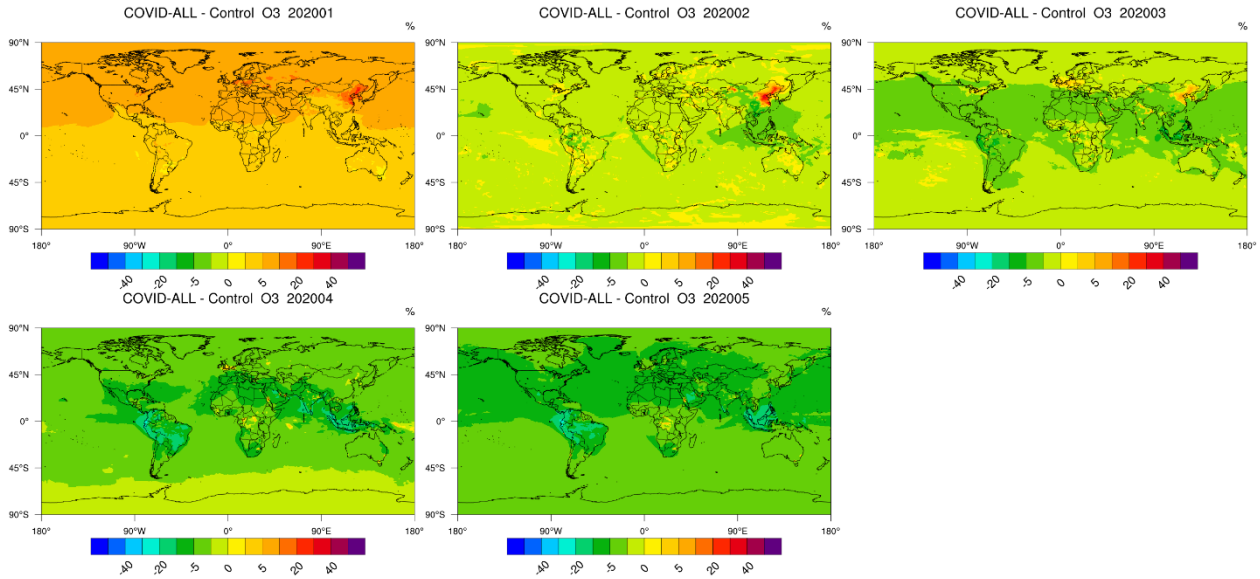

Reduction in all anthropogenic emissions (COVID-ALL)
OH

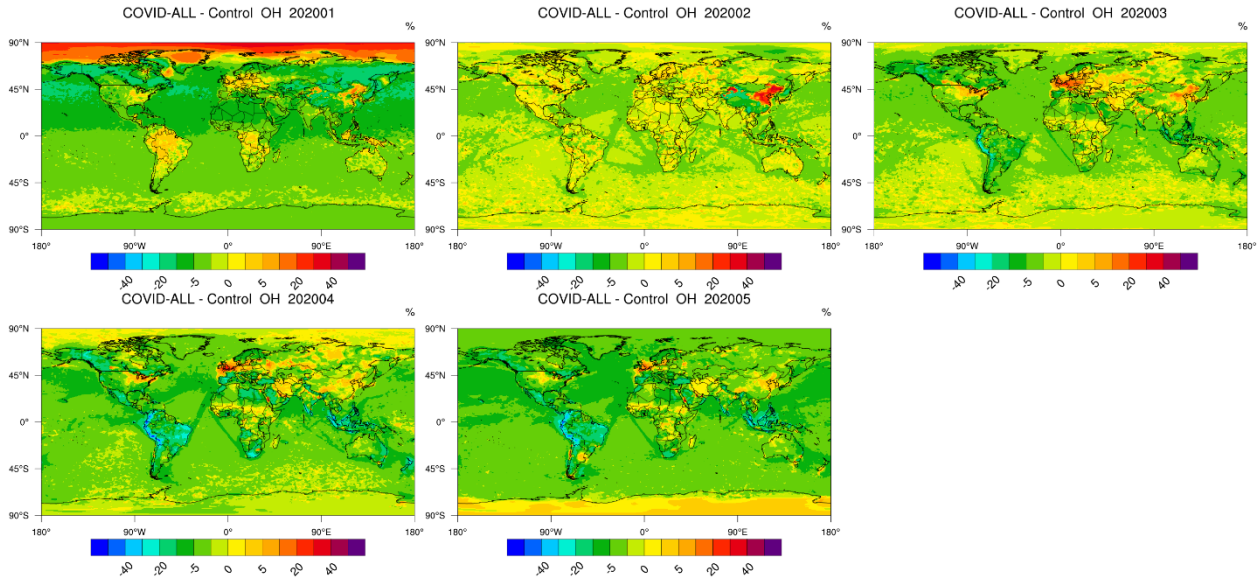

Reduction in all anthropogenic emissions (COVID-ALL)
HCHO

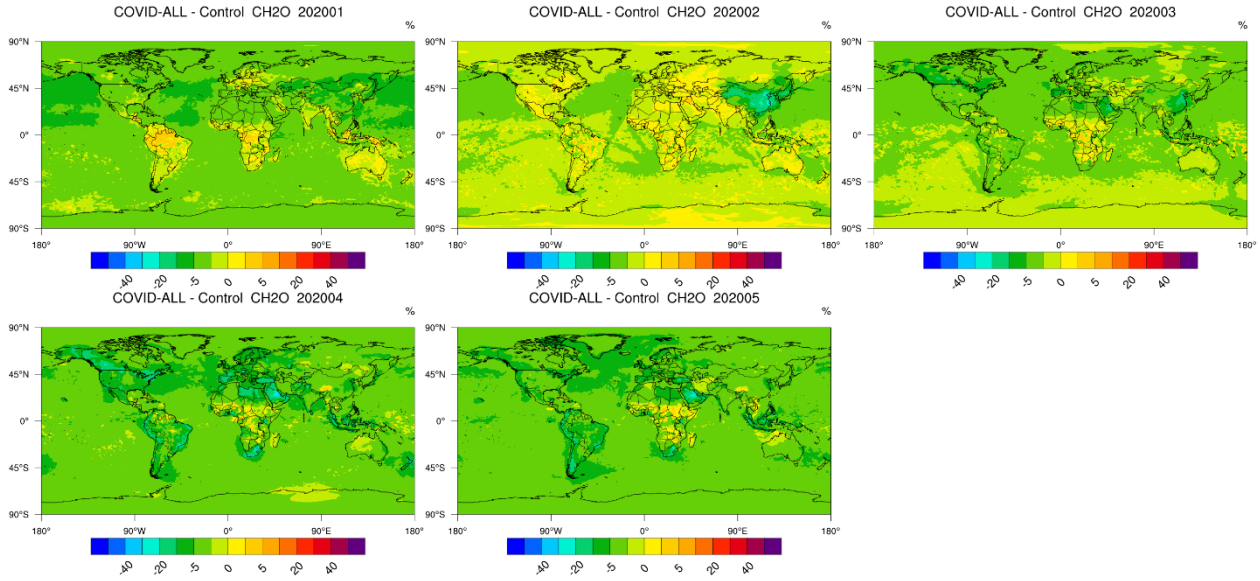

Reduction in all anthropogenic emissions (COVID-ALL)
PM2.5

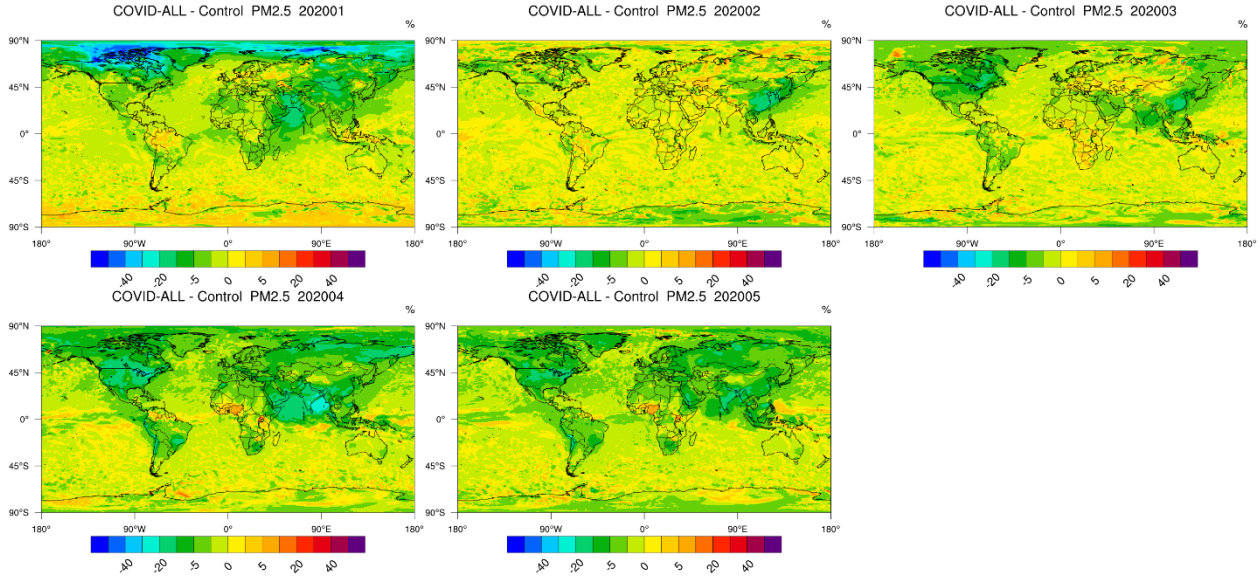

Figure S3. Evolution of the monthly mean change (percent) in the surface mixing ratio of NOx, ozone, OH, HCHO, and PM2.5 from January to May 2020 in response to the reduction in the anthropogenic emissions of primary pollutants resulting from the COVID-19 pandemic.

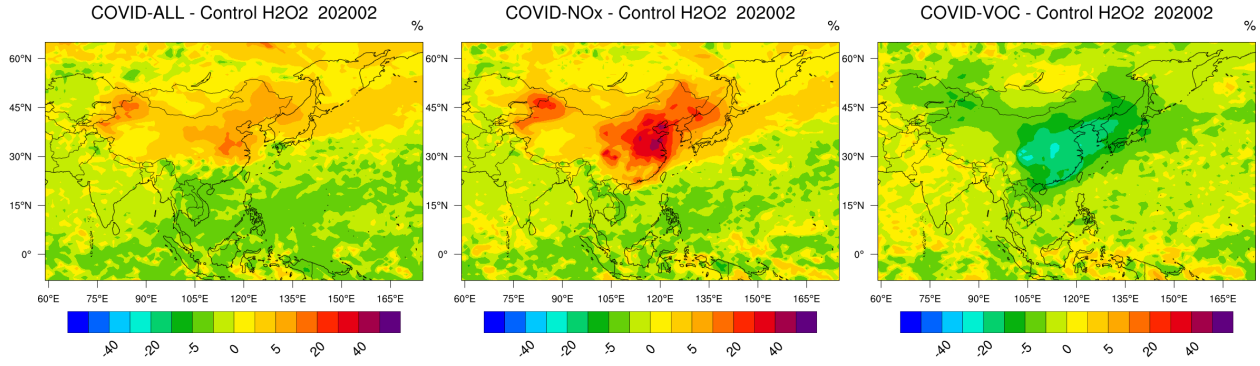

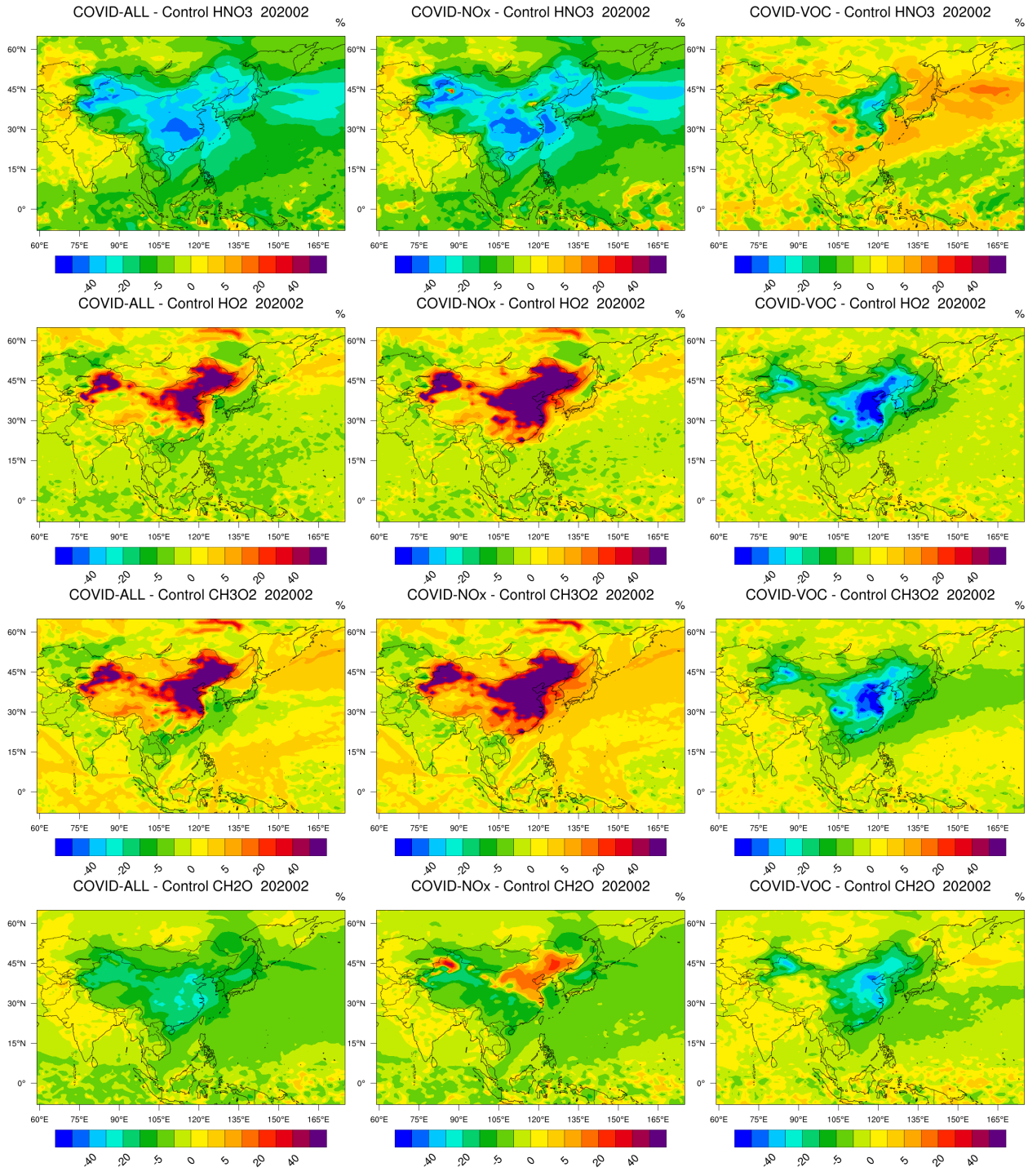

Figure S4. Percentage change in several chemical variables in China in response to reduced emissions of primary pollutants in February 2020 during the COVID-19 pandemic. From the top panels to the bottom panels: H_2O_2, HNO_3, HO_2, CH_3O_2, HCHO. Left column: reduction in all emissions; center panel: reduction in NOx emissions only; right panel: reduction in VOC and CO emissions only.

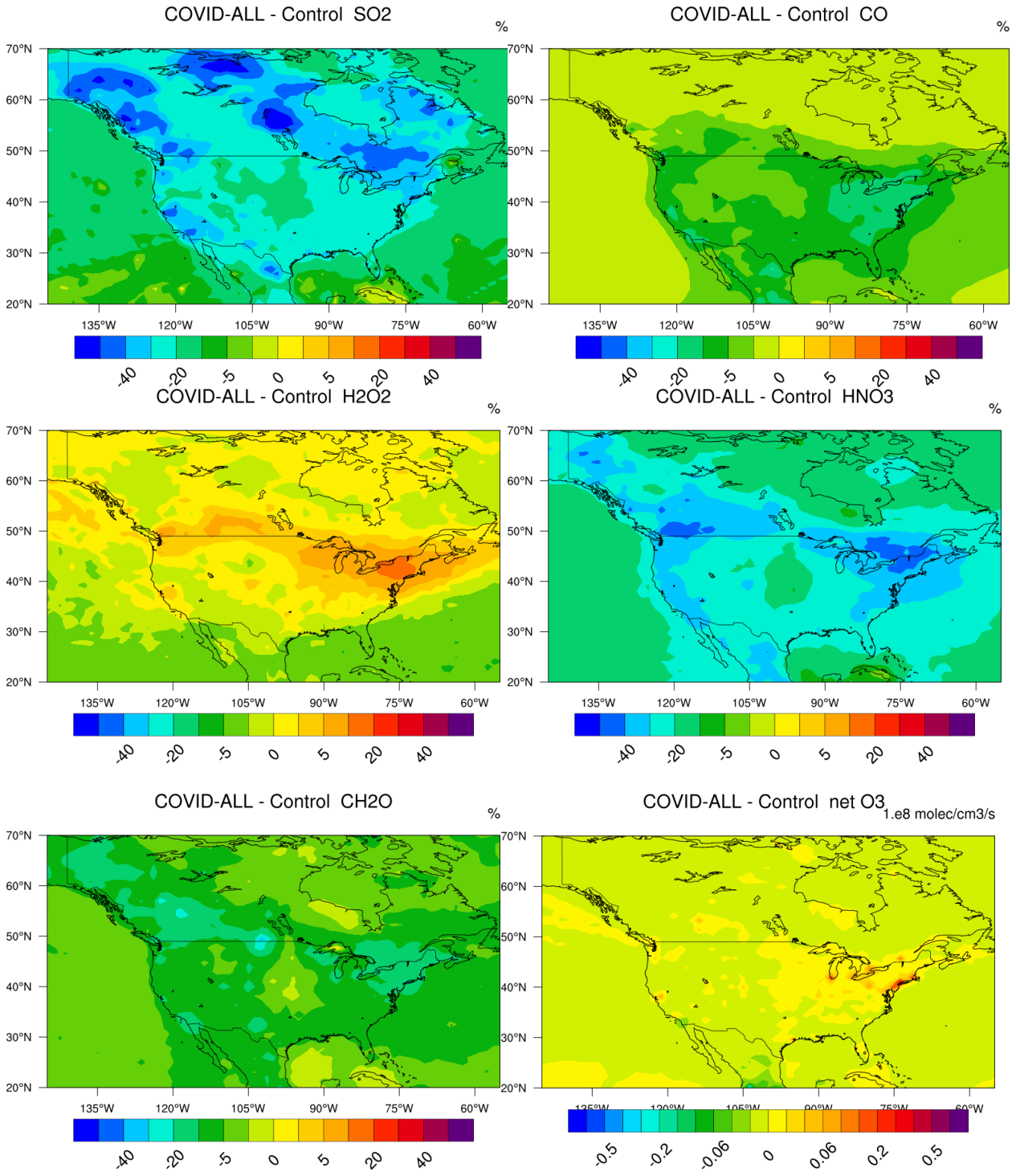

Figure S5. Change (from the top left panel to the bottom left panel) in the surface concentrations of SO_2, CO, H_2O_2, HNO_3, HCHO [percent] and in the net ozone production rate [cm^{-3} s^{-1}] in North America in response to reduced emissions of primary pollutants during the period 15 March - 14 April 2020 during the COVID-19 pandemic.